

5-2008

## Geology of the southern Reveille Range, Nye County, Nevada

Matthew Alan McKelvey  
University of Nevada, Las Vegas

Follow this and additional works at: <https://digitalscholarship.unlv.edu/thesesdissertations>



Part of the [Geology Commons](#), [Stratigraphy Commons](#), and the [Volcanology Commons](#)

---

### Repository Citation

McKelvey, Matthew Alan, "Geology of the southern Reveille Range, Nye County, Nevada" (2008). *UNLV Theses, Dissertations, Professional Papers, and Capstones*. 1447.  
<https://digitalscholarship.unlv.edu/thesesdissertations/1447>

This Thesis is protected by copyright and/or related rights. It has been brought to you by Digital Scholarship@UNLV with permission from the rights-holder(s). You are free to use this Thesis in any way that is permitted by the copyright and related rights legislation that applies to your use. For other uses you need to obtain permission from the rights-holder(s) directly, unless additional rights are indicated by a Creative Commons license in the record and/or on the work itself.

This Thesis has been accepted for inclusion in UNLV Theses, Dissertations, Professional Papers, and Capstones by an authorized administrator of Digital Scholarship@UNLV. For more information, please contact [digitalscholarship@unlv.edu](mailto:digitalscholarship@unlv.edu).

GEOLOGY OF THE SOUTHERN REVELLE RANGE,  
NYE COUNTY, NEVADA

by

Matthew Alan McKelvey

Bachelor of Science  
Austin Peay State University  
2001

A thesis submitted in partial fulfillment  
of the requirements for the

**Master Degree of Science in Geoscience  
Department of Geoscience  
College of Science**

**Graduate College  
University of Nevada, Las Vegas  
May 2008**

Copyright by Matthew A. McKelvey 2008  
All Rights Reserved



**Thesis Approval**  
The Graduate College  
University of Nevada, Las Vegas

APRIL 11, 2008

The Thesis prepared by

MATTHEW ALAN MCKELVEY

Entitled

GEOLOGY OF THE SOUTHERN REVEILLE RANGE, NYE COUNTY, NEVADA

is approved in partial fulfillment of the requirements for the degree of

MASTER OF SCIENCE IN GEOSCIENCE

*Examination Committee Chair*

*Examination Committee Member*

*Examination Committee Member*

*Graduate College Faculty Representative*

*Dean of the Graduate College*

## ABSTRACT

### GEOLOGY OF THE SOUTHERN REVEILLE RANGE, NYE COUNTY, NEVADA

by

Matthew Alan McKelvey

Dr. Eugene I. Smith, Examination Committee Chair  
Professor of geology  
University of Nevada, Las Vegas

The Reveille Range in central Nevada provides a unique window into the mid-Miocene geology and volcanology of the central Great Basin during the “ignimbrite flare up.” Although faulted along its margins, the interior of the range is relatively undeformed thus preserving volcanic centers. The Reveille Range contains three mid-Miocene caldera complexes. Previous studies have identified the Goblin Knobs caldera (25.6 Ma) in the central Reveille Range and the caldera of northern Reveille Range (25.3 Ma) to the north. These calderas are completely filled with intracaldera tuffs. This study has identified a younger third caldera located in the southern part of the Reveille Range, and the southern margin of the Goblin Knobs Caldera. The newly discovered caldera in the southern Reveille Range, herein named the Pyramid Spring caldera, contains intracaldera tuff, pumice-rich outflow sheets, and volcanoclastic sedimentary moat units dipping to the north off a possible resurgent dome. Crystal rich rhyolite domes occur along the eastern and northeastern margin of the caldera. An 8 km long composite dacite dike (Fang Ridge) is also associated with the caldera. Moat rocks include pyroclastic flows, debris flow

breccias, and fine to coarse grained immature sandstones that contain lithic fragments up to 5 cm in size. Of the three calderas in the Reveille Range, the Pyramid Spring caldera is the only one that is associated with outflow tuffs. Three cooling units were identified; the middle is welded and contains fiamme up to 15-20 cm in size. The outflow tuffs of the Pyramid Spring caldera are abruptly cut by the Goblin Knobs caldera. Besides the stratigraphic truncation, the Goblin Knobs caldera margin was identified by a zone of hydrothermal alteration (silicification) and mineralization and a section of outflow from the Pyramid Spring caldera that has slumped (back tilted) into the Goblin Knobs caldera. Correlation, age and geochemistry of Pyramid Spring caldera tuffs and indicate the presence of a previously unidentified volcanic center in the southern Reveille Range.

## TABLE OF CONTENTS

ABSTRACT.....	iii
TABLE OF CONTENTS.....	v
LIST OF FIGURES .....	viii
ACKNOWLEDGEMENTS.....	ix
CHAPTER 1 INTRODUCTION.....	1
Introduction.....	1
Previous Work .....	4
Volcanism .....	6
Regional Tectonics.....	7
Background on the Pahranaगत Formation and the Kawich caldera .....	9
The Kawich Caldera .....	9
The Pahranaगत Formation.....	11
Fang Ridge.....	11
Geochronology.....	12
Paleomagnetic Data for the Pahranaगत Formation .....	12
Petrology of the Pahranaगत Formation .....	13
Purpose of Research.....	14
CHAPTER 2 ANALYTICAL TECHNIQUES AND METHODOLOGY.....	16
$^{40}\text{Ar}/^{39}\text{Ar}$ Samples .....	16
Major and Trace Elements.....	18
Isotope Analysis.....	20
Paleomagnetic Sample collection and Analysis .....	20
CHAPTER 3 VOLCANIC STRATIGRAPHY AND FAULTS .....	22
Volcanic Stratigraphy .....	22
Lower Pyramid Spring tuff ( $Tps_1$ ) .....	22
Middle Pyramid Spring tuff ( $Tps_2$ ) .....	25
Upper Pyramid Spring tuff ( $Tps_3$ ).....	26
Reveille Peak .....	28
Rhyolite Domes .....	28
Volcaniclastic sedimentary units and pyroclastic flows .....	29
Fang Ridge.....	32
Faults.....	34

CHAPTER 4	IDENTIFICATION OF THE PYRAMID SPRING CALDERA .....	38
	Criteria for Recognizing a Caldera .....	38
	Caldera Wall .....	40
	Resurgent Dome.....	40
	Ring fracture and post-caldera domes.....	40
	Moat deposits and pyroclastic flows.....	43
	Outflow tuffs.....	45
	Summary .....	46
CHAPTER 5	GEOCHRONOLOGY .....	46
	Lower Pyramid Spring tuff (Tps <sub>1</sub> ).....	46
	Upper Pyramid Spring tuff (Tps <sub>3</sub> ).....	47
	Dome B.....	47
	Fang Ridge .....	47
CHAPTER 6	PALEOMAGNETIC ANALYSIS .....	52
	Lower Pyramid Spring tuff (Tps <sub>1</sub> ).....	53
	Middle Pyramid Spring tuff (Tps <sub>2</sub> ).....	54
	Upper Pyramid Spring tuff (Tps <sub>3</sub> ).....	54
	Tuff of Goblin Knobs(Tgk) .....	54
	Dome B .....	59
	Summary .....	59
CHAPTER 7	GEOCHEMISTRY .....	60
	Major Elements.....	60
	Trace Elements.....	60
	Isotopes .....	64
	Summary .....	69
CHAPTER 8	REGIONAL CORRELATIONS .....	71
	Geochemistry .....	71
	Geochronology.....	74
	Paleomagnetic Data .....	75
	Summary .....	75
CHAPTER 9	CONCLUSIONS .....	76
APPENDIX A	PETROGRAPHIC DESCRIPTIONS .....	77
APPENDIX B	<sup>40</sup> Ar/ <sup>39</sup> Ar LASER FUSION ANALYTICAL DATA .....	84
APPENDIX C	MAJOR AND TRACE ELEMENT GEOCHEMISTRY DATA.....	89
APPENDIX D	PALEOMAGNETIC DATA.....	91
REFERENCES CITED.....		93



VITA.....	97
-----------	----

## LIST OF FIGURES

Figure 1.	Map of geologic structures and calderas .....	2
Figure 2.	Location Map.....	3
Figure 3.	Gardner Map.....	5
Figure 4.	Magmochrons and extensional belts.....	8
Figure 5.	Kawich caldera .....	10
Figure 6.	Panorama of the southern Reveille Range.....	23
Figure 7.	Generalized geologic map of volcanic stratigraphy and structures.....	24
Figure 8.	Pumice Fragment.....	27
Figure 9.	Sedimentary section in the moat.....	31
Figure 10.	Fang Ridge.....	33
Figure 11.	Fault A .....	35
Figure 12.	Fault B .....	36
Figure 13.	Caldera elements based on Lipman description .....	39
Figure 14a.	Interpretation of generalized geologic map .....	41
Figure 14b.	Generalized cross section of the southern Reveille Range.....	42
Figure 15.	Isochron and probability plot of the lower Pyramid Spring tuff .....	48
Figure 16.	Probability plot of the upper Pyramid Spring tuff.....	49
Figure 17.	Isochron and probability plot of the DomeB .....	50
Figure 18.	Isochron and probability plot of the Fang Ridge dacite .....	51
Figure 19.	Paleomagnetic data for lower Pyramid Springs tuff.....	55
Figure 20.	Paleomagnetic data for middle Pyramid Springs tuff.....	56
Figure 21.	Paleomagnetic data for upper Pyramid Springs tuff.....	57
Figure 22.	Paleomagnetic data for tuff of Goblin knobs .....	58
Figure 23.	Irving-Baragar classification .....	61
Figure 24.	Major element variation plots.....	62
Figure 25.	Trace element variation plots .....	63
Figure 26a.	Spider diagrams for Pyramid Spring tuffs .....	65
Figure 26b.	Spider diagrams for Rhyolite domes .....	65
Figure 26c.	Spider diagrams for Fang Ridge .....	66
Figure 27.	$\epsilon_{Nd}$ vs. $Sr_i$ .....	67
Figure 28.	Pb isotopes.....	68
Figure 29.	Southern Reveille Range vs. Pahrnagat Range major elements.....	72
Figure 30.	Southern Reveille Range vs. Pahrnagat Range trace elements.....	73

## ACKNOWLEDGEMENTS

I would like to thank the Department of Geoscience for accepting me into this program and investing time and energy into furthering my education and research goals. I would also like to thank my advisor Dr. Eugene I. Smith. His passion for and geology, especially volcanology, proved to be very contagious. His knowledge and generosity helped make this project successful. Also, the rest of my committee, Dr. Andrew Hanson, Dr. Terry Spell, and Dr. Stephen Lepp deserve a great deal of credit for the advice and knowledge that they passed onto to me. I would also like to thank Dr. James Faulds from the Nevada Bureau of Mines and Geology/University of Nevada, Reno for his time and help with the paleomagnetic sampling and analysis of this project. I would like to thank Kathy Zanetti and Joseph Kula for all their help and time they provided me to make sure my geochronology was done correctly. I would like to thank all of my friends here and in Tennessee for helping me throughout this whole process. Last, but most important, I would like to thank my parents, Mark and Connie, and my brother, Mike, who have supported me through the good times and bad time and made me realize that this goal of mine was attainable.

## CHAPTER 1

### INTRODUCTION

During the Cenozoic, caldera forming eruptions produced numerous ash-flow tuffs within the Great Basin of western North America. According to estimates by Stewart and Carlson (1976) and Best et al. (1989), the Great Basin of the Basin and Range province contains approximately 70 known volcanic centers with more than 100 ash-flow tuffs. The majority of the ash-flow tuffs produced within the Basin and Range were erupted between 31 to 22 Ma during the ignimbrite flare-up (Best et al., 1993), however, minor ash-flow volcanism continued until 9.5 Ma. Within the Basin and Range province of Nevada, the central Nevada caldera complex covers more than 20,000 km<sup>2</sup> and contains numerous, large-volume ash-flow tuffs and intracaldera deposits (Best et al., 1995) (Figure 1).

The field area in the southern Reveille Range is located within the central Nevada caldera complex (Figure 2). The Reveille Range and adjacent areas contain numerous calderas, such as the Goblin Knobs caldera (central Reveille Range) and the Caldera of the northern Reveille Range in the northern Reveille Range (Rash, 1995; Martin and Naumann, 1995). West of the Reveille Range is the Kawich Caldera, located in the Kawich Range (Gardner et al., 1980; Best et al, 1995). A recent study in the Kawich Range by Honn (2005) has located five calderas and associated intracaldera tuffs.

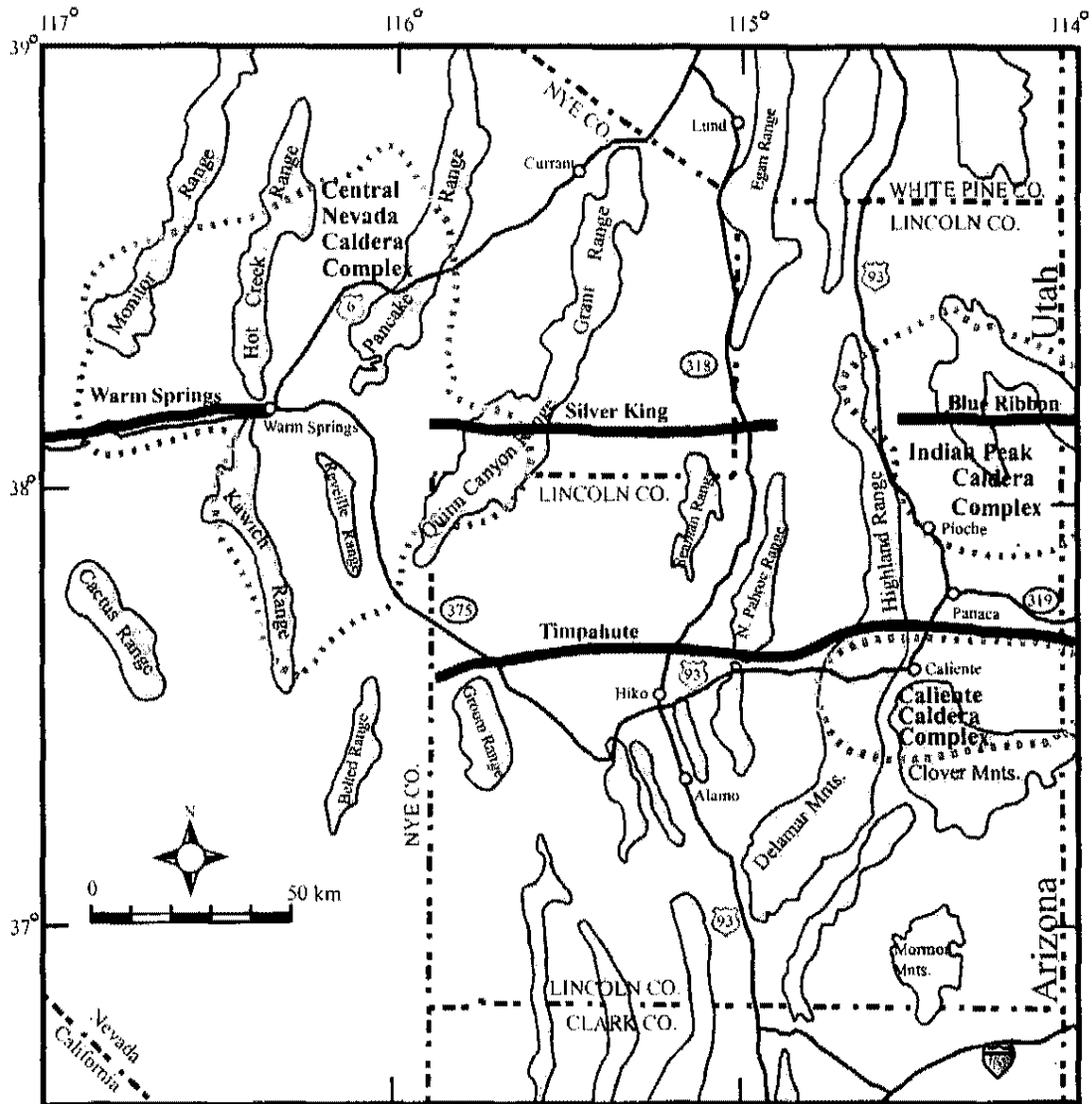


Figure 1. Caldera complexes and structural lineaments located within central Nevada. Caldera complexes include the Indian Peak, Caliente, and central Nevada (Red Dashed Lines). The structural lineaments include the Timpahute, Blue Ribbon, Silver King, and Warm Springs (Thick Black Line). Figure modified from Hurtubise (1994) and Rash (1995).

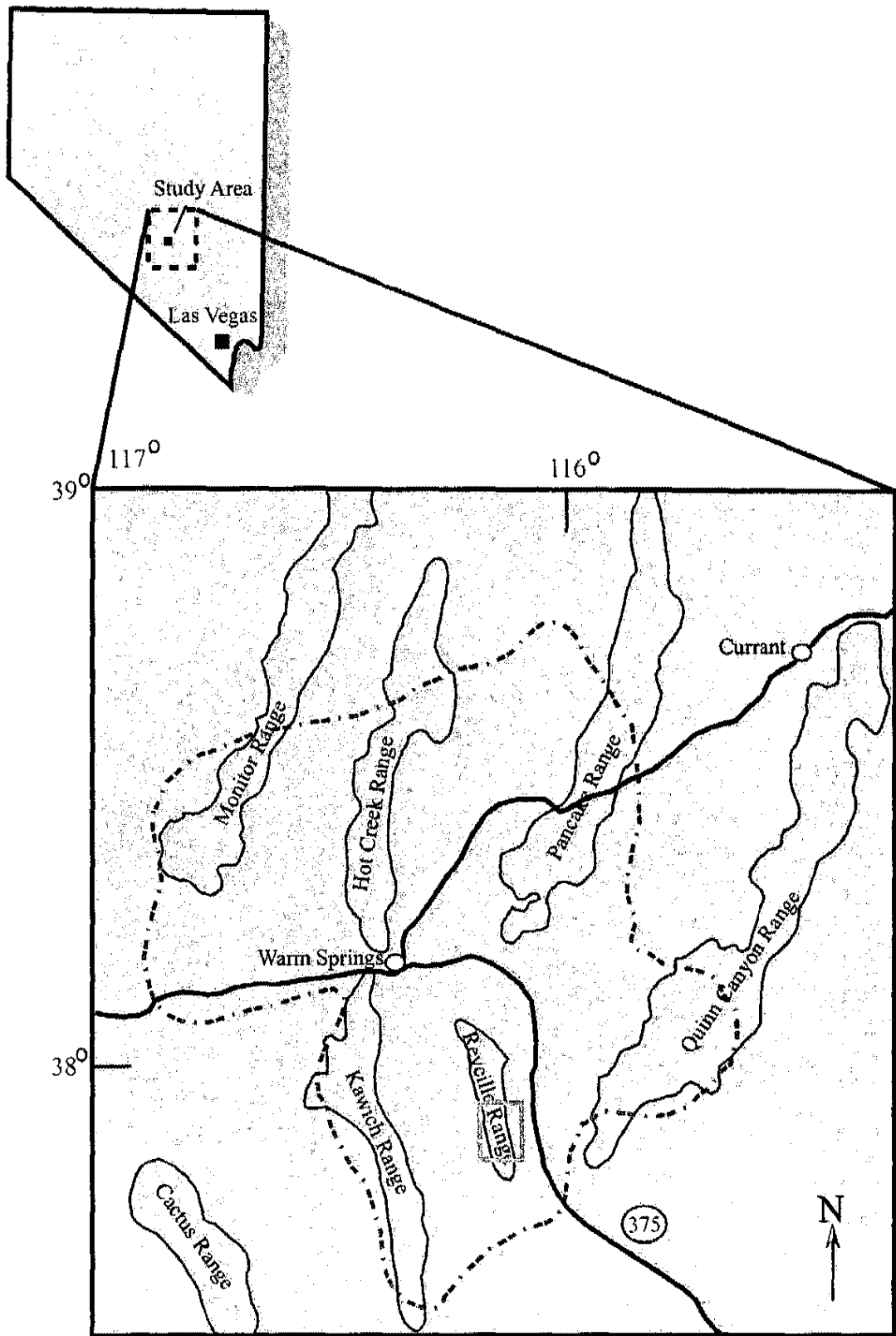


Figure 2. Location map of the area of study. Field area (red square) is located in the southern Reville Range. The Central Nevada Caldera Complex (blue dashed line) encompasses the field area.

## Previous Work

Geologic mapping by Ekren et al. (1973) provided a stratigraphic framework that other mapping projects have been based upon. During the mapping by Ekren et al. (1973) the study determined the existence of the Goblin Knobs caldera and the caldera of the northern Reveille Range. A later geologic study by Martin and Naumann (1995) mapped the Reveille 7<sup>1</sup>/<sub>2</sub>' quadrangle at a scale of 1:24,000 and located the northern margin of the Goblin Knobs caldera and the southern margin of the caldera of northern Reveille Range.

Gardner and others (1980) provided reconnaissance maps of the Kawich and Reveille Ranges (Figure 3). These reconnaissance maps are very generalized and do not differentiate the volcanic stratigraphy in the southern Reveille Range. Geologic studies by Best et al. (1995) used the reconnaissance maps by Gardner et al. (1980) to interpret the southern Reveille Range as the eastern margin of the Kawich caldera; the source of the Pahranaagat Formation.

The detailed geologic mapping of the Twin Springs Slough 7<sup>1</sup>/<sub>2</sub>' quadrangle, located in the northern Reveille Range, by Rash (1995) located the northern wall of the caldera of northern Reveille Range between the Pancake Range and the northern Reveille Range.

These previous mapping projects focused on the sedimentary stratigraphy or on the silicic volcanic units in the central and northern Reveille Range, but lacked any detail on the silicic volcanic units found in the southern Reveille Range.

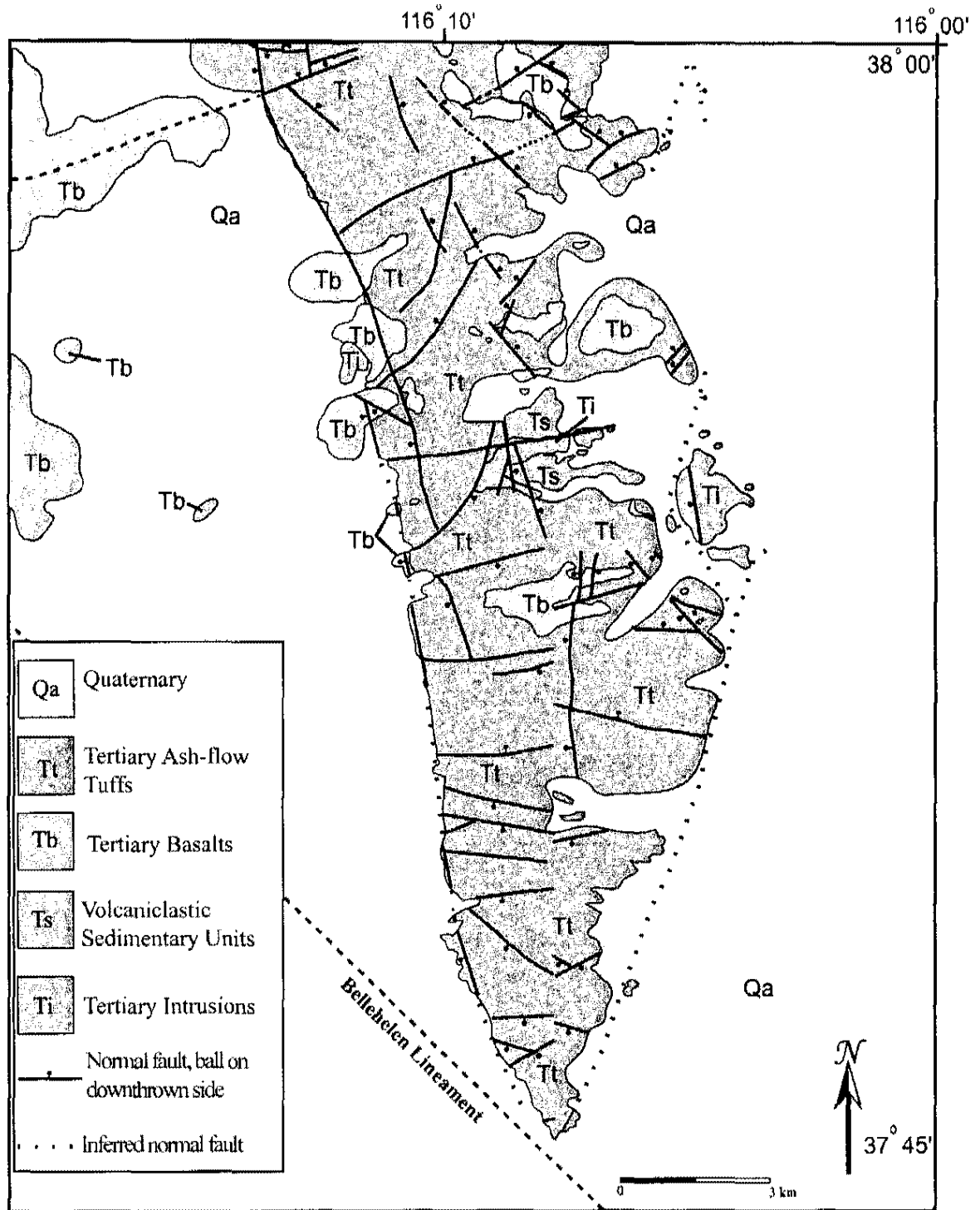


Figure 3. Generalized geologic map of the central and southern sections of the Reville Range. Figure is modified from Gardner and others (1980).



## Volcanism

Large-scale caldera related volcanism within the Basin and Range province began in the Eocene, at approximately 49 Ma, with the eruptions of the Challis volcanic field in central Idaho (Cater et al., 1979). Volcanism then migrated southwestward from the Challis volcanic field to the northeastern part of the Great Basin at about 35 – 30 Ma. The compositions of the volcanic rocks that were erupted between 35-30 Ma were predominately high-K andesite, dacite, and rhyolite with minor rhyolitic pyroclastic flows (Best and Christiansen, 1991).

The ignimbrite flare-up, a period of voluminous caldera-forming eruptions within the Great Basin, began about 31 Ma and ended around 20 Ma (Coney, 1978). During the ignimbrite flare-up caldera style eruptions began in central and western Nevada between 31 – 22 Ma and finally reached the southern and western sections of the Great Basin by 20 Ma (Figure 4) (Axen et al., 1993). During the ignimbrite flare-up high-K andesite, dacite, and rhyolite lavas were erupted; however, they were minor compared to the 35,000 km<sup>3</sup> of dacitic and rhyolitic ash-flows that were deposited at the same time (Best and Christiansen, 1991). Ash-flow volcanism began to decrease within the Great Basin after 20 Ma and was replaced by the extrusion of alkali basalts.

Pliocene to Quaternary basaltic volcanism has occurred in the Great Basin, Colorado Plateau, and the eastern front of the Sierra Nevada Range. A zone of alkali basaltic volcanism can be found in a southwest-northeast belt starting in Death Valley, CA and trending to the Lunar Crater Volcanic Field in central Nevada (Vaniman and Crowe, 1981).

These previous studies generalize the initiation of volcanism in the central Nevada caldera complex and suggest that eruptions occurred between 20-25 Ma. There has not been any detailed work to constrain the timing of volcanism that occurred in the southern Reveille Range.

### Regional Tectonics

The Reveille Range is located in the Basin and Range Province of central Nevada. During Cenozoic time the Basin and Range province underwent a period of large-scale extension and was extended 100%-300% in a general east-west direction (Wernicke, 1981). During the Eocene and Oligocene two north-south extensional belts formed in the Great Basin. The eastern belt is located near the Utah-Nevada border and the western belt stretches from the Funeral Mountains, California to the Albion Range, Idaho (Figure 4) (Axen et al., 1993). Extension was synvolcanic or post-volcanic in the northern section of both north-south extensional belts, while the extension in the southern section of both belts occurred prior to volcanism.

Several east-west striking topographic and structural lineaments occur in central Nevada including the Blue Ribbon-Silver King Lineament to the east of the Reveille Range which extends from Railroad Valley into southern Utah (Hurtubise, 1994). This lineament is composed of east-west striking normal faults. The Warm Springs Lineament begins in Hot Creek Valley and projects westward to Tonopah, Nevada (Hurtubise, 1994). The Timpahute Lineament is an east-west trending structure that is approximately 25 km wide and begins in the northern Groom Range. It strikes eastward into the eastern

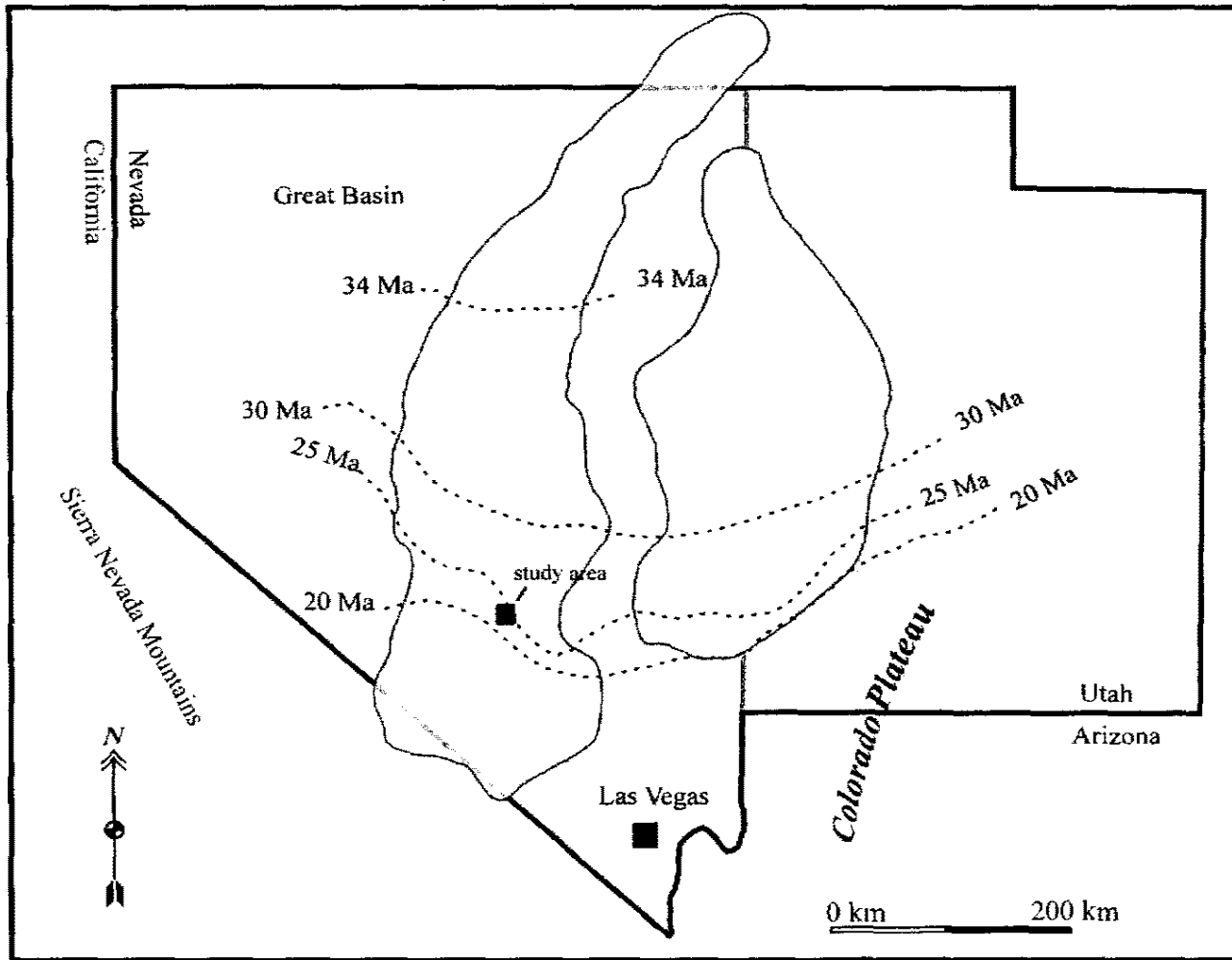


Figure 4. Map showing the Eocene to Oligocene extensional belts (gray shaded area). The dotted lines are magmochrons that indicate the southward migration of large scale volcanism in the Great Basin. The magmochrons record the initiation of volcanism. Figure is modified from Axen and others (1993).

section of the Caliente Caldera Complex and possibly into Utah (Hurtubise, 1994) (Figure 1).

#### Background on the Pahrnagat Formation and the Kawich caldera

The Pahrnagat Formation and the Kawich caldera are located in central Nevada in what is known as the central Nevada caldera complex. The Miocene Pahrnagat Formation and the Kawich caldera formed during the ignimbrite flare-up in central Nevada. The Kawich caldera is considered the source of the Pahrnagat Formation, which is a regionally extensive ash-flow sheet that is exposed over an area of 33,000 km<sup>2</sup> in the southern Great Basin of Nevada. According to Best et al. (1995) the Pahrnagat Formation is also known as the Pahrnagat Lakes Tuff, granite-weathering tuff, tuff of Saulsbury Wash, and the upper tuff of White Blotch Spring.

#### The Kawich Caldera

The Kawich caldera is located near the southern margin of the central Nevada caldera complex in the Kawich Range (Figure 5). The Kawich caldera has an area of 1040 km<sup>2</sup>, however east-west crustal extension has increased the area of the caldera to 1550 km<sup>2</sup> (Best et al., 1995). The intracaldera tuff that is located in the Kawich caldera is at least 1 km thick and had an original volume of 1000 km<sup>3</sup> (Best et al., 1995). Due to the lack of detailed work in the Kawich caldera the history of collapse, resurgence, and the magmatic evolution of the intracaldera rocks is generally unknown.

A recent study by Honn (2005) indicated that the Kawich caldera as described by Best et al. (1995) does not exist. Honn (2005) identified five previously undocumented

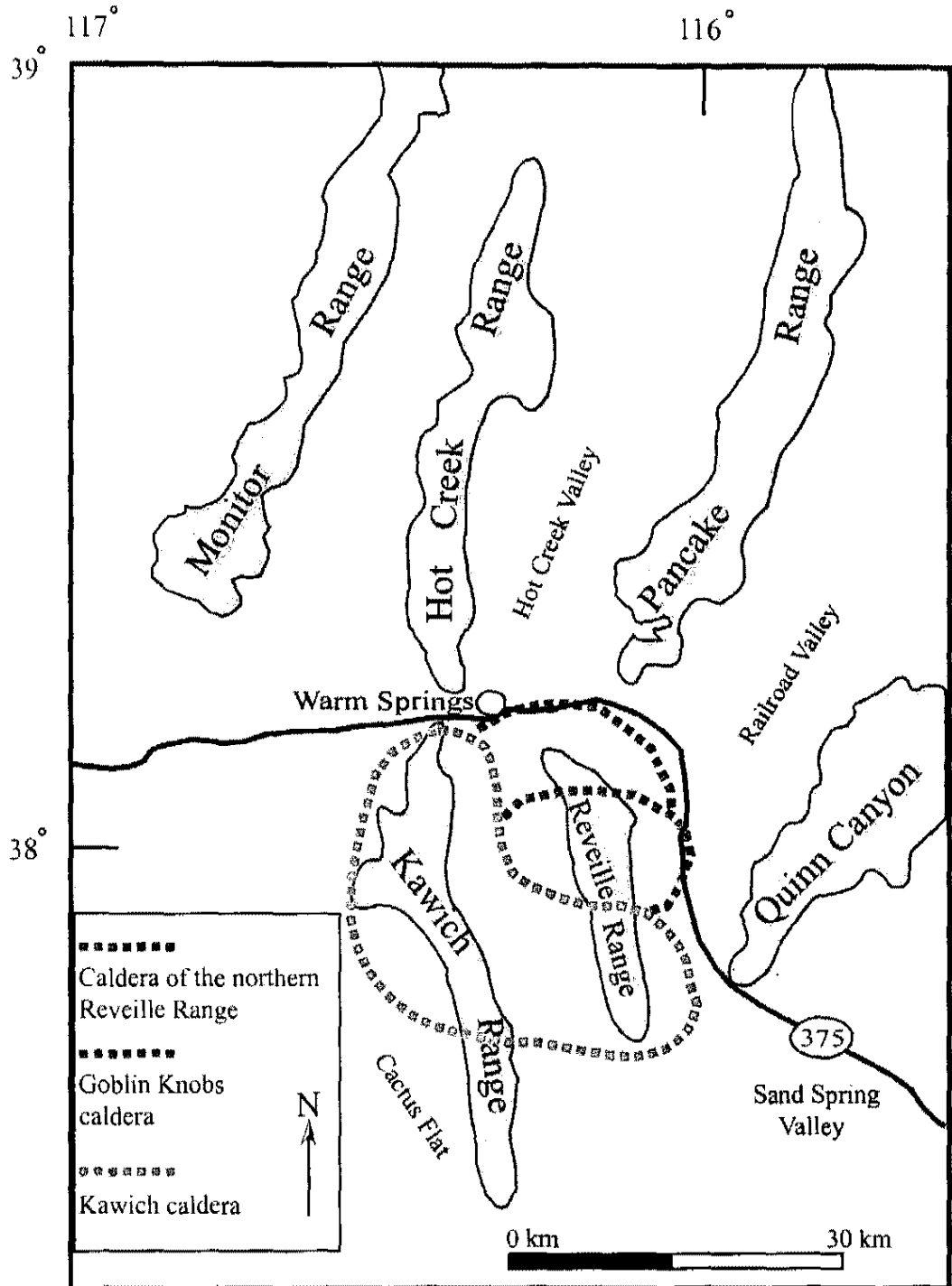


Figure 5. Calderas located in the Kawich and Reville Range. Red dotted line indicates the margin of the Kawich Caldera proposed by Best and others (1995). Blue Dotted line indicated the margin of the caldera of the northern Reville Range proposed by Rash (1995). The green dotted line indicates the margin of the Goblin Knobs caldera proposed by Martin and Naumann (1995) and Rash (1995).

calderas in the region that Best et al. (1995) suggested contains just the Kawich caldera. Geochemical analysis of the ash-flow tuffs from the Honn (2005) study indicated that the Pahranaagat Formation was not present.

### The Pahranaagat Formation

The Pahranaagat formation is divided into two petrographic types based on the degree of welding, abundance of pumice fragments, and mafic phenocrysts (Best et al., 1995). The first petrographic type is the Saulsbury type that “characterizes the proximal parts of the outflow sheet around the caldera” (Best et al., 1995). The Saulsbury type is partly to densely welded and contains a small percentage of pumice clasts. Mafic phenocrysts are rare in Saulsbury type tuff and consist mainly of biotite with a few amphiboles (Best et al., 1995).

The Alamo petrographic type forms the distal parts of the outflow sheet (Best et al., 1995). The Alamo type tuff is less densely welded in comparison to the Saulsbury type (Best et al., 1995) and contains white to light gray pumice lapilli and local blocks in a pink to pale orange or purple-gray devitrified matrix (Best et al., 1995). Stratigraphically the Alamo type overlies the Saulsbury type.

### Fang Ridge

Fang Ridge is an east-west trending dacite dike (Best et al., 1995) that forms a prominent ridge within the Reveille Range. The study by Best et al. (1995) identified Fang Ridge as an east-west trending dike that was composed of dacite. The dacite that composes Fang Ridge is 2 Ma to 3 Ma younger than the Pahranaagat Formation.

Emplacement of the Fang Ridge dacite is unrelated to the magma that produced the Pahranaagat Formation (Best et al., 1995).

However, there has been no study conducted on the relationship or origin of the Fang Ridge dacite. Best et al. (1995) inferred, without any in depth geochronological or geochemical studies, that there is no relationship between Fang Ridge and other volcanic units in the southern Reveille Range.

### Geochronology

$^{40}\text{Ar}/^{39}\text{Ar}$  dating of the Pahranaagat Formation by Best et al. (1995) yielded an age of 22.639 Ma  $\pm$  0.009 Ma. According to Best et al. (1995) the outflow and intracaldera tuff are analytically indistinguishable in age, which suggests that geographic variation in the Pahranaagat Formation does not effect the age. In 2005, Dr. Eric Christiansen re-dated the tuff using the  $^{40}\text{Ar}/^{39}\text{Ar}$  technique and obtained an age of 22.78 Ma.

These previous geochronological studies on the Pahranaagat tuff did not include the volcanic stratigraphy in the southern Reveille Range. There is a lack of geochronologic data to determine whether their inferences that the southern Reveille Range containing the Pahranaagat tuff were accurate.

### Paleomagnetic data

Paleomagnetic data for Tertiary volcanic rocks in central Nevada reported by Scott et al. (1995) were primarily from Lincoln County, Nevada, east-southeast of the Reveille Range. Paleomagnetic studies focused primarily on ash-flow tuffs that were erupted from the Indian Peak caldera and Caliente caldera complexes. These studies identified several

distinct paleomagnetic poles for the ash-flow tuffs that were erupted during the caldera forming events at the Indian Peak caldera and Caliente caldera complex. Also, paleomagnetic data were collected by Best et al. (1995) from the Pahrnagat Formation. They used these data to suggest that the Pahrnagat Formation erupted from the Kawich Caldera.

Very few paleomagnetic studies have been carried out on the Pahrnagat Formation. Best et al. (1995) conducted the most comprehensive paleomagnetic studies on the Saulsbury and the Alamo petrographic types of the Pahrnagat Formation and their results are included in Appendix B. Their data show a reversed magnetic polarity that ranges from  $-39^{\circ}$  to  $-70.9^{\circ}$  inclination. The average inclination of the Pahrnagat tuff is  $-58.4^{\circ}$  (Best et al., 1995).

Previous studies have used the paleomagnetic data from other localities in the central Nevada caldera complex and other caldera complexes in central Nevada to infer the presence of the Pahrnagat tuff in the southern Reveille Range. However, there have been no paleomagnetic studies done in the southern Reveille Range to determine whether these inferences are correct.

#### Petrology of the Pahrnagat Formation

Elemental and modal compositions and the nature of the plagioclase phenocrysts in pumice fragments in the outflow sheet of the Pahrnagat Formation have indicated four pumice groups (Best et al., 1995). Three of the pumice groups are rhyolite and one is a trachydacite (Best et al., 1995). The rhyolitic pumice groups are subdivided into a quartz-



rich high silica rhyolite, quartz-poor high silica rhyolite, and a low silica rhyolite (Best et al., 1995).

The high silica rhyolite pumice groups are compositionally gradational with each other (Best et al., 1995). The high silica rhyolite pumice groups have euhedral to subhedral plagioclase and sanidine crystals, low to medium amounts of biotite, Fe-Ti oxides, and contains some amphibole (Best et al., 1995). The low silica rhyolite pumice has more biotite, Fe-Ti oxides, amphibole, and clinopyroxene than the high-silica rhyolite pumices (Best et al., 1995). Trachydacite pumice group is similar in mineralogy to the low silica rhyolite pumice group, except that the trachydacite pumice group does not contain quartz or sanidine (Best et al., 1995).

The Best and others (1995) study of the Pahranaagat tuff did not include any detailed work on the volcanic stratigraphy located in the southern Reveille Range. Their research focused primarily on the Pahranaagat tuff at different localities in central Nevada.

### Purpose of Research

This thesis is an in depth study of the volcanic stratigraphy, geochronology, and paleomagnetism of the volcanic rocks in the southern Reveille Range. The data that was gathered during this study of the Reveille Range was correlated to the data of previous studies in the area to determine any relationship between other caldera forming events in the region. The study provides a better understanding of the volcanic evolution of the region and increases our knowledge of the volcanic stratigraphy, timing of volcanism, and magmatism that occurred during or just before a major episode of continental extension within the central Nevada caldera complex.

The questions that this thesis will answer are (1) Is there evidence for a caldera in the southern Reveille Range? (2) What is the relationship of the ash-flow tuffs in the southern Reveille Range to the tuffs located in other parts of the range? (3) Is the model proposed by Best et al. (1995) for the Kawich Caldera in the southern Reveille Range correct? (4) Are the tuffs in the southern Reveille Range equivalent to the Pahrnagat Formation? and (5) What is the origin of Fang Ridge?

## CHAPTER 2

### ANALYTICAL TECHNIQUES AND METHODOLOGY

Twenty three samples were collected for X-ray fluorescence (XRF), thermal ionization mass spectrometry (TIMS), and  $^{40}\text{Ar}/^{39}\text{Ar}$  analyses. Twenty of the samples were collected from tuffs or domes and three were collected from the Fang Ridge dacite dike. Analysis was done on pumice fragments that were removed from the tuffs, but whole rock samples were analyzed for the domes and the dacite dike.

#### $^{40}\text{Ar}/^{39}\text{Ar}$ Samples

The following section, which is quoted directly from the UNLV Nevada Isotopic Geochronology Laboratory procedure hand-out explains how  $^{40}\text{Ar}/^{39}\text{Ar}$  analysis were conducted.

“Samples analyzed by the  $^{40}\text{Ar}/^{39}\text{Ar}$  method at the University of Nevada, Las Vegas were wrapped in Al foil and stacked in sealed 6 mm inside diameter Pyrex tubes. Individual packets averaged 3 mm thick and neutron fluence monitors (FC-2, Fish Canyon Tuff sanidine) were placed every 5-10 mm along the tube. Synthetic K-glass and optical grade  $\text{CaF}_2$  were included in the irradiation packages to monitor neutron induced argon interferences from K and Ca. Loaded tubes were packed in an Al container for irradiation. Samples were irradiated at McMaster Nuclear Reactor at McMaster University, Ontario, Canada. The samples were in-core for 7 hours in the 5C position

where they are surrounded by fuel rods on all four sides. Correction factors for interfering neutron reactions on K and Ca were determined by repeated analysis of K-glass and CaF<sub>2</sub> fragments. Measured (<sup>40</sup>Ar/<sup>39</sup>Ar)<sub>K</sub> values were 0.01868 (± 52.3%). Ca correction factors were (<sup>36</sup>Ar/<sup>37</sup>Ar)<sub>Ca</sub> = 2.5867 (± 10.31%) × 10<sup>-4</sup> and (<sup>39</sup>Ar/<sup>37</sup>Ar)<sub>Ca</sub> = 8.0803 (± 27.74%) × 10<sup>-4</sup>. J factors were determined by fusion of 3-7 individual crystals of neutron fluence monitor which gave reproducibility's of 0.1% to 0.4% at each standard position. Variation in neutron flux along the 100 mm length of the irradiation tubes was <4%. An error in J of 0.4933% was used in age calculations.

Irradiated crystals together with CaF<sub>2</sub> and K-glass fragments were placed in a Cu sample tray in a high vacuum extraction line and were fused using a 20 W CO<sub>2</sub> laser. Sample viewing during laser fusion was by a video camera system and positioning was via a motorized sample stage. Reactive gases were removed by three GP-50 SAES getters prior to being admitted to a MAP 215-50 mass spectrometer by expansion. The relative volumes of the extraction line and mass spectrometer allow 80% of the gas to be admitted to the mass spectrometer for laser fusion analyses. Peak intensities were measured using a Balzers electron multiplier by peak hopping through 7 cycles; initial peak heights were determined by linear regression to the time of gas admission. Mass spectrometer discrimination and sensitivity was monitored by repeated analysis of atmospheric argon aliquots from an on-line pipette system. Measured <sup>40</sup>Ar/<sup>36</sup>Ar ratios were 287.75 ± 0.50% during this work, thus a discrimination correction of 1.02695 (4 AMU) was applied to measured isotope ratios. The sensitivity of the mass spectrometer was ~6 × 10<sup>-17</sup> mol mV<sup>-1</sup> with the multiplier operated at a gain of 52 over the Faraday. Line blanks averaged 2.0 mV for mass 40 and 0.01 mV for mass 36 for laser fusion analyses. Discrimination,

sensitivity, and blanks were relatively constant over the period of data collection. Computer automated operation of the sample stage, laser, extraction line and mass spectrometer as well as final data reduction and age calculations were done using LabSPEC software written by B. Idleman (Lehigh University). An age of 27.9 Ma (Steven et al., 1967; Cebula et al., 1986) was used for the Fish Canyon Tuff sanidine flux monitor in calculating ages for samples.

For each sample inverse isochron diagrams are examined to check for the effects of excess argon. Reliable isochrons are based on the MSWD criteria of Wendt and Carl (1991) and must comprise contiguous steps and a significant fraction of the total gas released. All analytical data are reported at the confidence level of  $1\sigma$  (standard deviation)".

#### Major and Trace Element Samples

Thirteen samples were analyzed for major and trace elements. Analyses were done at the Rock Chemistry Laboratory at the University of Nevada, Las Vegas. Samples for X-ray fluorescence (XRF) were crushed using the Chipmunk rock crusher to approximately 1 cm. Each sample was sieved to remove all fine particles and weathered pieces of sample that may add contamination to the sample. The samples analyzed on the XRF were further ground to a fine powder using the Bico shatter box. In order to avoid contaminating the samples the tungsten-carbide coated rings were used.

Samples were analyzed using the PANalytical X-ray fluorescence spectrometer. The XRF is designed to acquire quantitative elemental distributions for major and trace elements in whole rock samples using calibration curves derived from analyzing U.S.G.S.

and international rock standards. Analytical procedures were followed as outlined by Norrish and Hutton (1969).

### Loss on Ignition

Loss on ignition (LOI) was calculated for each sample. L.O.I. is the measure of the concentration of volatiles in the sample. One and a half grams of sample measured to  $\pm 0.0005$  were used for L.O.I. analysis. The samples were heated in ceramic crucibles to  $950^{\circ}\text{C}$  for one hour to burn off any volatiles that may have been present in the sample. The samples were placed in a  $120^{\circ}\text{C}$  oven and slowly cooled. Samples were then placed in a dessicator and cooled to room temperature. After the sample had cooled, it was reweighed. The formula used to calculate L.O.I. is:

$$L.O.I. = (The\ weight\ lost\ after\ being\ heated / The\ original\ weight) \times 100.$$

After LOI determination the samples were made into fusion disks. This was done by measuring 1 gram ( $\pm 0.0002$ ) of sample to 6 grams ( $\pm 0.0002$ ) of flux. The flux is composed of 50% lithium tetraborate and 50% lithium monoborate. Each sample was heated to  $1050^{\circ}\text{C}$  in a carbon crucible for thirty minutes. The sample was stirred every 10 minutes to ensure that it was fully disaggregated in the liquid. To prevent cracking of the fusion disks, several steps had to be taken. After the final stirring the sample was quenched for fifteen seconds using an aluminum disk to initially draw off excess heat from the sample. The sample was then placed on a hot plate for approximately 1 minute before being placed in a  $400^{\circ}\text{C}$  oven for an hour. The samples were then cooled in a  $120^{\circ}\text{C}$  oven over night before being placed into the dessicator for storage.

## Isotope Analyses (TIMS)

Five samples were analyzed for Pb, Nd, and Sr isotope ratios by thermal ionization mass spectrometry (TIMS). Isotopic analysis was performed by J.D. Walker at the University of Kansas Tectonics and Crustal Evolution Laboratory using a VG Sector variable 6-collector mass spectrometer.

Samples that were prepared for TIMS used the same preparation technique for the XRF samples, but steel rings were used instead of the tungsten-carbide rings.

The lab uses procedures from Patchett and Ruiz (1987), Richard et al. (1976), and Krogh (1973) for obtaining Sm-Nd and Rb-Sr abundances. Powdered samples analyzed for Rb-Sr were dissolved with HF-HNO<sub>3</sub> acid in sealed containers. Elemental separations used HCl elution on cation exchange columns.

## Paleomagnetic Samples Collection and Analysis

Forty six samples were collected for paleomagnetic analysis from five sites. Thirty four samples were collected from the ash-flow tuffs or intracaldera tuffs and twelve samples from the dome east northeast of Fang Ridge. Paleomagnetic sample collection and analysis was conducted using the methodology outlined by Knight et. al (1986) and Hudson et al., (2000). A short description of the analytical terminology is provided below.

The K-value is the Fisher precision parameter which how many samples are aligning in the same direction. The higher the K-value for a sample site indicates that the data from that sample site are more accurate. The  $\alpha_{95}$  value between the five samples was 3.5%. The  $\alpha_{95}$  is a semi-angle of 95% confidence cone centered on the mean. The lower

the  $\alpha_{95}$  value the more accurate the data. The N-value is the number of samples used per site.



## CHAPTER 3

### VOLCANIC STRATIGRAPHY AND FAULTS OF THE SOUTHERN REVEILLE RANGE

This chapter describes the volcanic stratigraphy (Figure 6 and Figure 7) that was identified during field work in the southern Reveille range. All information presented in this chapter and following chapters are data that was acquired during thesis research.

#### Volcanic Stratigraphy

##### Ash-flow tuffs

There are three ash-flow tuff units (Tps<sub>1</sub>, Tps<sub>2</sub>, and Tps<sub>3</sub>) in the southern Reveille Range (Figure 7). The ash-flow tuffs are herein named the lower, middle and upper Pyramid Spring tuff.

##### *Lower Pyramid Spring tuff*

The lower Pyramid Spring tuff (Tps<sub>1</sub>) crops out 0.5 km to the north of Fang Ridge in the eastern part of the field area but abuts against Fang Ridge in the western section of the field area. The ash-flow tuff is moderately-welded and pumice poor at the base of the section and grades into a poorly welded pumice rich unit at the top of the section.

The tuff is composed of a fine-grained matrix with field estimated modal phenocrysts of quartz (15-20%) up to 1.5 mm in size, sanidine (30-40%) up to 2 mm, plagioclase up to 2 mm, and minor amounts of biotite and Fe-oxides (0-5%) up to 0.5 mm. Pumice

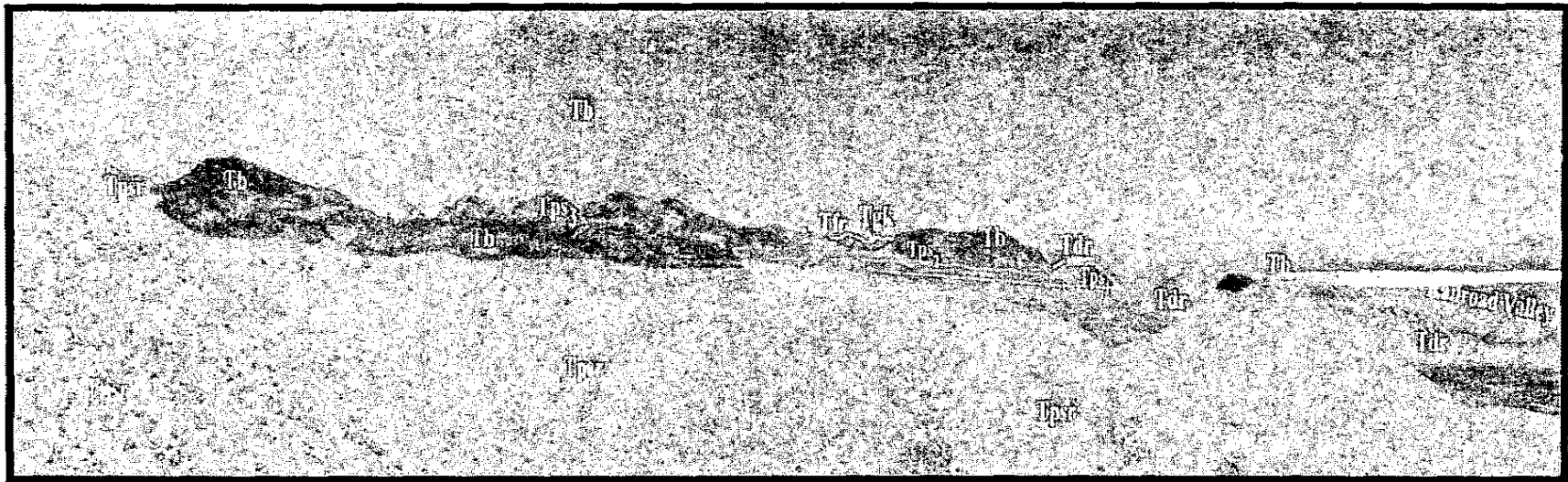


Figure 6. View of the southern Reveille Range looking to the north. Figure shows the approximate location of the geologic units within the field area. In the distance the Pancake Range is visible.

- Reveille Peak
  Tertiary basalts
  Dome A-D
  Lower Pyramid Spring tuff
- Middle Pyramid Spring tuff
  Upper Pyramid Spring tuff

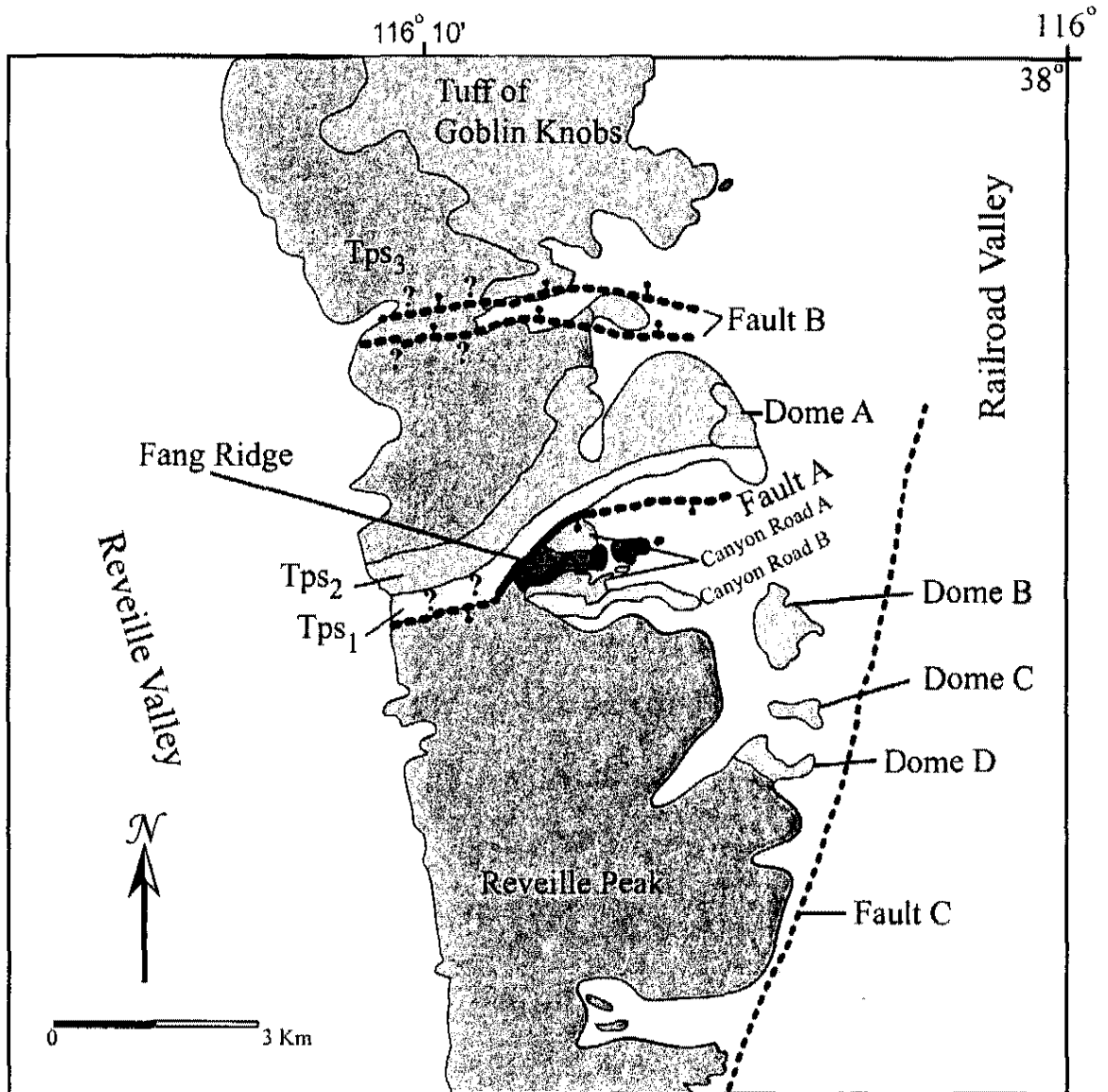


Figure 7. Generalized geologic map of the volcanic stratigraphy and structures in the southern Reville Range. The Paleozoic and Pliocene basalts have been removed for clarity. Figure modified from Gardner and others (1980).

fragments range from 5-8 cm in length. Lithic fragments comprise less than 2% of the unit.

The foliation defined by elongated pumice fragments in the lower Pyramid Spring tuff has an east-west strike with a dip of 5-20° to the north. The strike and dip of foliation stays constant throughout the entire unit.

#### *Middle Pyramid Spring tuff*

The middle Pyramid Spring tuff (Tps<sub>2</sub>) lies above the lower tuff and consists of a pumice poor basal section that grades into a pumice rich section at the top of the unit. In general the lower part of the section is moderately welded, while the top is poorly welded. The middle Pyramid Spring tuff is distinguished from the lower Pyramid Spring tuff by the presence of a pumice poor basal section stratigraphically above the pumice rich section of the lower Pyramid Springs tuff. Pumice fragments are large and range in length from 10-15 cm.

Phenocrysts comprise approximately 45-50% of the rock. Estimated modal phenocrysts include plagioclase (25-35%) up to 1.5 mm in size, quartz (15-20%) up to 1.0 mm, sanidine (30-40%) up to 2 mm, and biotite (0-5%) up to 0.5 mm. Pumice fragments range from 10-20 cm in length. The middle Pyramid Spring tuff contains lithic fragments (<2%) composed predominantly of fine-grained carbonate and rhyolite.

The foliation defined by elongated pumice fragments in the middle Pyramid Spring tuff has an east-west strike with a dip of 15-25° to the north. The flow foliation stays constant throughout the entire unit.

### *Upper Pyramid Spring tuff*

The upper Pyramid Spring tuff (Tps<sub>3</sub>) lies at the top of the section. It is predominantly a cliff forming unit in the field area. Unlike the lower and middle Pyramid Springs ash-flow tuffs, this unit does not have a pumice poor basal section. The unit is ~150 m thick and contains pumice fragments throughout the whole section. Pumice fragments range from 15 cm to approximately 0.5 m in length (Figure 8). The upper Pyramid Spring tuff flowed farther to the north than the lower and middle units and north of fault B it lies on the Tuff of Goblin Knobs. The upper unit was identified by Martin and Naumann (1995) as the tuff of Southern Reveille Range.

Estimated modal phenocrysts include plagioclase (25-30%) up to 2 mm in size, quartz (15-25%) up to 1.5 mm, sanidine (30-40%) up to 2 mm, and biotite (0-5%) up to 0.5 mm. Fragments of fine-grained carbonate and rhyolite comprise 1% of the total volume. Pumice clasts are compacted and define a well-developed foliation.

The upper Pyramid Spring tuff is easily identifiable in the field because it has a distinctive weathering pattern in which large elongated voids are produced when the pumice fragments are eroded. These voids can be in excess of 3 m in length.

The foliation defined by elongated pumice fragments in the upper Pyramid Spring tuff has an east-west strike with a dip of 20-30° to the north. The dip of the upper Pyramid Spring tuff becomes steeper to the north. Dips of 20° are common just north of fault A, but to the north of fault B dip increases to 30°.

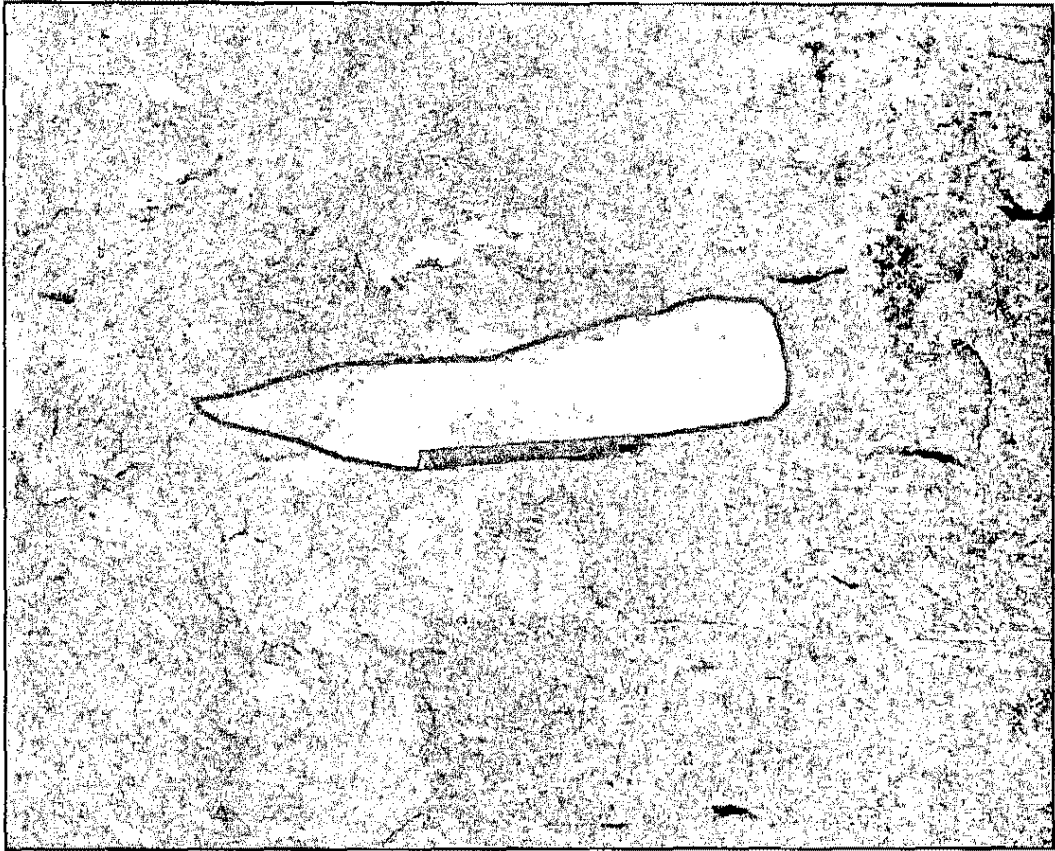


Figure 8. Size of pumice fragments (Green outline) located in upper Pyramid Springs ash-flow tuff. Pencil in photograph is approximately 15 cm in length. The light peach color areas within the outcrop are also pumice fragments.

## Reveille Peak

Reveille Peak (Tpsr) is located approximately 2.5 km to the south of Fang Ridge (Figure 7). The peak is composed of red to purple rhyolite ash-flow tuff forming a monotonous section nearly 1000 m thick. The tuff is non-bedded and moderately welded and contains sparse inclusions of granite (xenoliths). Zones of vitrophyre are rare and generally found in lower to middle sections of the Reveille Peak section. Phenocrysts make up 40-45% of the rock and include plagioclase (25-35%) up to 1 mm in size, quartz (15-20%) up to 1.5 mm, sanidine (30-40%) up to 2 mm, and biotite (0-5%) up to 0.5 mm.

## Rhyolite Domes

There are four domes that crop out along the eastern margin of the field area. The domes will be referred to as Dome A, Dome B, Dome C, and Dome D (Figure 7).

### Dome A

Dome A (Tdr) is the northern most of the domes in the southern Reveille Range. Dome A intrudes the two lowermost units of the Pyramid Spring tuff. The dome is composed of white to peach colored flow-banded rhyolite. Phenocrysts comprise 55-60% of the rock and include quartz (20-25%) up to 1-2 mm, plagioclase (25-30%) up to 2 mm, sanidine (30-40%) up to 1 mm, and biotite (0-10%) up to 0.5 mm. Flow foliation in Dome A strikes roughly north-south with a dip between 75-85° to the east. The flow foliation is defined by bands of Fe-oxides and biotite.

### Dome B

Dome B (Tdr) is located 1.5 km east southeast of Fang Ridge. The dome is composed of white to peach colored rhyolite. The phenocrysts of Dome B make up 40-45% of the

rock. The phenocrysts include quartz (15-25%) up to 1 mm, plagioclase (20-25%) up to 1 mm, sanidine (35-45%) up to 1.5 mm, and biotite (0-5%) up to 0.5 mm. Flow foliation is north-south with a dip of 80-85° to the east. The foliation is defined by bands of Fe-oxides and biotite.

#### Dome C

Dome C (Tdr) is located approximately 3 km to the southeast of Fang Ridge. The dome is composed of white to peach colored rhyolite. The phenocrysts of Dome C make up 35-40% of the rock and are similar in percentage to that of Dome B. The foliation of Dome C is roughly north-south striking with a dip of 75-85° to the east.

#### Dome D

Dome D (Tdr) is located 1 km to the southwest of Dome C. The dome is composed of white to peach colored rhyolite. The phenocrysts make up 30-35% of the rock. The phenocrysts include quartz (15-25%) up to 1 mm in size, plagioclase (25-30%) up to 1 mm, sanidine (30-40%) up to 1.5 mm, and biotite (0-5%) up to 0.5 mm. Crystals are anhedral to subhedral with some resorbed crystals of quartz. Flow foliation is north-south with a dip of 85-90° to the east.

#### Volcaniclastic sedimentary units and pyroclastic flows

There are two areas to the north and south of Fang Ridge that contain volcaniclastic sedimentary units and pyroclastic flow. These sections will be referred to as Canyon Road A and Canyon Road B. The Canyon Road A section occurs both to the north and south of Fang Ridge (Figure 7).



## Volcaniclastic Sedimentary Units

The volcaniclastic units crop out approximately 0.25 km to the south of Fang Ridge and crop out adjacent to Fang Ridge to the north (Figure 9). Volcaniclastic sedimentary rocks and minor pyroclastic flows comprise the Canyon Road A section. The volcaniclastic section grades from clast supported breccia consisting of pumice and rock fragments that range in composition from dacite to rhyolite upward into fine-grained sandstones consisting of reworked accretionary lapilli in an ash matrix. The sedimentary section is 15-30 m thick and is described in detail below.

### *Breccias*

The breccias are clast supported with a medium grained matrix. The lithic fragments within the breccia range from 2 cm to 5 cm and consist predominantly of volcanic material, such as pumice, dacite, and rhyolite fragments. Individual beds of breccia range in thickness from 5-10 m and are poorly sorted.

### *Coarse-grained Sandstones*

The coarse grained sandstones consist of sub-angular to sub-rounded grains of quartz and lithic fragments. Some of the coarser-grained sandstones contain large ripple marks with a mud-like drape on the rippled surface. The mud-like drapes are approximately 1-2 cm thick. The coarse grained sandstones contain beds about a meter thick. The thickness of coarse grained sandstone unit ranges from 5 to 10 m.

### *Fine-grained Sandstones*

The fine-grained sandstones consist of accretionary lapilli within an ash matrix. The grains are well rounded and very well sorted. The fine grained sandstones show evidence of soft sediment deformation and are thinly bedded (approximately 1-2 mm thick). This

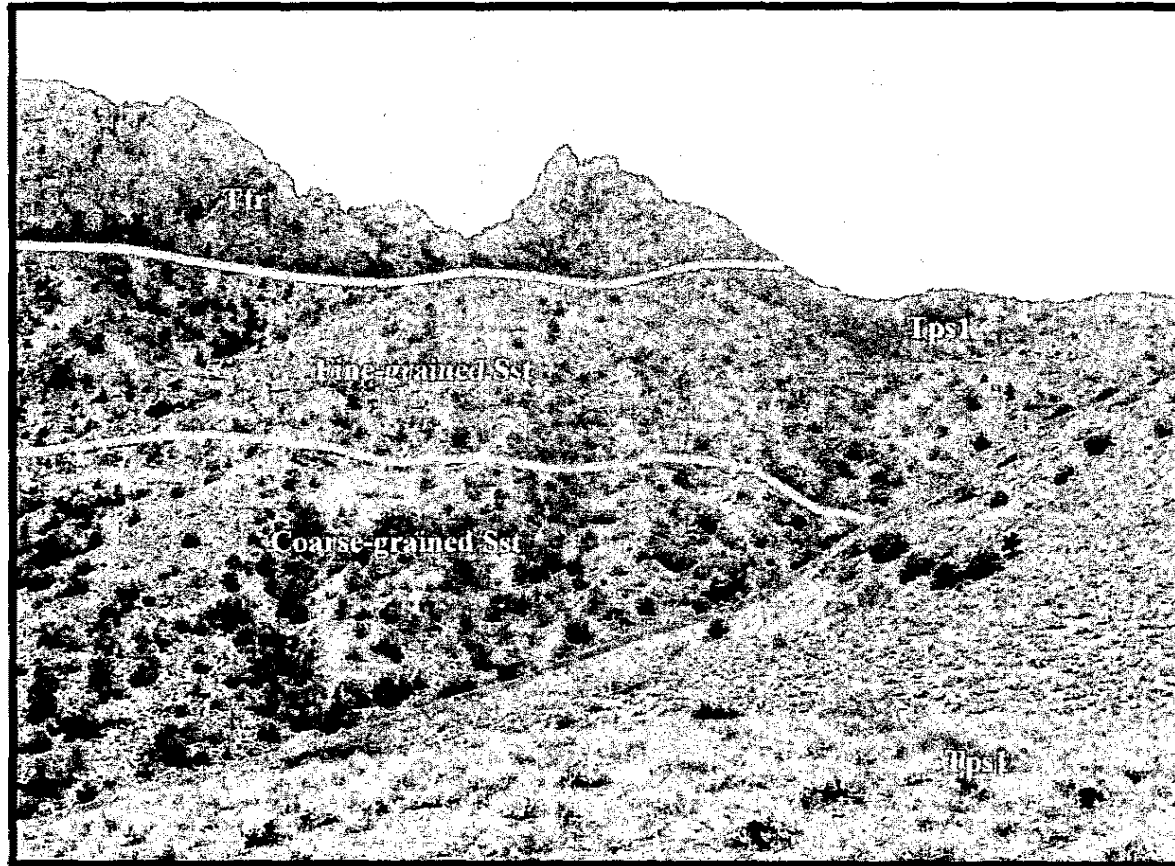


Figure 9. Volcaniclastic sedimentary units (fine grained Sst and coarse grained Sst) wedged between Fang Ridge (Tfr) and the lower Pyramid Spring tuff (Tps<sub>1</sub>).

unit coarsens upwards. The fine grained sandstone unit are approximately 5-10 m thick.

### *Pyroclastic flows*

The Canyon Road B locality is comprised of pyroclastic flows (Tpf). The pyroclastic flows are generally 3-5 m thick. The phenocryst assemblage of the pyroclastic flows includes quartz (25-30%) up to 1 mm in size, plagioclase (30-35%) up to 1 mm, and sanidine (30-35%) up to 1 mm. The phenocrysts are supported in an ash matrix that consists of 55-60% of the rock. The pyroclastic flows contain minor amounts of lithic fragments consisting predominantly of rhyolite tuff and minor amounts of volcanoclastic sedimentary rock.

### Fang Ridge

Fang Ridge (Tfr) is a dacite dike that is up to 100 m in height and approximately 7 km long that extends east-west through the center of the field area (Figure 10). Some parts of Fang Ridge are dark brown in color while others are white-tan in color. Fang Ridge has extensive columnar jointing throughout. Small intrusions of Fang Ridge dacite crop out to the north of the main Fang Ridge dike and intrude the lower and middle Pyramid Springs tuffs. Fang Ridge dike, also intrudes into the volcanoclastic units of Canyon Road A.

Fang Ridge is composed of homogenous dacite. Phenocrysts include quartz (35-40%), plagioclase (40-45%), biotite (15-20%), and minor amounts of sanidine (<2%). Quartz phenocrysts are anhedral with a faint yellow color. The plagioclase phenocrysts are milky white and are anhedral to subhedral. Biotite phenocrysts are generally found in euhedral books approximately 2 mm thick and 1-2 mm across.

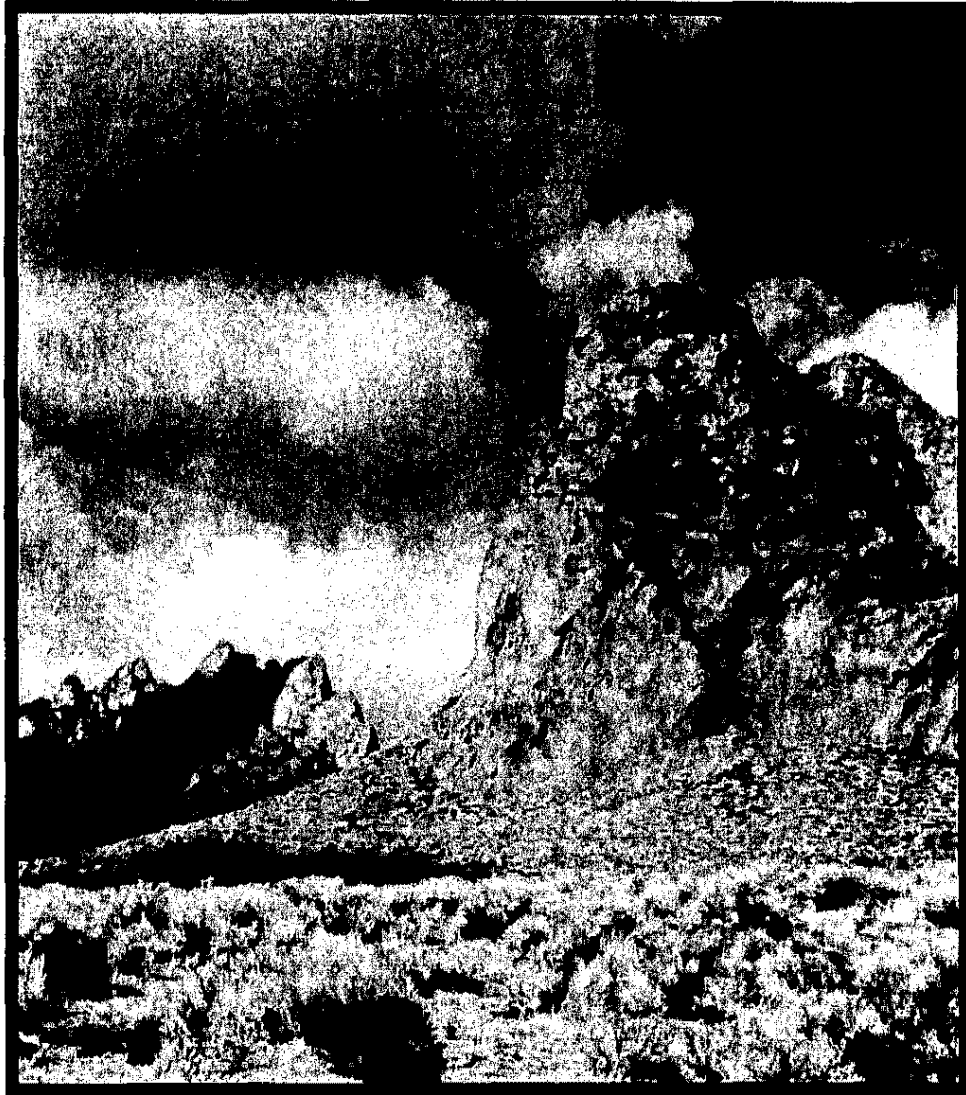


Figure 10. Photo of Fang Ridge dacite located in the southern Reveille Range. Photo is taken looking to the west.

## Faults

In the southern Reveille Range there are three major faults. These are referred to as Fault A, Fault B, and Fault C (Figure 7).

### *Fault A*

Fault A is a normal fault that strikes east-west and dips 60-65° to the south. The trace of Fault A changes strike by 20 degrees. In the east it strikes N 90 E to N 70 E. The fault then curves and strikes N 90 E along the trend of Fang Ridge (Figure 7). The eastward and westward projection of the fault can not be determined because it is covered by alluvium to the east and debris from Fang Ridge and Pyramid Spring tuff to the west. The fault separates the three Pyramid Springs ash-flow tuffs, north of the fault, from the volcanoclastic units and the volcanic domes to the south (Figure 11).

### *Fault B*

Fault B consists of two east-west striking normal faults that dip to the north (Figures 7 and 12). The fault zone is located at the northern boundary of the field area. The Pyramid Springs ash-flow tuffs south of the fault zone dip to the north, but between the two fault strands the Pyramid Springs ash-flow tuffs dip to the south. The northern strand of Fault B locally places the Pyramid Springs ash-flow tuff against the tuff of Goblin Knobs. The fault zone is characterized by hydrothermal alteration, stains of iron oxide and calcite veins.

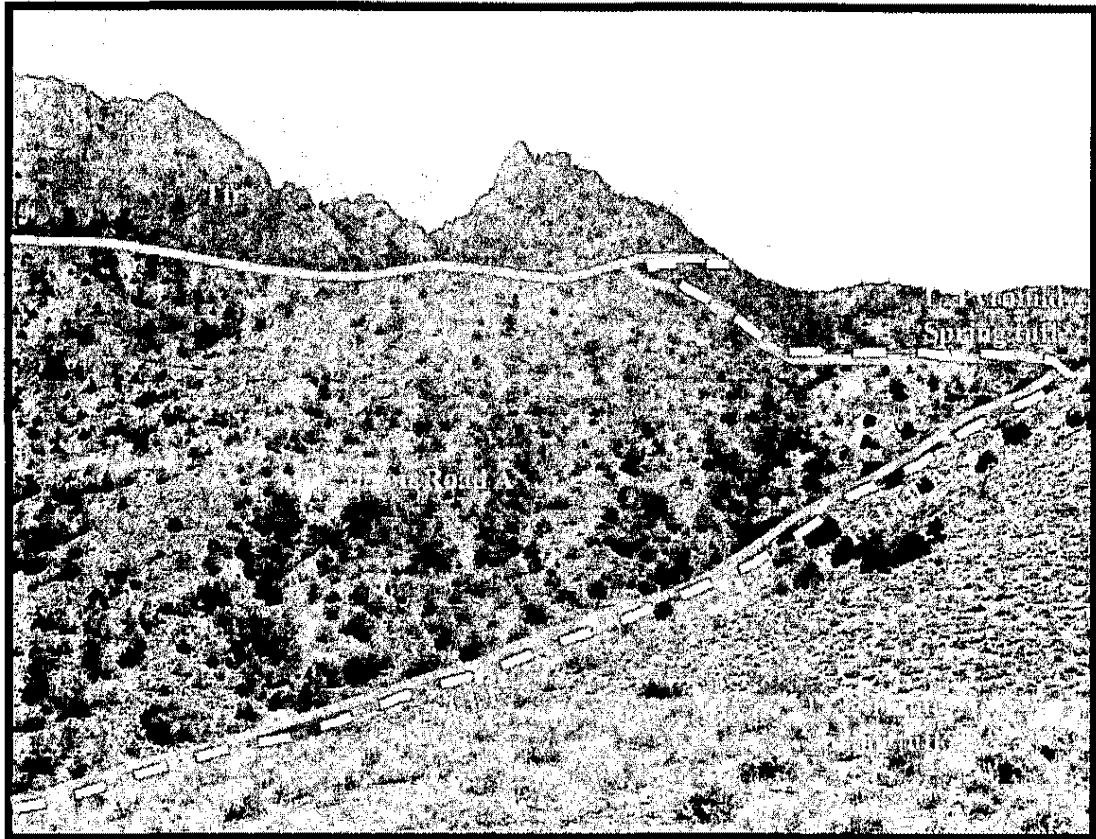


Figure 11. Volcaniclastic sedimentary units (Canyon Road A) wedged between Fang Ridge (Tfr) and the lower Pyramid Spring tuff. White dashed line denotes the trace of Fault A. Photo taken looking to the west.

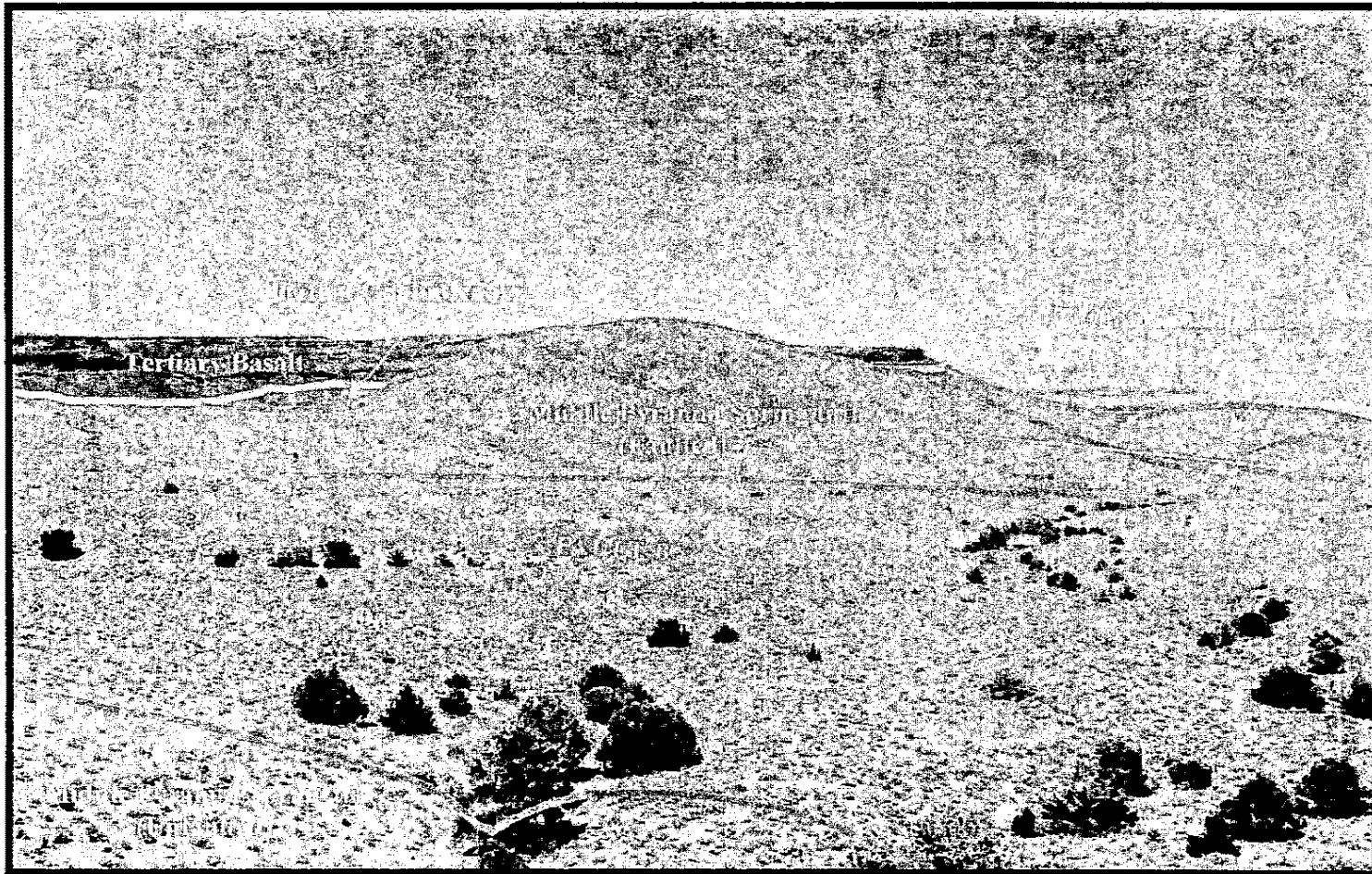


Figure 12. Fault rotated blocks of the middle Pyramid Spring tuff. The middle Pyramid Spring tuff in the foreground is unfaulked and dips to the north. The section of middle Pyramid Spring tuff in the background is faulted and dips to the southwest. Photo taken looking to the northeast.

### *Fault C*

Fault C is a north-south striking fault located on the eastern margin of the southern Reville Range. Fault C separates the valley fill sequence of Railroad Valley from the volcanic units in the Reville Range.



## CHAPTER 4

### IDENTIFICATION OF THE PYRAMID SPRING CALDERA

#### Criteria for Recognizing a Caldera

A caldera is characterized by several features that are associated with its formation and post-collapse volcanic history (Lipman, 1997) (Figure 13). These features are:

1. An erosional caldera wall that is commonly scalloped.
2. A resurgent dome that represents a structurally uplifted caldera floor.
3. Bounding faults (ring faults) that accommodate the subsidence during the caldera collapse. Post-caldera domes are commonly associated with the ring bounding faults.
4. Intracaldera fill deposited in the area that subsides during caldera collapse. This material can be deposited during the collapse of the caldera in the form of ash-flow tuffs, volcanic domes or megabreccias. The intracaldera fill, however, can also be composed of sedimentary units or other volcanic material eroded from the resurgent dome of the caldera.
5. Outflow tuffs that are produced during the eruption of a caldera.

Based on field work completed for this thesis, the geology of the southern Reveille Range is interpreted as representing a caldera. This caldera is herein named the Pyramid Spring caldera. Evidence for the caldera is provided below.

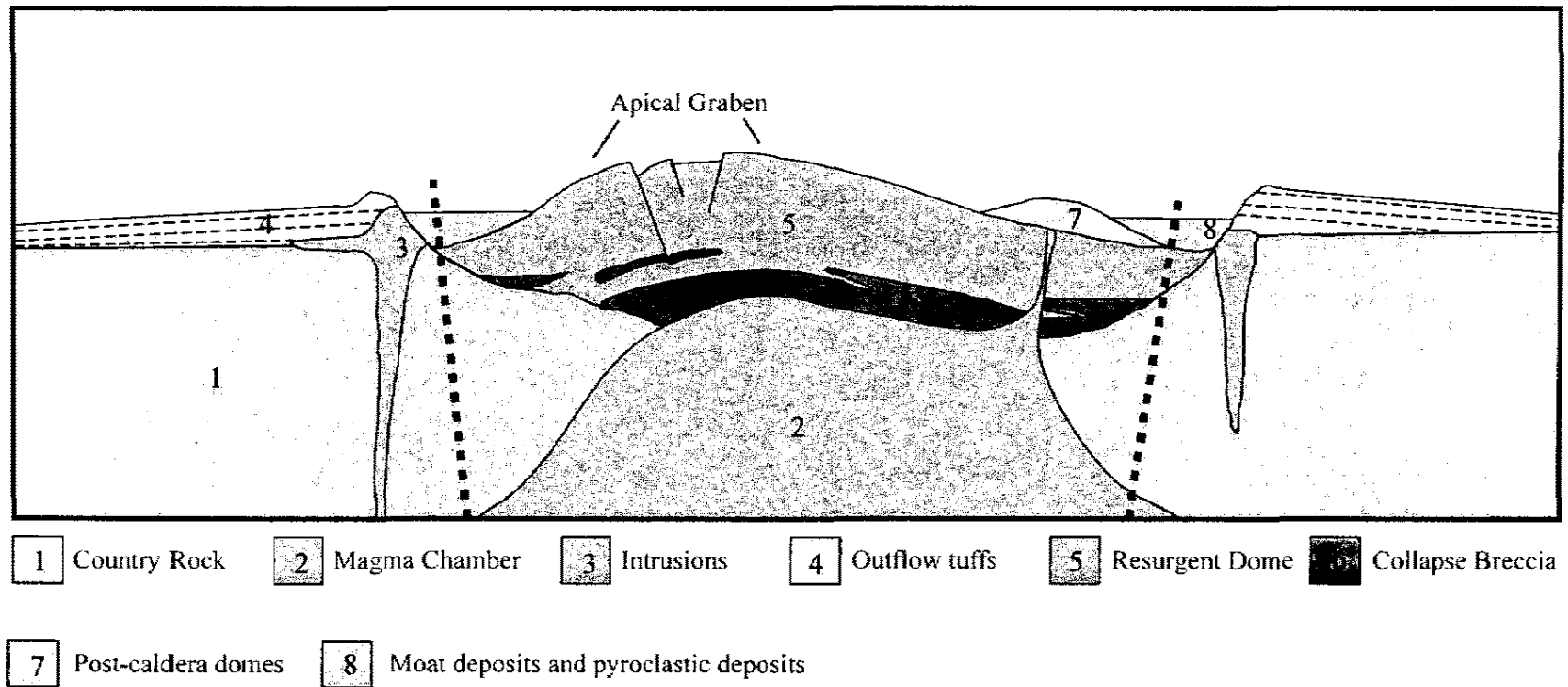


Figure 13. Diagram shows common elements that can be found in a caldera that has undergone collapse and resurgence of the caldera floor. Figure was modified from Lipman (1984).

## The caldera wall

The caldera wall separates the collapsed caldera moat from the outflow tuffs produced during the eruption. Fault A is interpreted to be the caldera wall in the southern Reveille Range. The caldera wall (Fault A) separates the caldera moat units of Canyon Road A and Canyon Road B from the outflow units of the Pyramid Spring tuff (Figure 14a and 14b). The caldera moat and outflow units will be described later in this chapter. Also, the change in strike on the fault trace of Fault A from N 90 E to N 70 E and back to N 90 E is characteristic of the lobate nature of caldera walls.

## Resurgent dome

A resurgent dome represents the structurally uplifted caldera floor. The caldera floor is the area inside the perimeter of the collapsed region. The resurgent dome of the Pyramid Springs caldera is interpreted to be Reveille Peak (Figure 14a and 14b). The resurgent dome is characterized by thick monotonous sections of tuff that lack any coherent stratigraphy. The tuff that comprises Reveille Peak is nearly 1000 m thick, lacks bedding, and is moderately welded, which are all features characteristic of intracaldera tuff (Lipman, 1997).

## Ring fracture and post-collapse domes

The ring fracture is generally characterized by the formation of post-collapse domes along the fractures created prior to and during collapse of the caldera. Although, identifying the trace of the ring fracture in the field is difficult, post-collapse domes can help delineate its approximate location. Domes A-D are interpreted as post-collapse

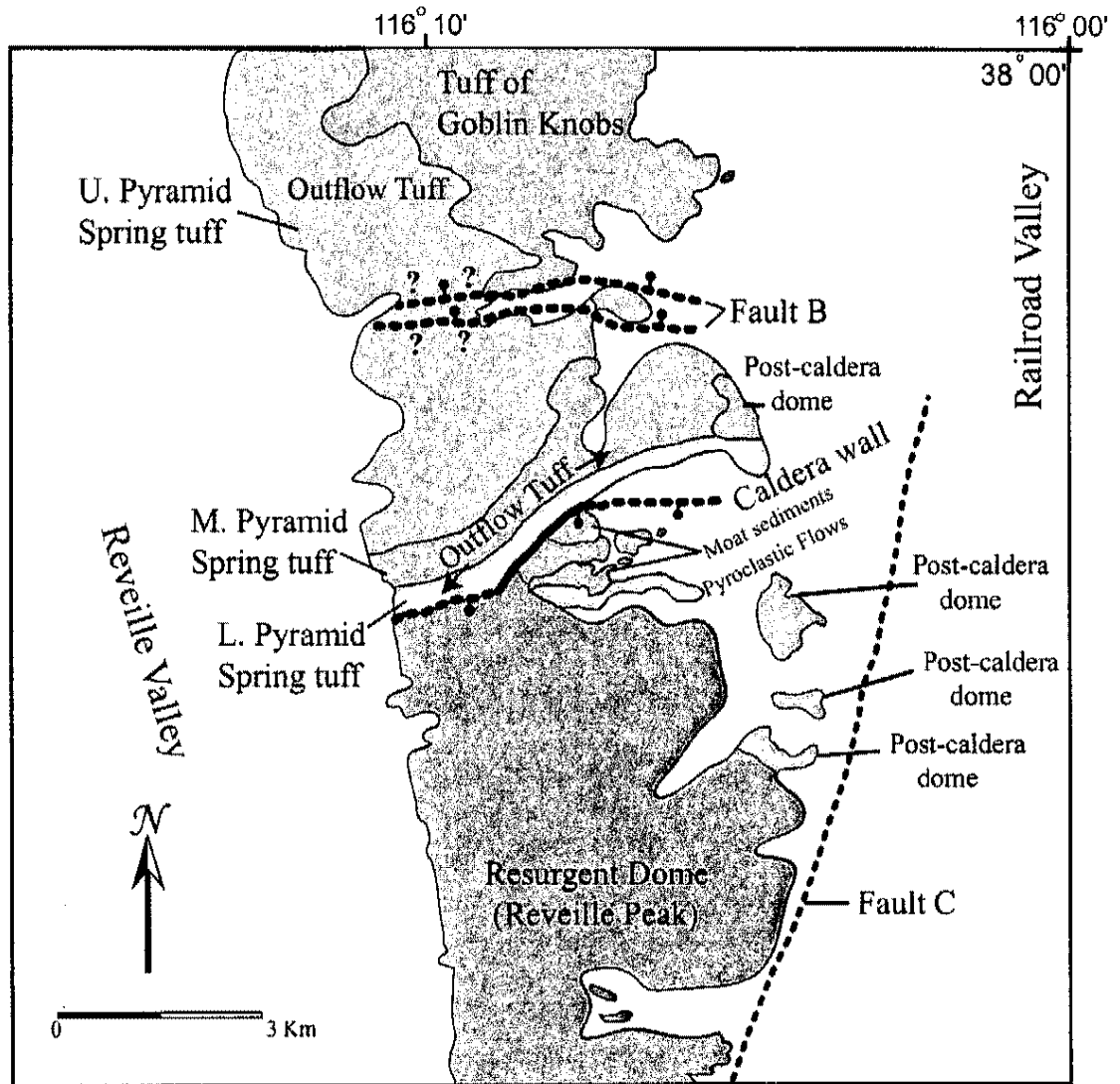


Figure 14a. Generalized geologic map showing the interpretation of each volcanic unit in the southern Reville Range. Paleozoic and Pliocene units have been removed for clarity purposes. Figure is modified from Gardner (1980).

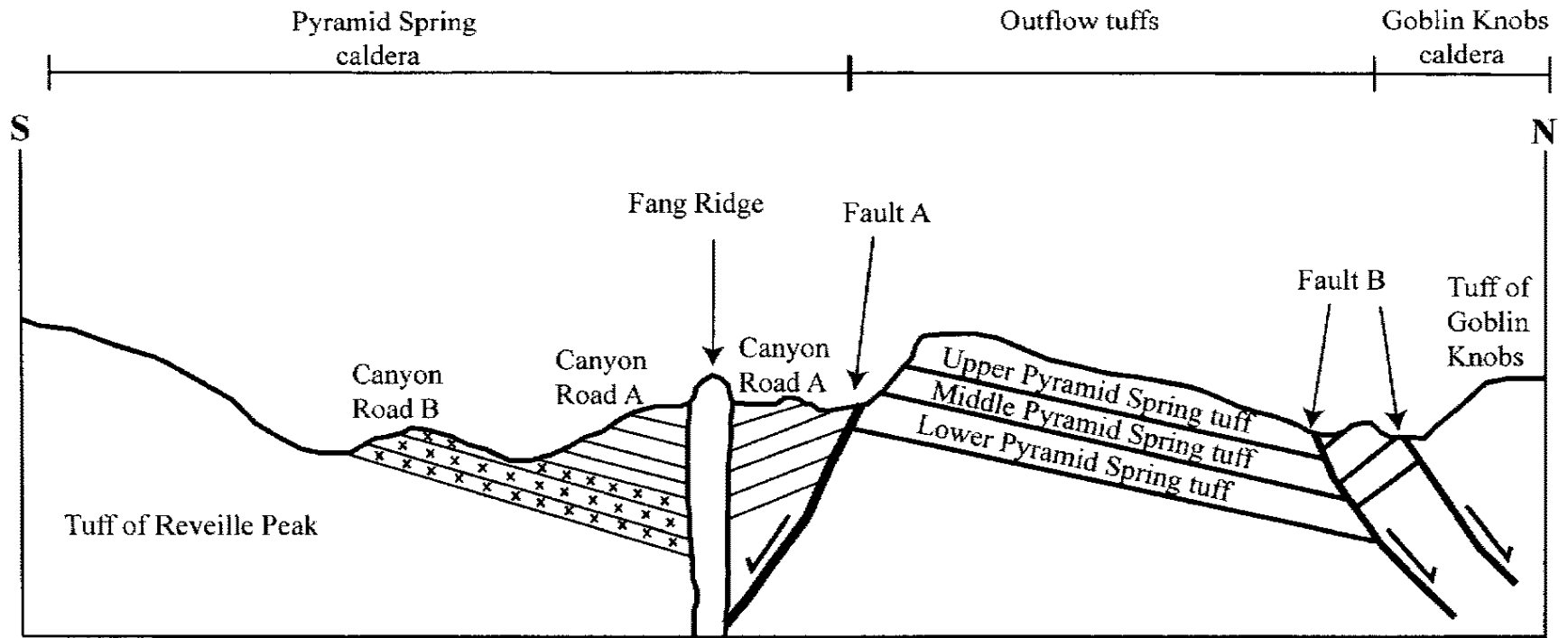


Figure 14b. Generalized N-S cross-section of the southern Reveille Range. The cross-section is not to scale.

domes (Figure 14a and 14b). These domes form a north-south trend with a slight curvature concave toward the west. While the domes do not provide absolute evidence of the existence of the ring fracture in the subsurface, they are suggestive of its presence.

#### Moat deposits and pyroclastic deposits

The volcanoclastic and pyroclastic units of Canyon Road A and Canyon Road B areas are interpreted as moat deposits in the Pyramid Spring caldera (Figure 14a and 14b). These units form in a topographic low between the resurgent dome and the caldera wall. They dip to the north on the north flank of the resurgent dome, but dip southwest just south of the caldera wall.

#### *Canyon Road A*

The volcanoclastic sedimentary units of Canyon Road A are characteristic of deposits found in the moat of a caldera. There are several characteristics to these deposits that would suggest deposition in a lacustrine setting in a caldera moat. Although, it is not necessary for caldera moats to contain water, lakes are very common within calderas (Schmincke, 2004).

The breccia of Canyon Road A exhibits features characteristic of deposition in a subaerial environment, but this unit grades upward into a coarse-grained sandstone with ripple marks that was probably deposited in an aqueous environment. This could indicate deposition of the breccia before the caldera moat began to fill with water.

The coarse-grained sandstones exhibit sedimentary structures that are characteristic of deposition in a lacustrine setting. These include ripple marks and mud drapes. Ripple marks are found throughout the entire unit. Mud drapes deposited on the

ripple marks are composed of silt to very fine-grained sandstones and mirror the ripple marks found in coarse-grained sandstones. The mud drapes are then overlain by another deposit of coarse-grained sandstone.

The fine-grained sandstones are predominantly composed of accretionary lapilli, or ash particles that were deposited in an aqueous environment. The fine-grained sandstones also show evidence of soft sediment deformation; a process that is common in aqueous environments.

### *Canyon Road B*

The pyroclastic flows of the Canyon Road B are probably related to post-caldera eruptions. They likely formed during the initial stages of dome formation. The presence of tuff clasts probably derived from Reveille Peak and clasts of volcanoclastic sedimentary rocks document the eruption of these tuffs during post-caldera activity.

### Outflow tuffs

The lower Pyramid Spring tuff, the middle Pyramid Spring tuff, and the upper Pyramid Spring tuff are interpreted as the outflow units from the Pyramid Spring caldera (Figure 14a and 14b). The identification of three distinct stratigraphic units and the overall outcrop location of the units (especially the upper Pyramid Spring tuff) are characteristic of outflow tuffs. Highly flattened pumice (fiamme) is very common in outflow tuffs, but is very rare in intracaldera tuffs. The highly flattened large (15 cm-0.5 m long) fiamme in the upper Pyramid Spring tuff support the interpretation of the Pyramid Spring tuff being an outflow unit. In addition, the Pyramid Spring tuff only

crops out to the north of the caldera wall, which fits with the Pyramid Spring tuff is an outflow unit of the Pyramid Spring caldera.

Although a direct correlation between outflow units and intracaldera tuffs is often difficult, there are similarities between the Pyramid Spring tuff and the tuff on Reveille Peak that suggest a correlation. These similarities include mineralogy and chemistry affinities (see chapter 7). Based on these similarities, the tuff on Reveille Peak is interpreted as the intracaldera equivalent of the Pyramid Spring outflow units.

### Summary

Field research and observations were able to identify most of the features required to meet criteria for identifying a caldera outlined by Lipman (1997). Observations used to identify the Pyramid Spring caldera include:

1. Locating the caldera wall of the Pyramid Spring caldera (Fault A).
2. Identifying the resurgent dome at Reveille Peak.
3. Identifying the post-caldera domes that may suggest the presence of a ring fault in the subsurface (Domes A-D).
4. Identification of the caldera moat deposits and the pyroclastic flows that document post-caldera volcanic activity (Canyon Road A and B locations).
5. The identification of the Pyramid Spring tuff as the outflow unit that was produced during the formation of the Pyramid Spring caldera.



## CHAPTER 5

### GEOCHRONOLOGY

Four samples were collected for  $^{40}\text{Ar}/^{39}\text{Ar}$  geochronology. Samples were analyzed at the Nevada Isotope Geochronology Laboratory (NIGL) at the University of Nevada, Las Vegas. The samples included two samples from the Pyramid Spring tuff (Lower Pyramid Spring tuff and Upper Pyramid Spring tuff), one sample from Dome B, and one sample from Fang Ridge. The samples were crushed and sieved then analyzed under a binocular microscope and 60 crystals of sanidine were extracted from each sample.

#### Lower Pyramid Spring tuff

The Lower Pyramid Springs Ash-flow tuff was dated at  $22.89 \text{ Ma} \pm 0.15 \text{ Ma}$  (weighted mean age). The sample has an isochron age of  $22.76 \text{ Ma} \pm 0.140 \text{ Ma}$ .  $^{40}\text{Ar}/^{36}\text{Ar}$  for the lower Pyramid Springs tuff is  $274 \pm 6.5$  (Figure 15). The initial  $^{40}\text{Ar}/^{36}\text{Ar}$  ratio for the lower Pyramid Springs tuff is lower than the 295.5 standard for the present day  $^{40}\text{Ar}/^{36}\text{Ar}$  atmospheric ratio. The weighted mean age of  $22.89 \text{ Ma} \pm 0.15 \text{ Ma}$  was used for this study because the  $^{40}\text{Ar}/^{36}\text{Ar}$  ratio produced an irregular intercept. For complete details on the analyses refer to Appendix B.

#### Upper Pyramid Spring tuff

The Upper Pyramid Springs Ash-flow tuff was dated at  $22.86 \text{ Ma} \pm 0.15 \text{ Ma}$  (weighted mean age). An isochron age could not be defined for the Upper Pyramid

Springs Ash-flow tuff because of the high radiogenic yield for the sample. High radiogenic yields indicate that any initial argon in the sample did not have an effect on the sample. Figure 16 shows the weighted mean age of the sample.

#### Dome B

Dome B is one of four post-caldera domes in the field area. The weighted mean age of the rhyolite dome is  $22.79 \text{ Ma} \pm 0.15 \text{ Ma}$ . The isochron age for this sample is  $22.79 \text{ Ma} \pm 0.14 \text{ Ma}$  (Figure 17). The initial  $^{40}\text{Ar}/^{36}\text{Ar}$  ratio for the rhyolite of North Dome is  $291 \pm 6$  indicating no excess argon is present. The weighted mean age of  $22.79 \text{ Ma} \pm 0.15 \text{ Ma}$  is used for this study.

#### Fang Ridge

The age of the Fang Ridge dacite is  $21.39 \pm 0.21 \text{ Ma}$  (Figure 18). Analysis was done on plagioclase crystals instead of sanidine due to the lack of sanidine in the sample.

The analysis of Fang Ridge was done on ten out of fifteen samples. The procedure for rejecting five analyses was for any sample that had a  $1 \sigma$  standard deviation greater than one million years.

### Lower Pyramid Spring tuff-Sanidine

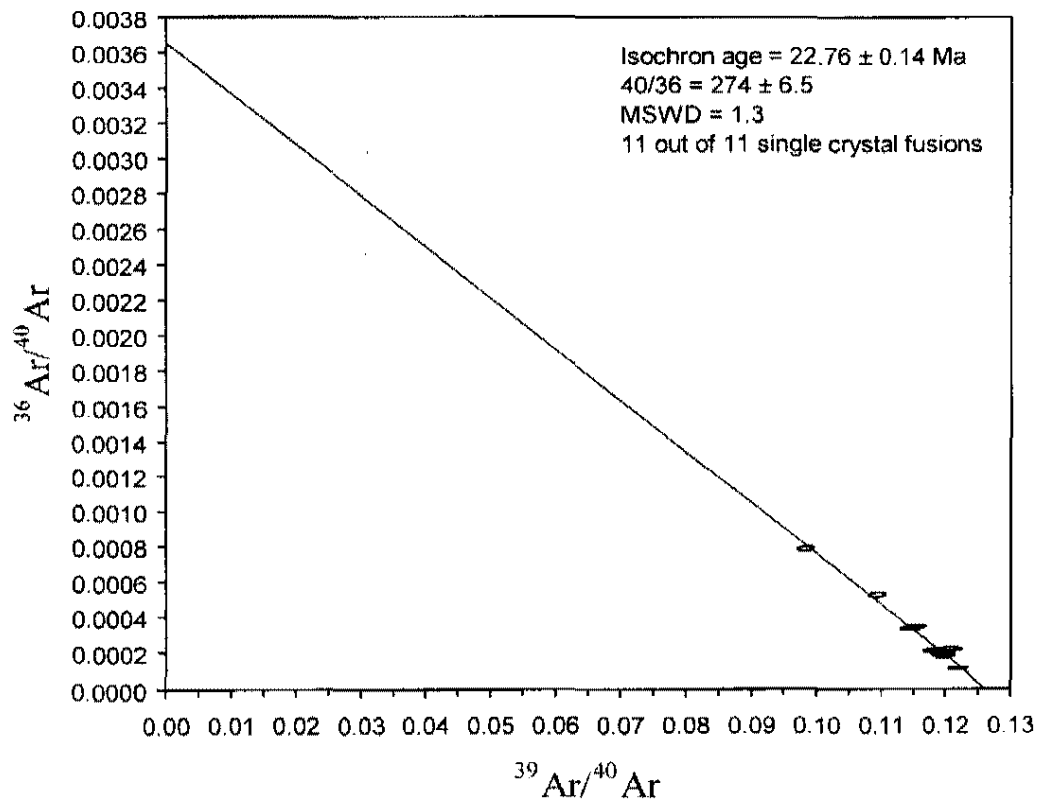


Figure 15. Probability plot and isochron for the lower Pyramid Spring tuff.

Upper Pyramid Spring tuff - Sanidine

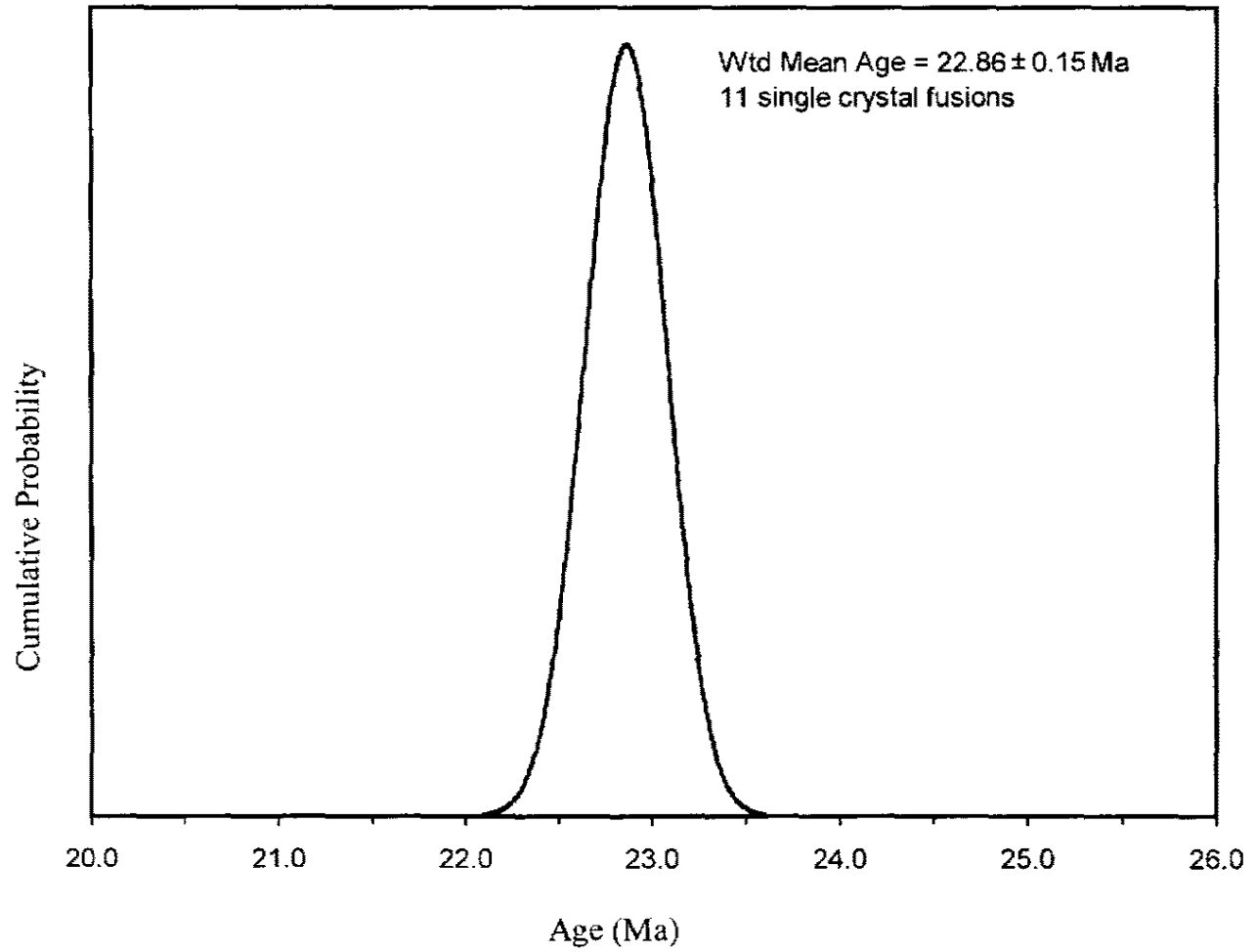


Figure 16. Probability plot for the upper Pyramid Spring tuff.

Dome B - Sanidine

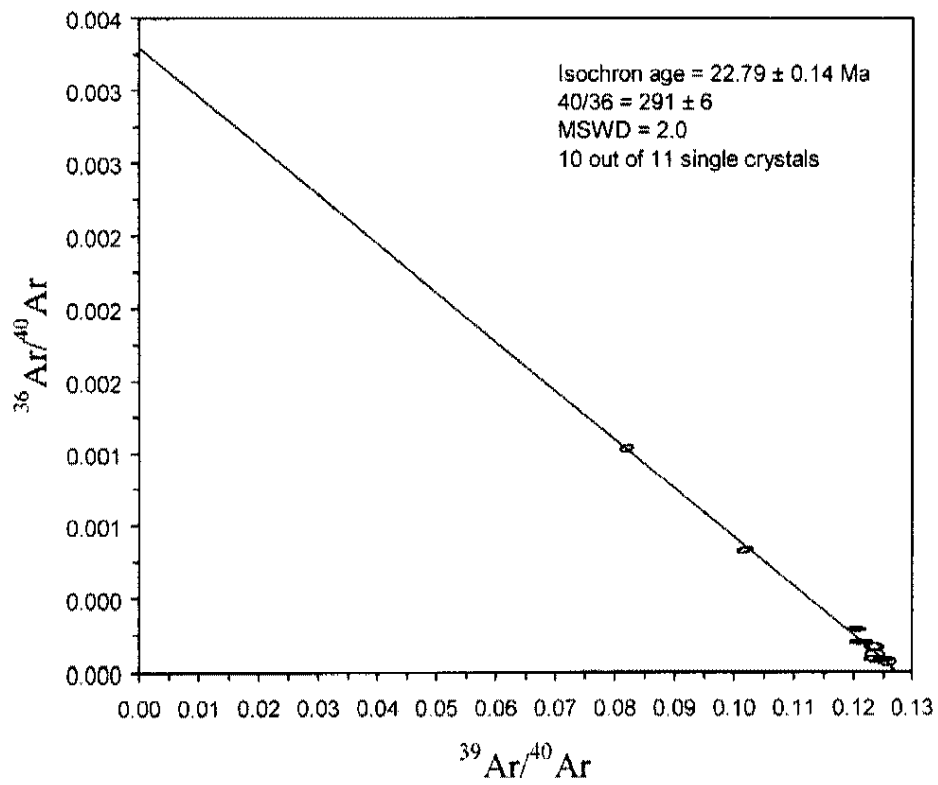
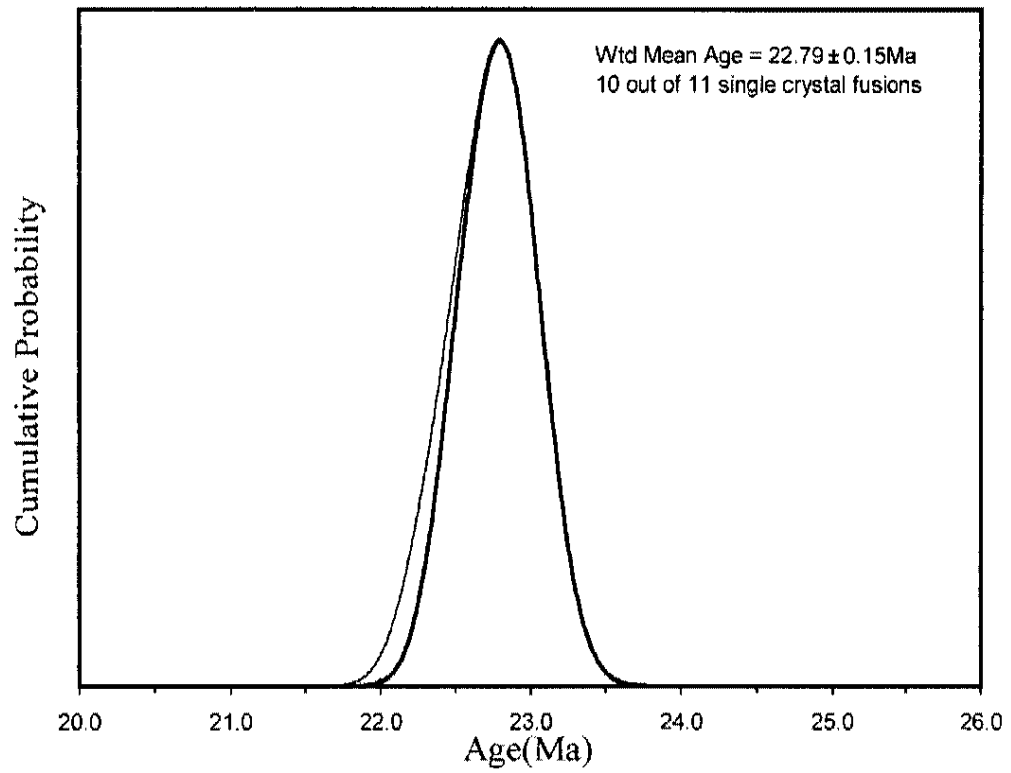


Figure 17. Probability plot and isochron for Dome B.

Fang Ridge Dacite - Plagioclase

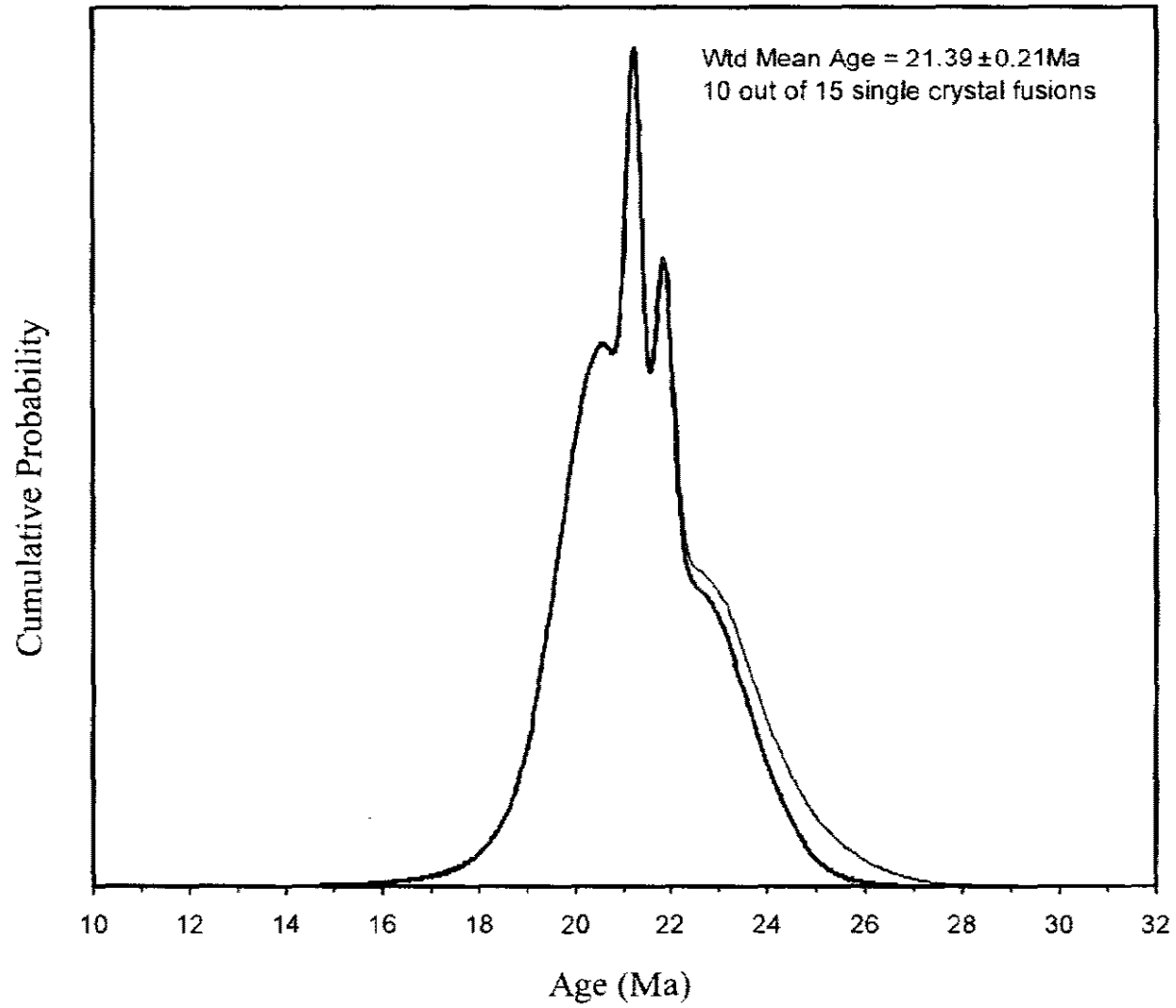


Figure 18. Probability plot for Fang Ridge.

## CHAPTER 6

### PALEOMAGNETIC ANALYSIS

The paleomagnetic investigations were done to correlate ash-flow tuffs with regional units and included analysis of characteristic remanent magnetization (ChRM) from five sites in the ash-flow tuffs from the Reveille Range. Conventional paleomagnetic methods (e.g., Knight et al., 1986; Hudson et al., 2000) were employed in this study. The following description of the technique is from Faulds (personal communication, 2006).

A portable drill was used to collect cores from each site. Samples were prepared for analysis using non-magnetic saw blades. All analyses were conducted at the Keck Paleomagnetic Laboratory at the University of Nevada, Reno. Remanent magnetizations were measured on an Agico JR-5A magnetometer. To isolate components of the natural remanent magnetization, all samples were subjected to either alternating field or thermal demagnetization techniques. Demagnetization trajectories were then monitored on orthogonal demagnetization diagrams. ChRMs were calculated using standard methods such as the multivariate technique of principal component analysis (e.g., Kirschvink, 1980). Conventional statistical analyses on a sphere (e.g., Fisher, 1953; McFadden and Lowes, 1981) were employed to determine site means and dispersion parameters.

Four of the five sites yielded grouped site means, with an  $\alpha_{95} < 10^\circ$  and  $k > 100$  ( $k$  is a precision parameter denoting the concentration of the distribution about the mean direction).

Most samples behaved simply during demagnetization. After removal of magnetizations with highly variable direction at low inductions, a single ChRM was recognized between 30 and 100 mT (milliTesla). At higher inductions, demagnetization trajectories typically continued straight to the origin. These thermoremanent magnetizations are typical of ash-flow tuffs.

Demagnetization behaviors suggest that fine-grained, pseudo-single domain titanomagnetite is the principal carrier of the ChRMs in the ash-flow tuffs. Alternating field demagnetization commonly removed nearly all magnetization by 100 mT. Titanomagnetite typically loses most magnetization by 100 mT.

#### Lower Pyramid Spring tuff

Twelve paleomagnetic cores were drilled in the lower Pyramid Spring tuff, only six samples were used to acquire data. The other six samples were either partial cores or what is known as LBO. LBO stands for loose but OK, which means that the core was broken during the drilling process and was loose within the drilled hole. These types of samples can produce inaccurate data and were not used during the analysis process.

Five of the six cores produced a paleomagnetic pole direction of  $-50.5^\circ$  inclination and  $218.1^\circ$  declination. The K-value for the samples was 490.1. This K-value is acceptable because it is higher than 100. Figure 19 shows the Zijiderveld and stereonet plots for this unit.



### Middle Pyramid Spring tuff

Eight sample locations were drilled in the middle Pyramid Spring tuff, however, only five of the sample cores were useable. The other three samples were partial cores or LBO's. Four of the five samples had an average paleomagnetic direction of  $-41.4^{\circ}$  inclination and  $201.1^{\circ}$  declination. The K-value of the samples was 616.4 and the  $\alpha_{95}$  value was 3.7%. Figure 20 shows the stereonet and the Zijiderveld plots for the samples.

### Upper Pyramid Spring tuff

Twelve sample locations were drilled in the upper Pyramid Spring tuff. Only six of the twelve samples were used because they were either partial cores or LBO's. Five of the six samples produced an average paleomagnetic pole direction of  $-42.5^{\circ}$  inclination and  $213.4^{\circ}$  declination. The K-value for the samples was 1008.6 and the  $\alpha_{95}$  value was 2.4%. Figure 21 shows the stereonet and the Zijiderveld plots for the samples.

### Tuff of Goblin Knobs (Tgk)

Eleven samples were drilled within the tuff of Goblin Knobs. Six samples were used because the other five were partial cores or LBO's. Five of the six samples produced an average paleomagnetic pole direction of  $8.6^{\circ}$  inclination and  $27.2^{\circ}$  declination. The K-value is 338.1 and the  $\alpha_{95}$  value was 3.7%. Figure 22 shows the stereonet and the Zijiderveld plots for the samples.

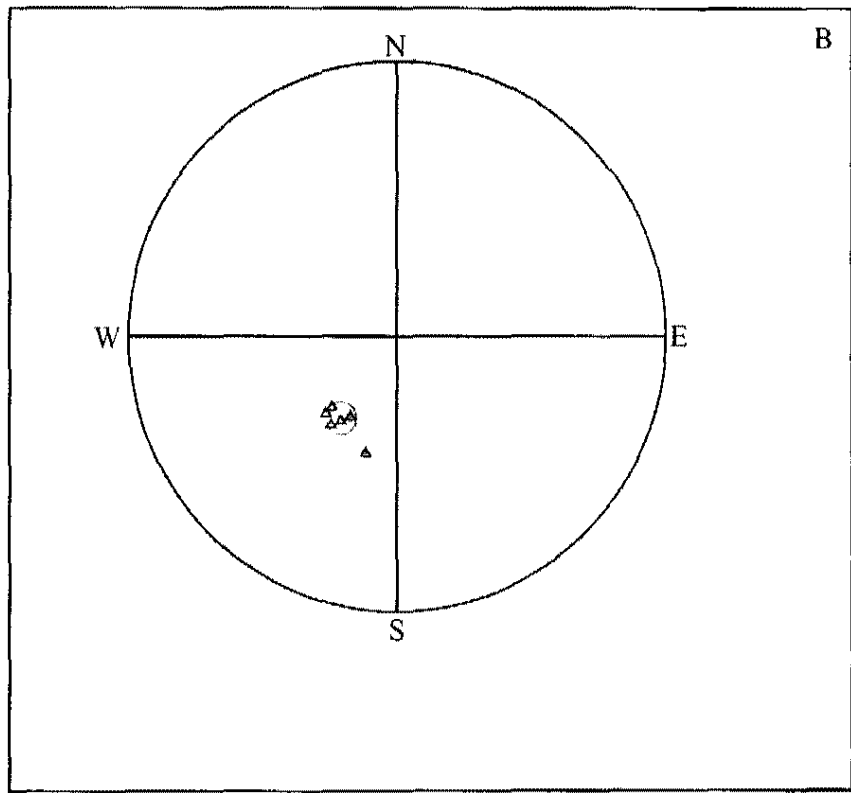
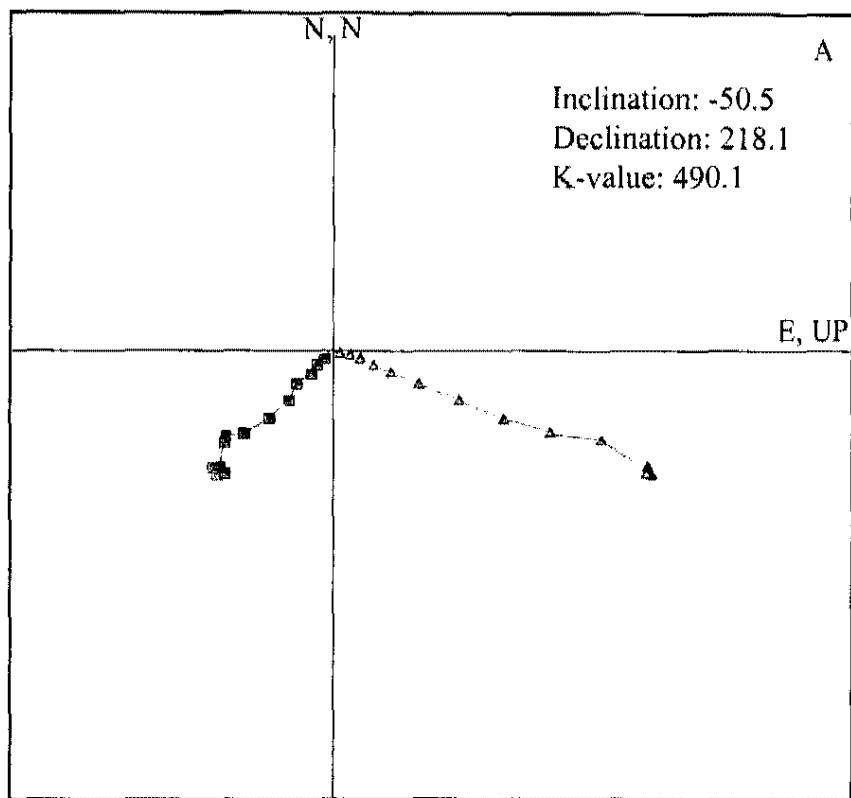


Figure 19. Paleomagnetic plots for the lower Pyramid Spring tuff. Figure (A) is a Zijderveld plot of the unit and (B) is the stereonet projection of the unit.

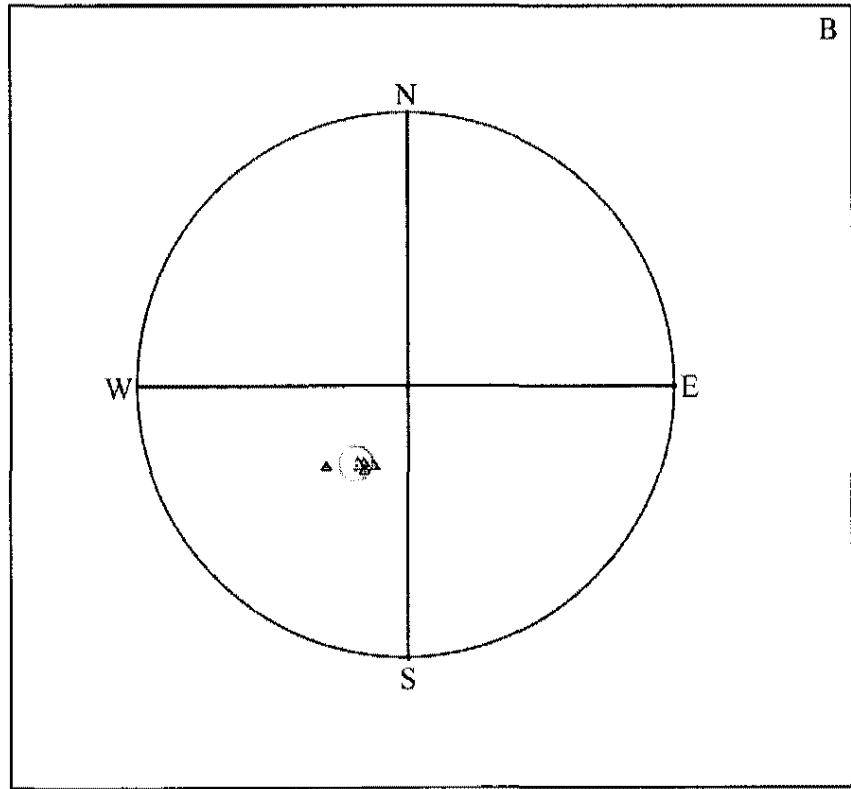
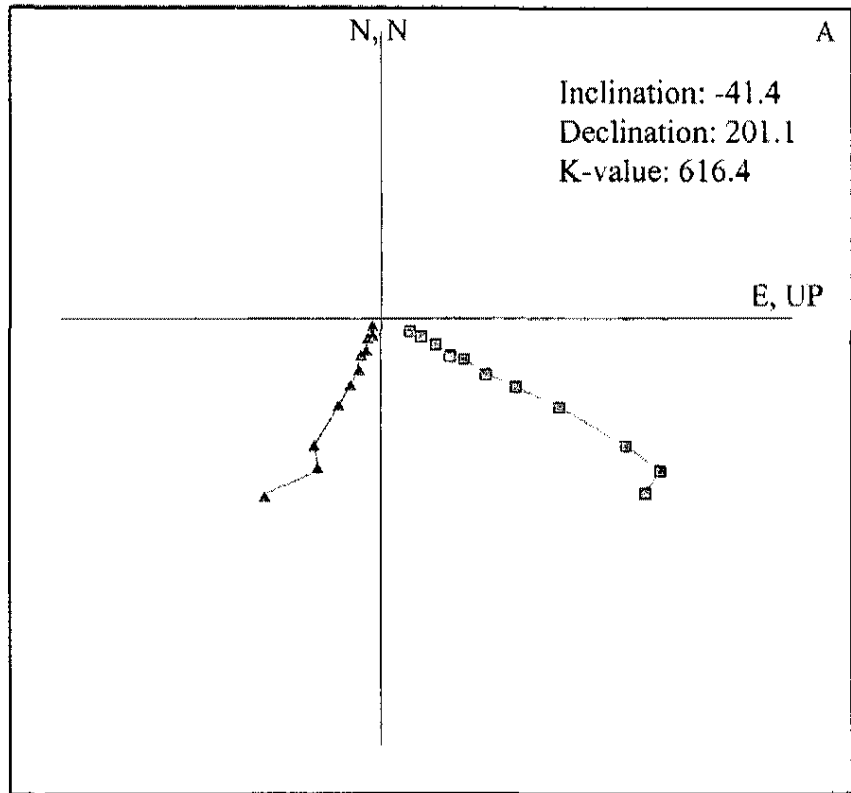


Figure 20. Paleomagnetic plots for the middle Pyramid Spring tuff. Figure (A) is a Zijderveld plot of the unit and (B) is the stereonet projection of the unit.

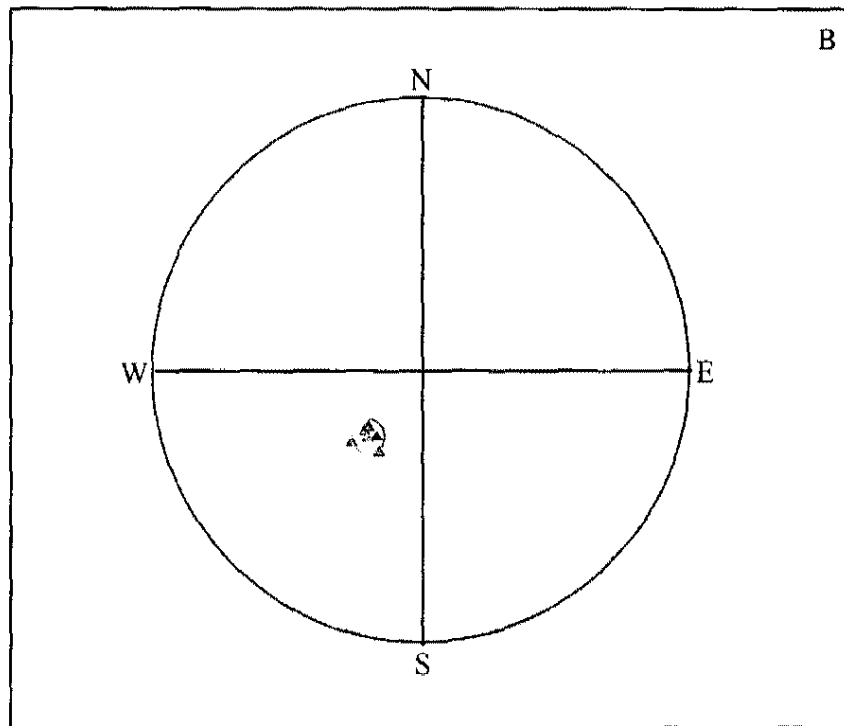
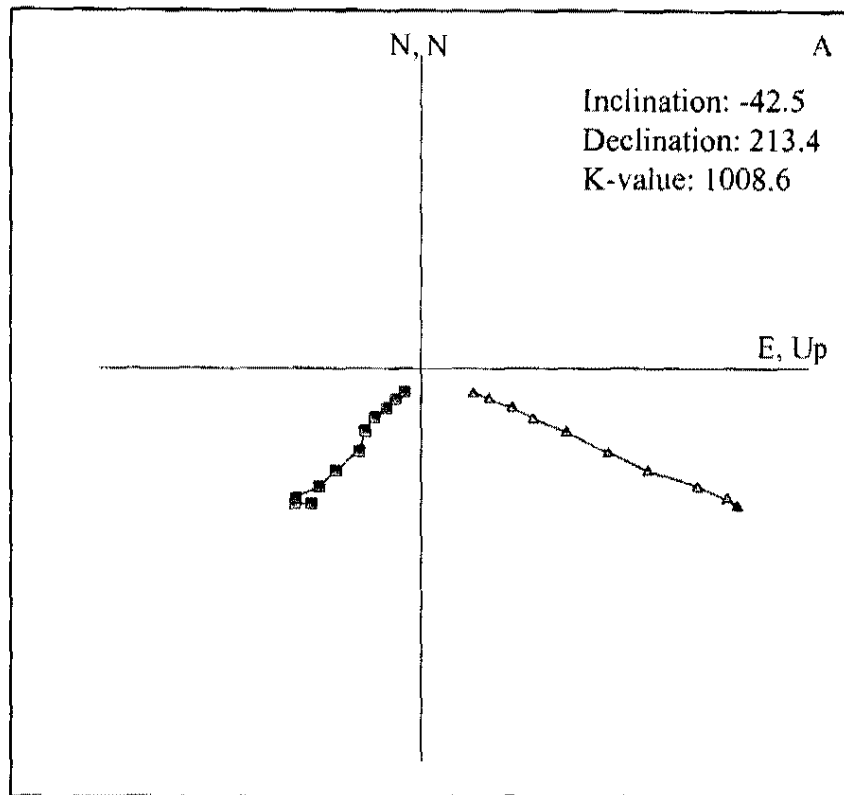


Figure 21. Paleomagnetic plots for the upper Pyramid Springs tuff. Figure (A) is a Zijderveld plot of the unit and (B) is the stereonet projection of the unit.

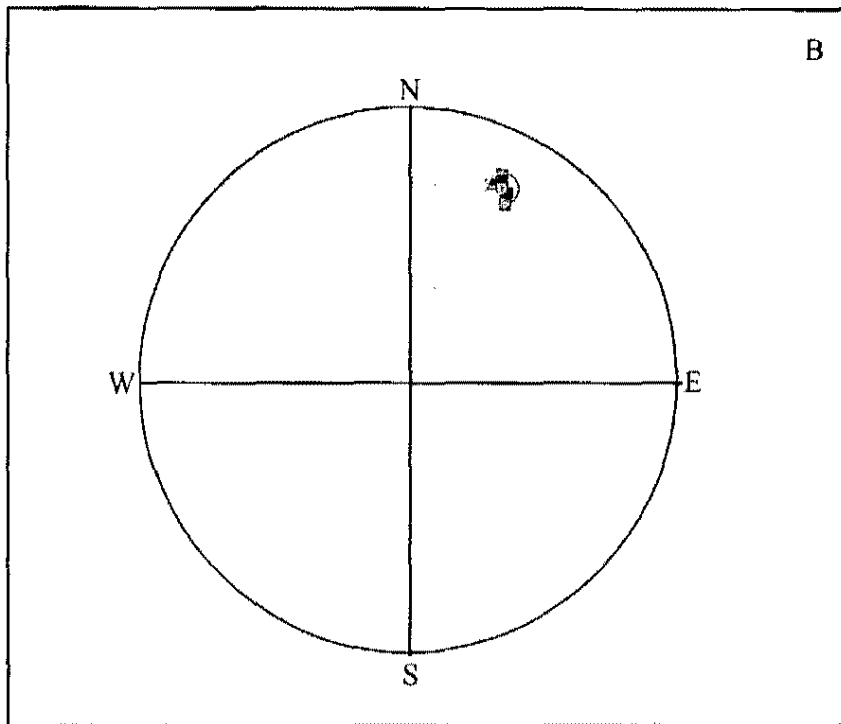
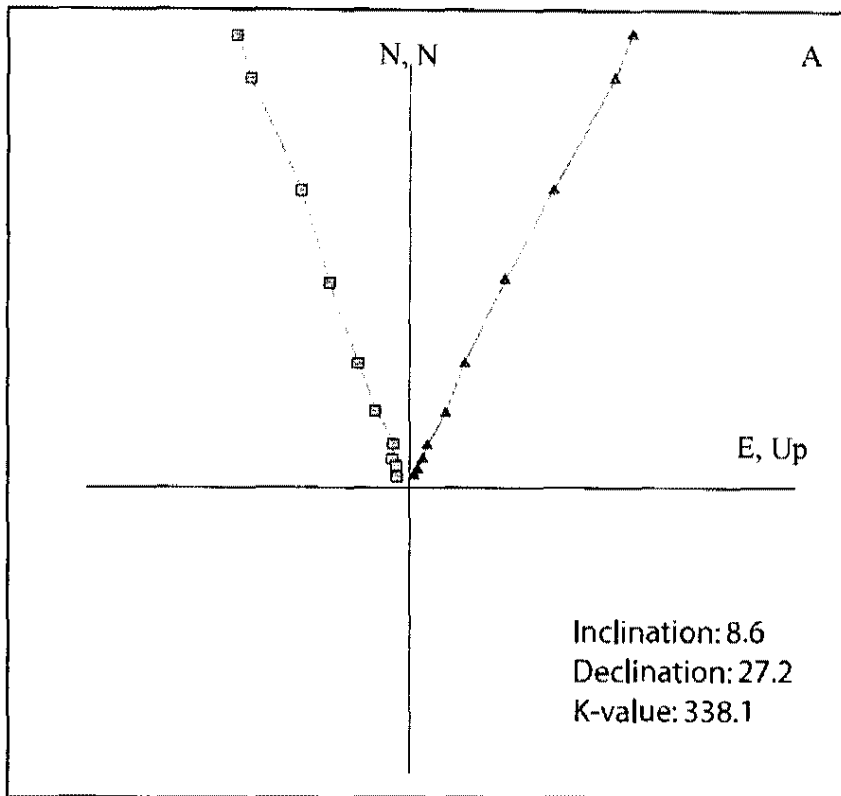


Figure 22. Paleomagnetic plots for the tuff of Goblin Knob. Figure (A) is the Zijderveld plot of the unit and (B) is the stereonet projection of the unit.

## Dome B

Ten samples were drilled in the Dome B. The data collected from this unit showed no apparent trend or stable demagnetization trends. This can be explained by meteorologic resetting of magnetization (most likely by lightning strikes) or by coarse magnetic grains, which alter the magnetic field of surrounding smaller grains. Since, coarse magnetic grains are not present at Dome B, meteorological resetting of the magnetization is most likely the cause of the unstable magnetic trends.

## Summary and Interpretation

The purpose of the paleomagnetic analysis was for correlation purposes between the Pyramid Spring tuff, tuff of Goblin Knobs, and the Pahranaagat Formation. The observations for the Pyramid Spring the tuff and Goblin Knobs is:

1. The paleomagnetic directions from the Pyramid Spring tuff range between  $-41.4^{\circ}$  to  $-50.5^{\circ}$  inclination and  $201.1^{\circ}$  to  $218.1^{\circ}$  declination.
2. The average inclination of the three units of the Pyramid Spring tuff is  $-44.8^{\circ}$  and the average declination  $210.9^{\circ}$ .
3. It is most likely that the three units of the Pyramid Spring tuff were erupted from the same volcanic center over a relatively short period of time. The three units of the Pyramid Spring tuff have similar paleomagnetic poles, mineralogy, and ages.
4. The tuff of Goblin Knobs has a normal polarity; therefore it is not correlative to the Pyramid Spring tuff, which has a reversed polarity. Geochronological data and geochemical data support this observation.

## CHAPTER 7

### GEOCHEMISTRY

The geochemistry of the volcanic rocks presented in this chapter will be used in subsequent chapters to discuss the petrogenesis of the ash-flow tuffs and to correlate with other ash-flow tuffs in the region. The complete geochemistry data set is provided in Appendix C.

#### Major Elements

The upper, middle and lower members of the Pyramid Spring tuff range from dacite and rhyolite (64.80 – 70.43 wt. % SiO<sub>2</sub>; 15.35 – 18.52 wt. % Al<sub>2</sub>O<sub>3</sub>; 6.00 – 6.78 wt. % K<sub>2</sub>O) according to the Irvine and Baragar (1971) classification (Figure 23). The Fang Ridge dike is an andesite to a dacite (65.26 – 67.11 wt. % SiO<sub>2</sub>; 14.29 – 14.67 wt. % Al<sub>2</sub>O<sub>3</sub>; 4.24 – 4.38 wt. % K<sub>2</sub>O). The post-collapse domes (Dome B and Dome C) are rhyolite (73.45 – 75.83 % SiO<sub>2</sub>; 12.30 – 13.59 wt. % Al<sub>2</sub>O<sub>3</sub>; 4.60 -5.12 wt. % K<sub>2</sub>O) (Figure 24). The resurgent dome of Reveille Peak is a rhyolite (75.83 wt. % SiO<sub>2</sub>; 12.95 wt. % Al<sub>2</sub>O<sub>3</sub>; 4.66 wt. % K<sub>2</sub>O).

#### Trace Elements

The trace element variation diagrams (Figure 25) show clear differences between the dacite of Fang Ridge, post-caldera domes, and the Pyramid Spring tuff. However, the

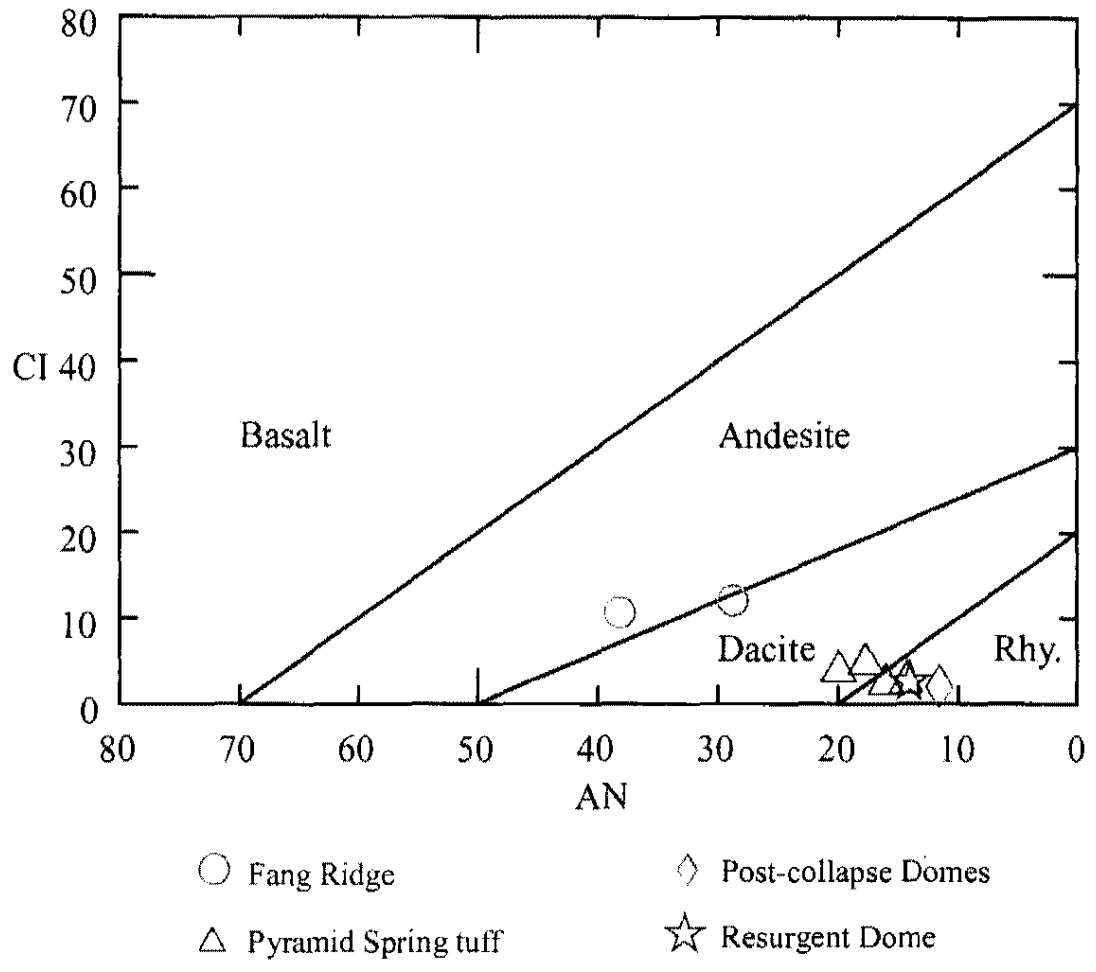


Figure 23. Irving and Baragar (1971) classification of the volcanic rocks in the southern Reville Range.



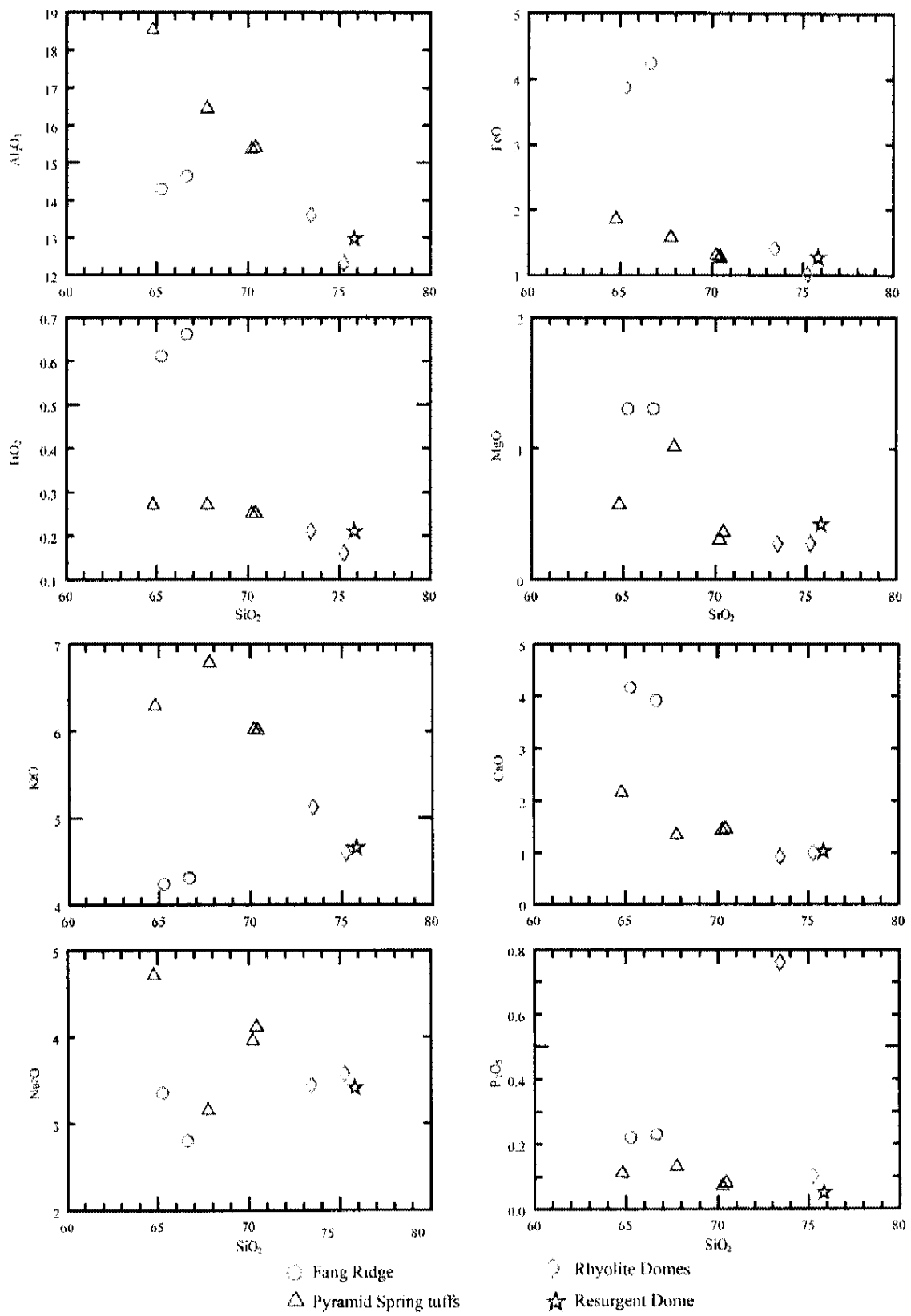


Figure 24. Major element variation diagrams for units in the southern Reville Range.

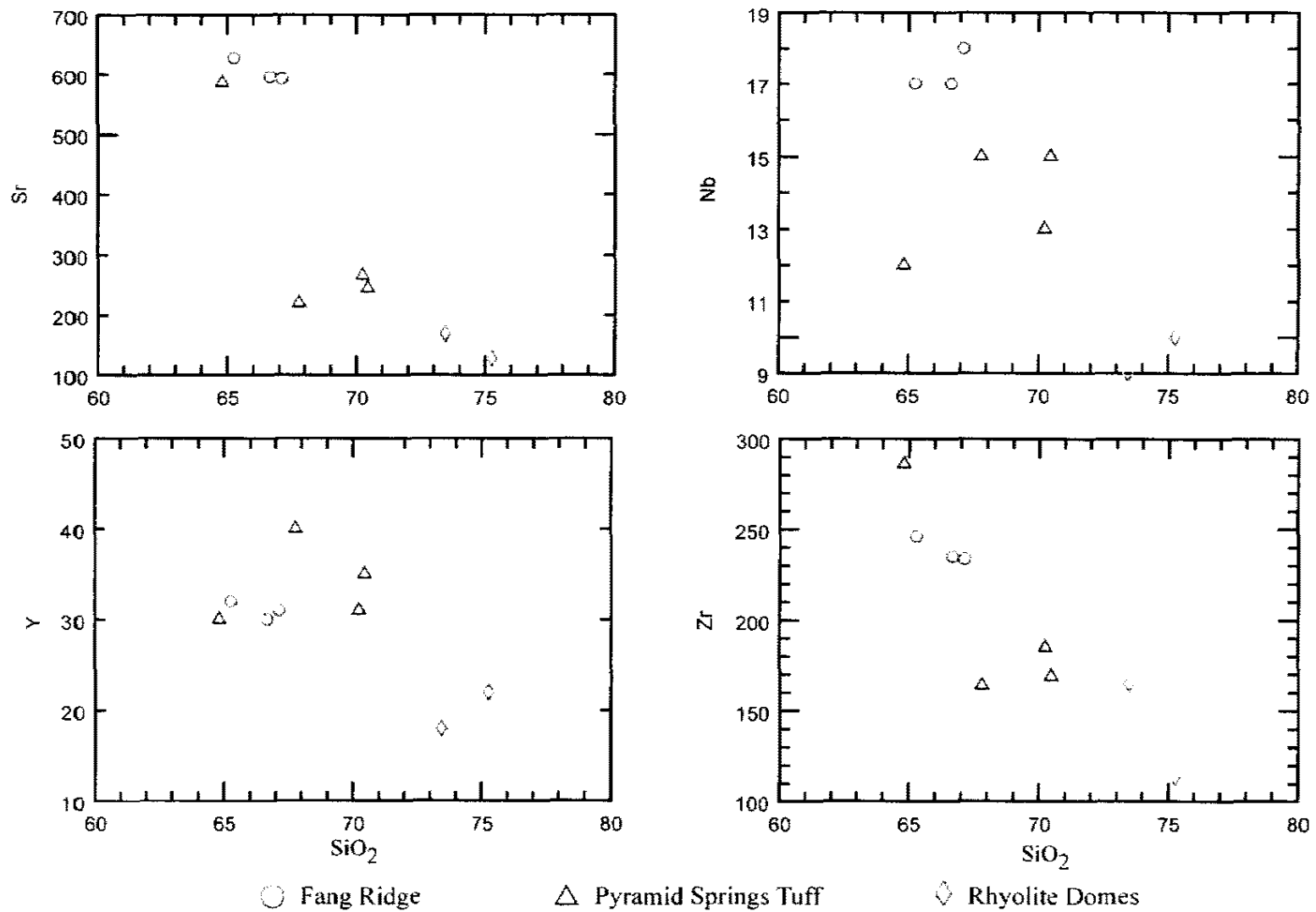


Figure 25. Trace Element variation diagrams for the dacites and rhyolites.

Pyramid Spring tuff, the post-caldera domes, and the resurgent dome show chemical affinities to one another. Trace element concentrations (except for Y) are higher in the domes and ash-flow tuffs than in the Fang Ridge dacite. In general, the post-caldera domes have the lowest concentration of trace elements compared to ash-flow tuffs (Figure 25).

Primitive mantle normalized element variation diagrams (Sun and McDonald, 1989) show that the Pyramid Spring tuff and the post-caldera domes have high large-ion lithophile (LIL), and light rare-earth element (LREE) concentrations, but low values of Nb, Sr, P, Ti and sometimes Ba compared to primitive mantle (Fig. 26a and 26b). Fang Ridge is enriched in both LREE and HREE in relation to the Pyramid Spring tuff and post-caldera domes (Fig 26c), but shows lower values of Ba, Nb, Sr, P and Ti compared to primitive mantle.

### Isotopes

The  $^{87}\text{Sr}/^{86}\text{Sr}$  ratio for two of the three members of the Pyramid Spring tuff are similar (0.7097227 and 0.7092529); however, the initial  $^{87}\text{Sr}/^{86}\text{Sr}$  for Dome B is slightly lower (0.7089105) than the Pyramid Spring tuff. Fang Ridge has an initial  $^{87}\text{Sr}/^{86}\text{Sr}$  between 0.7077212 and 0.7077336.

$\epsilon_{\text{Nd}}$  for the Pyramid Spring tuffs range from -7.60 to -7.78, while Dome B has an  $\epsilon_{\text{Nd}}$  of -7.76. Fang Ridge's  $\epsilon_{\text{Nd}}$  ranges from -8.22 to -8.56 (Figure 27).

Plots of  $^{206}\text{Pb}/^{204}\text{Pb}$  vs.  $^{207}\text{Pb}/^{204}\text{Pb}$  and  $^{208}\text{Pb}/^{204}\text{Pb}$  (Figure 28) indicate small variation

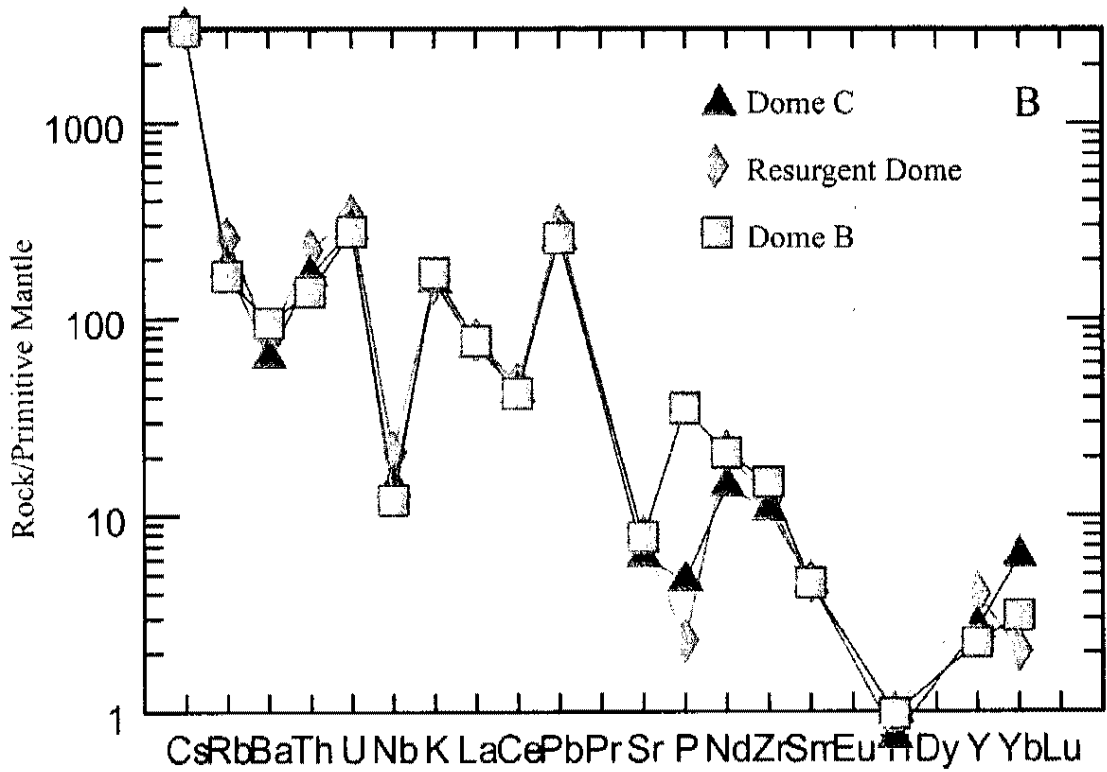
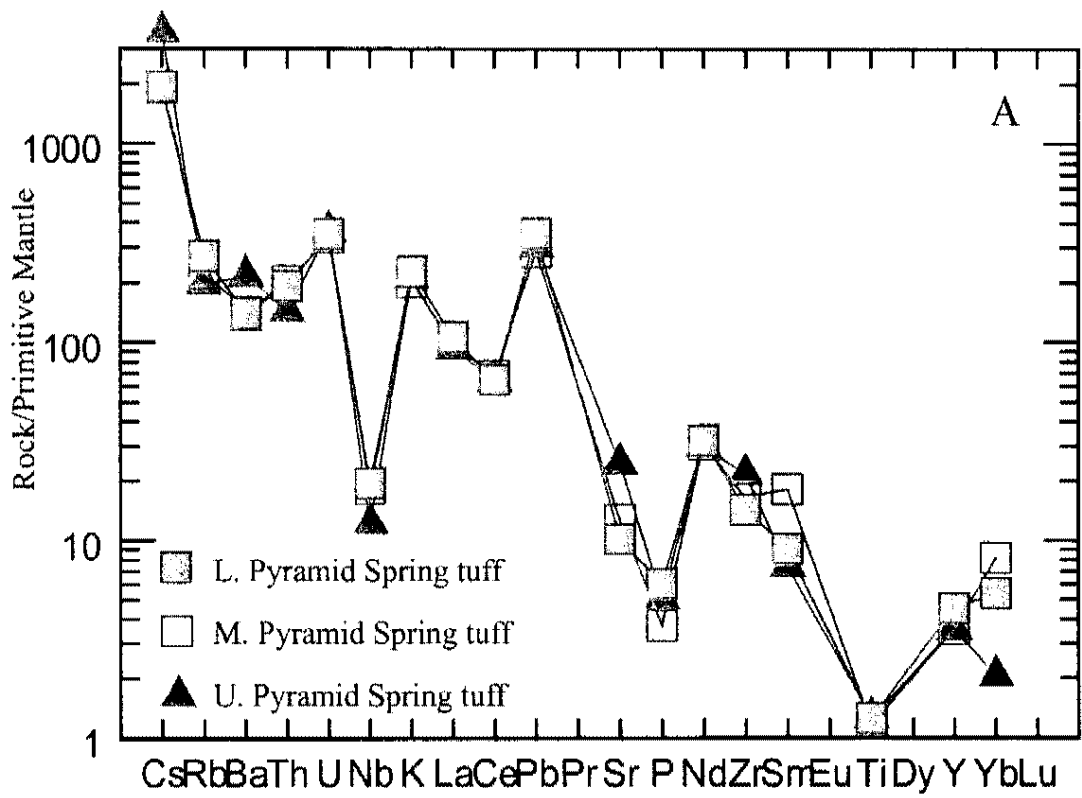


Figure 26a and 26b. Primitive Mantle normalized spider diagrams for (a) Pyramid Spring tuff, (b) Post-caldera domes.

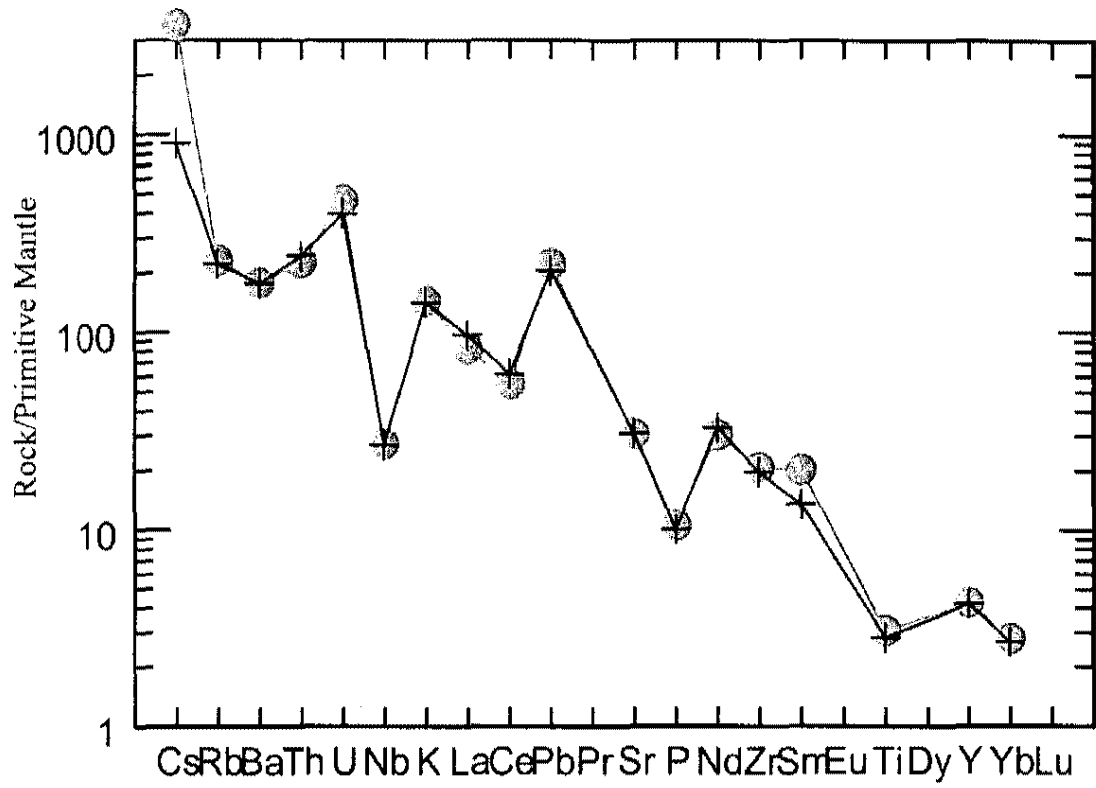


Figure 26c. Primitive Mantle normalized spider diagrams for Fang Ridge.

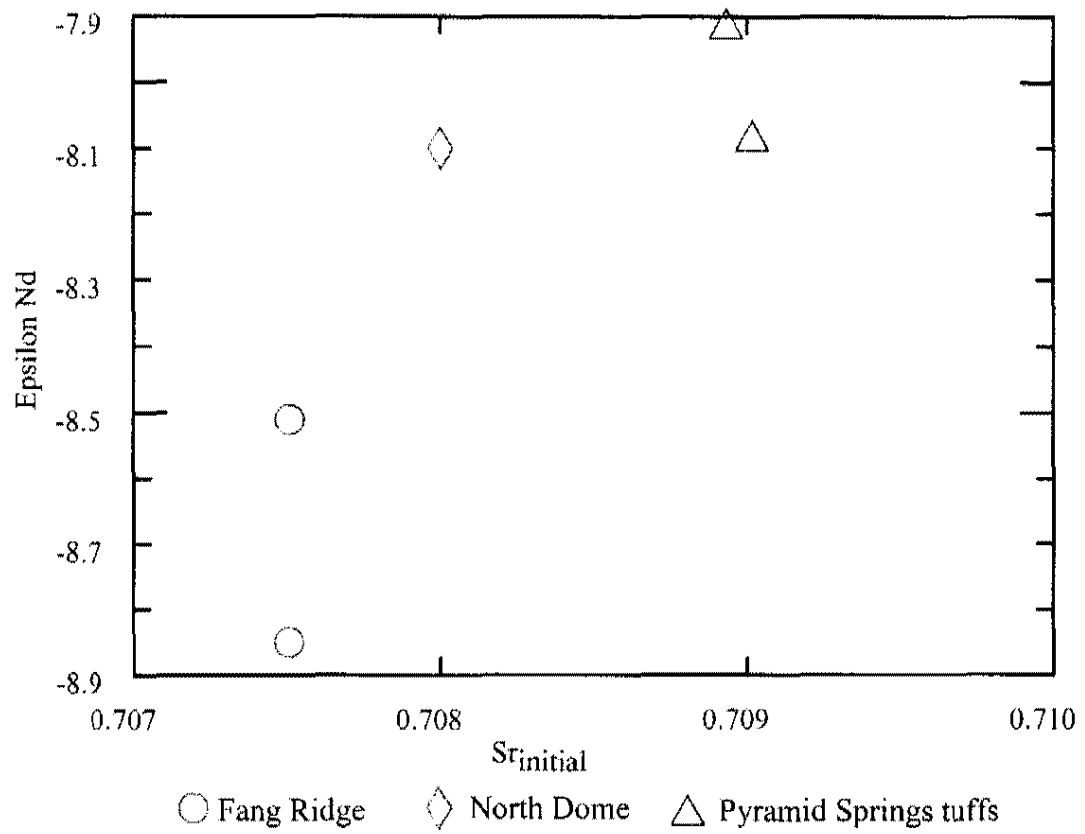


Figure 27. Trace element plot of initial Sr versus epsilon Nd.

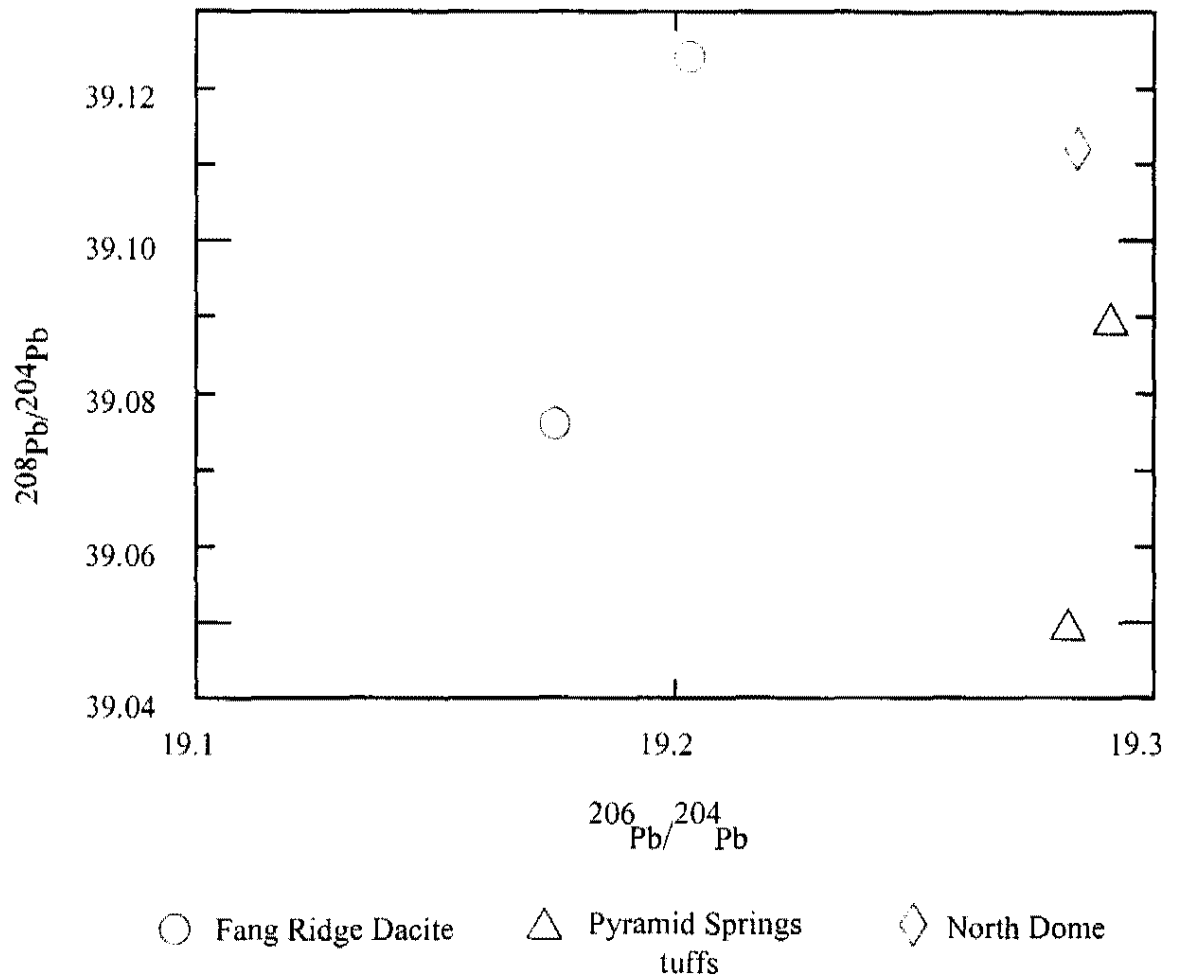


Figure 28. Element variation diagram for  $^{208}\text{Pb}/^{204}\text{Pb}$  vs.  $^{206}\text{Pb}/^{204}\text{Pb}$  for the volcanic units in the southern Reville Range.

in  $^{206}\text{Pb}/^{204}\text{Pb}$ , but little difference in  $^{207}\text{Pb}/^{204}\text{Pb}$  and  $^{208}\text{Pb}/^{204}\text{Pb}$  (Figure 28). The Pyramid Spring tuffs and Dome B are similar and have  $^{206}\text{Pb}/^{204}\text{Pb}$  values that range from 19.282 to 19.291.  $^{206}\text{Pb}/^{204}\text{Pb}$  for Fang Ridge is lower and ranges from 19.175 to 19.203.

### Summary

The major purpose of geochemical analysis for this project was for correlation purposes (see Chapter 8); therefore only general observations will be made concerning volcanic rock petrogenesis. These observations include:

1. Major elements indicate that the four major rock groups (Pyramid Spring tuff, post-caldera domes, resurgent dome, and Fang Ridge) are chemically different. The Pyramid Spring tuff, post-caldera domes, and resurgent dome geochemically lie on the same trend for MgO, FeO, TiO<sub>2</sub>, CaO, P<sub>2</sub>O<sub>5</sub>, Sr, and Y; however, the ash-flow tuffs have lower SiO<sub>2</sub> than the rhyolite domes.
2. The composition of Fang Ridge dacite is remarkably homogenous. Major element chemistry suggests that Fang Ridge dacite is not cogenetic with the Pyramid Spring tuff or the post-caldera domes because the concentrations of TiO<sub>2</sub>, FeO, CaO, and MgO are higher, and Al<sub>2</sub>O<sub>3</sub>, K<sub>2</sub>O, and Na<sub>2</sub>O are lower than the Pyramid Spring tuff and post-caldera domes. The 1.3 m.y. difference in age between the formation of Fang Ridge and the eruption of the Pyramid Spring tuff and domes supports this conclusion as do Sr, Nd and Pb isotopes. Isotopic ratios clearly indicate a different crustal source for Fang Ridge dacite.
3. Similarities in major, trace element geochemistry and isotopic ratios between the three members of the Pyramid Spring tuff indicate that these units are cogenetic



and most probably comagmatic. A comagmatic relationship is supported by similar ages and paleomagnetic poles.

## CHAPTER 8

### REGIONAL CORRELATIONS

One of the most important questions dealt with in this thesis is whether the tuffs in the southern Reveille Range are equivalent to the Pahranaagat Formation. During the 1990's the Reveille Range and surrounding areas were the focus of studies dealing with the formation of the Kawich caldera and the emplacement of the Pahranaagat Tuff (Best et al., 1995). Their study concluded that the Kawich caldera produced the Pahranaagat Tuff at  $22.64 \text{ Ma} \pm 0.01 \text{ Ma}$  and suggested that the Pahranaagat Tuff is correlative with the Pyramid Spring tuff in the southern Reveille Range. Contrary to the conclusions of Best et al. (1995), I conclude that the Pyramid Spring tuff is not correlative with the Pahranaagat Formation. The following paragraphs summarize the evidence to support this conclusion.

#### Geochemistry

The major element variation diagrams of volcanic rocks in the southern Reveille Range show trends different from major element variation of the Pahranaagat Formation (Figure 29). The Pyramid Spring tuffs have lower concentrations of CaO, FeO, and  $\text{TiO}_2$  than the Pahranaagat Formation. Trace element variations of the Pyramid Spring tuff are more limited in concentration than the Pahranaagat Formation (Figure 30), but these differences may not be significant. In a recent study, Honn (2005)

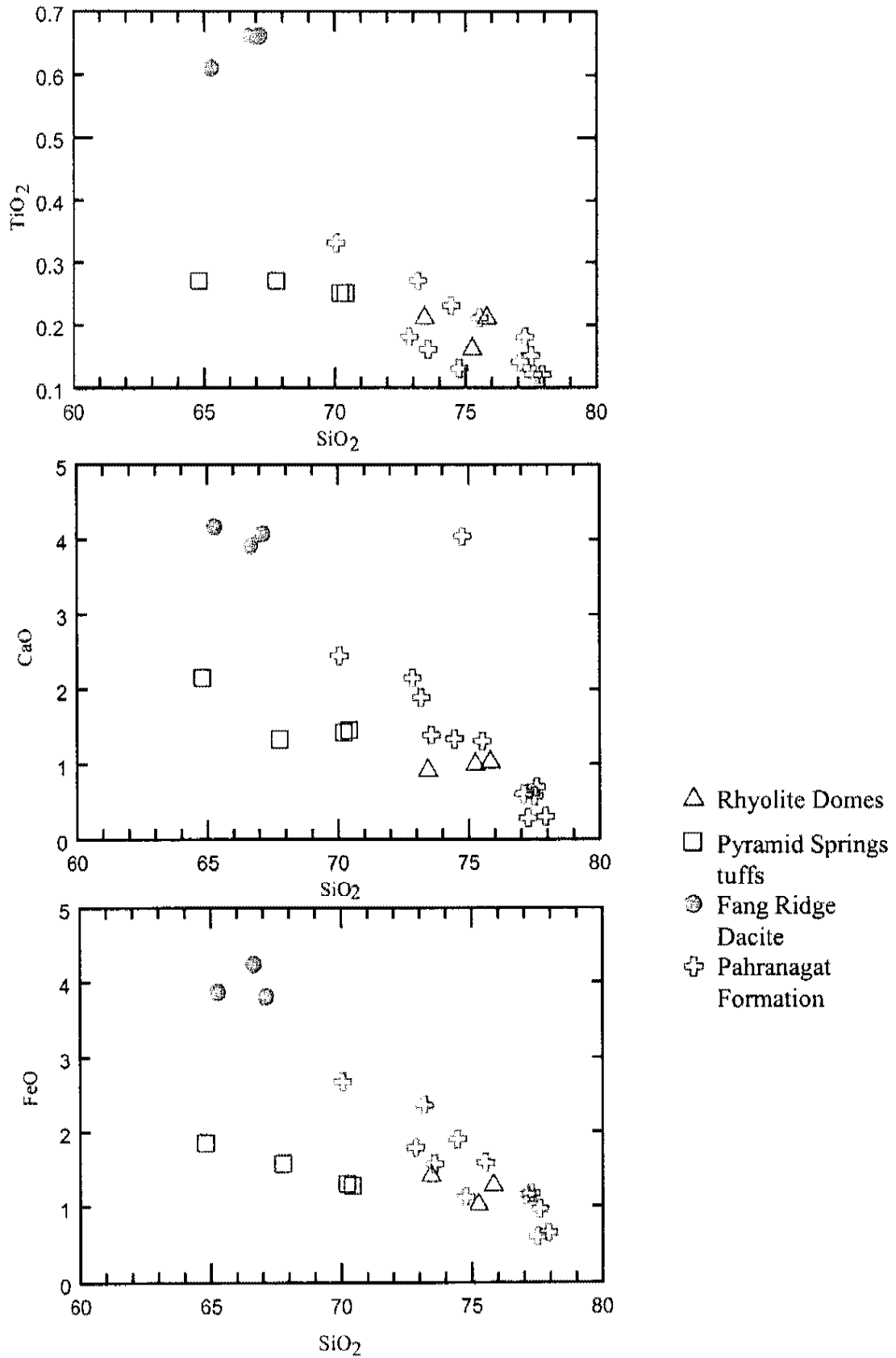


Figure 29. Element variation diagrams for the volcanic rocks in the southern Reveille Range and the Pahrnagat Formation.

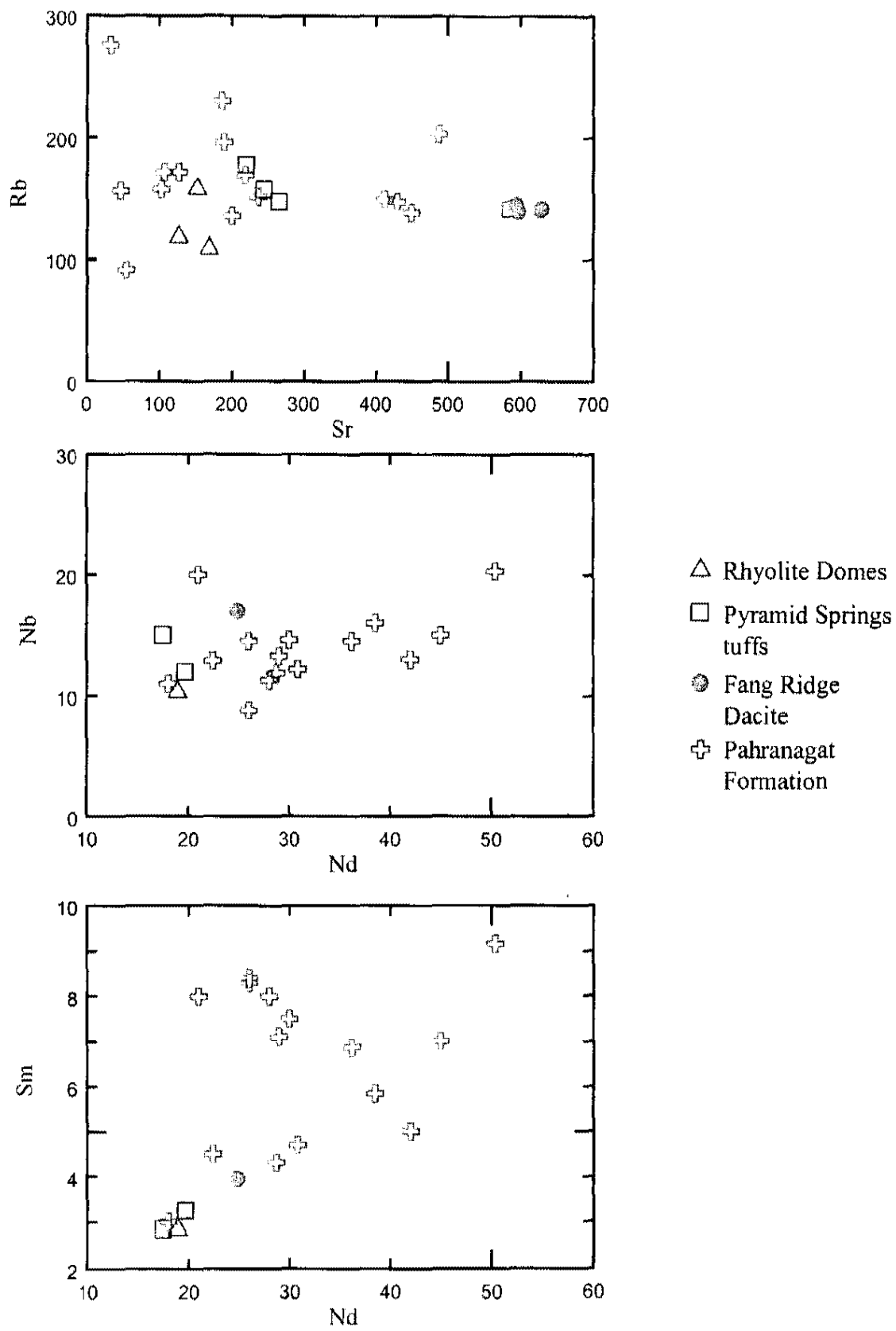


Figure 30. Trace element variation diagram of the volcanic rocks in the southern Reveille Range and the Pahrnagat Formation.

indicated that the trace elements abundances of tuffs in the Kawich Range are indistinguishable from the Pahranaagat Formation and concluded that they are correlative with the Pahranaagat Formation.

### Geochronology

Geochronological interpretations are based on one sigma errors. If two sigma errors are used the ages of the Pyramid Spring tuffs will coincide with the ages for the Pahranaagat Formation.

Best et al. (1995) dated the Pahranaagat Tuff at  $22.64 \pm 0.01$  Ma. However, in 2005 an unpublished age of 22.78 (personal communication; Christiansen, 2005) was reported for the Pahranaagat Tuff. The 22.78 Ma date used an older Fish Canyon tuff standard (28.02 Ma) for the fluence monitor. In comparison, dates reported in this thesis used a newer Fish Canyon tuff standard (27.90 Ma). To address the fluence monitor differences between this thesis and the study conducted by Dr. Eric Christiansen, dates for samples from the southern Reveille Range were corrected using the fluence monitor of the older Fish Canyon Tuff standard (28.02 Ma). The age of the samples from the southern Reveille Range increased by  $\sim 100$  Ka after the age correction. The corrected age of the lower Pyramid Spring tuff is  $22.99 \pm 0.150$  Ma and the corrected age of upper Pyramid Spring tuff is  $22.95 \pm 0.146$  Ma.

Based on this information, the corrected ages for the ash-flow tuffs in the southern Reveille Range are on average 150,000 years older than that of the Pahranaagat Tuff. This difference is slightly larger than the error reported for the dates and is probably significant.

## Paleomagnetic Data

Paleomagnetic data from Best et al. (1995) focused on the Pahranaagat Formation, which according to their model erupted from the Kawich caldera. The Pahranaagat Formation is documented in several of the mountain ranges that surround the Reveille Range. The data from Best et al. (1995) is summarized in Appendix D and is compared to new paleomagnetic data from the Pyramid Spring tuff in the paragraphs below.

The average inclination of the Pahranaagat tuff is  $-58.6^\circ$ , a value that is  $14^\circ$  higher than the average inclination of  $-44.8^\circ$  for the Pyramid Spring tuff. This observation, therefore, suggests that the Pyramid Spring tuff is not correlative with the Pahranaagat formation. The only tuff that is possibly correlative to the Pyramid Spring tuff is the tuff exposed in Cedar Pass in the southern Kawich Range. Hypothetically, it is possible that either the eruption that produced the tuff at Cedar Pass is coeval with the eruptions in the southern Reveille Range or is correlative with the Pyramid Spring tuff. Unfortunately, exposures of the tuff at Cedar Pass lie in a restricted entry area, so samples could not be obtained for this study.

## Summary

The Pyramid Spring tuff is probably not correlative with the Pahranaagat Formation. This conclusion is based on:

1. A more restricted range of major element variation for the Pyramid Spring tuff compared to the Pahranaagat Formation.
2. An older age of about 190,000 years for the Pyramid Spring tuff.
3. A significance difference in the inclination of paleomagnetic poles for the Pyramid Spring tuff.

## CHAPTER 8

### CONCLUSIONS

A major contribution of this project was the discovery of the Pyramid Spring caldera and the identification of outflow tuffs that erupted from the caldera. Additionally, field work determined that the Pyramid Spring caldera is younger than the Goblin Knobs caldera located just to the north.

New  $^{40}\text{Ar}/^{39}\text{Ar}$  dates demonstrated that there are three magmatic events that occurred before the eruption of Pliocene basalt in the southern Reveille Range. The first event was the formation of the Pyramid Spring caldera at 22.9 Ma. At 22.8 Ma rhyolitic eruptions produced post-caldera domes. Fang Ridge dacite was emplaced along the northern Pyramid Spring caldera wall at 22.3 Ma.

The paleomagnetic, geochemical and  $^{40}\text{Ar}/^{39}\text{Ar}$  ages suggest that the Pyramid Spring tuff is not correlative with the Pahranaagat Formation. Furthermore, paleomagnetic and geochronological data indicate that the Pyramid Spring tuff erupted over a short period of time due to the small deviation of paleomagnetic poles from each unit of the Pyramid Spring tuff and their very similar  $^{40}\text{Ar}/^{39}\text{Ar}$  ages.

APPENDIX A

PETROGRAPHIC DESCRIPTIONS



## Appendix A: Petrographic Descriptions

The stratigraphic nomenclature used in this thesis is from Gardner et al. (1980), Naumann et al. (1991), Martin and Naumann (1995), Rash (1995), Best et al. (1995) with the exception of six newly identified units. Gardner et al. (1980) and Best et al. (1995) did not differentiate the ash-flow tuffs within the southern Reveille Range. Detailed mapping by Naumann et al. (1991), Martin and Naumann (1995), and Rash (1995) focused on the stratigraphic relations of the Tertiary units within the central and northern Reveille Range. Naumann et al. (1991) were able to recognize four types of basalts by geochemistry, petrography, geochronology, and field relations. Martin and Naumann (1995) and Rash (1995) were able to correct the errors in the stratigraphic contacts mapped by Ekren et al. (1973).

The following stratigraphic descriptions explain units on Plate 1. The ages of the basalts and tuff of Goblin Knobs were obtained from the studies of Naumann et al. (1991), Martin and Naumann (1995), and Rash (1995). The descriptions of the units are based on hand sample and thin section analysis.

### Tuff of Goblin Knobs (Tgk) (Reveille Range)

The tuff of Goblin Knobs ( $25.69 \pm 0.58$  Ma, biotite; Rash, 1995) is pale yellowish-brown densely welded tuff exposed primarily within the central Reveille Range. The Tuff of Goblin Knobs consists of 30-40% phenocrysts of quartz (25-30%) up to 5.6 mm in size, sanidine (15-35%) up to 3.3 mm in size, plagioclase (40-50%) up to 3.1 mm in size, biotite (1-15%) up to 3.1 mm in size. Also, the Tuff of Goblin Knobs contains trace amounts of hornblende (trace), up to 3.2 mm in size, Fe-Ti oxides (trace-2%) up to 0.06

mm in size, apatite (trace) up to 0.02 mm in size, and zircon (trace) up to 0.08 mm in size. White to gray pumice (2-5%) is generally flattened and ranges in length from 5 to 65 mm.

The Tuff of Goblin Knobs contains lithic fragments (5-7%) that include carbonate, quartzite, and porphyritic volcanic fragments (predominantly). The thickness of the tuff of Goblin Knobs ranges from 0-1700 m. Information for the tuff of Goblin Knobs was obtained from Naumann and Martin (1995) and Rash (1995).

#### Lower Pyramid Spring Tuff (Tps<sub>1</sub>) (Reveille Range)

The lower Pyramid Springs tuff is pink to purple in color. The tuff is a densely welded tuff at the base and grades into a moderately welded tuff at the top of the unit; phenocrysts which make up 35-40% of the rock include plagioclase (25-35%) up to 2 mm in size, quartz (15-20%) up to 1.5 mm in size, sanidine (30-40%) up to 2 mm in size, and biotite (0-5%) up to 0.5 mm in size, sanidine (30-40%) up to 2 mm in length. The lower Pyramid Spring tuff contains minor lithic fragments (<2%) that are predominately composed of carbonate. The age of the lower Pyramid Spring tuff is 22.892 Ma ± 0.154 Ma.

#### Middle Pyramid Spring Tuff (Tps<sub>2</sub>) (Reveille Range)

The middle Pyramid Spring tuff is pink to purple in color. The tuff has a densely welded tuff at the basal section and grades into a moderately welded tuff at the top of the unit. Phenocrysts comprise approximately 35-40% of the rock. Phenocrysts include plagioclase (25-35%) up to 1.5 mm in size, quartz (15-20%) up to 1.0 mm in size,

sanidine (30-40%) up to 1-2 mm in size, and biotite (0-5%) up to 0.5 mm in size. The pumice fragments can range from 10-20 cm in length. The middle Pyramid Spring tuff contains minor amounts of lithic fragments (<2%) composed predominantly of carbonate and volcanic fragments.

#### Upper Pyramid Spring Tuff (Tps<sub>3</sub>) (Reveille Range)

The upper Pyramid Spring tuff is yellowish to pink in color. The tuff is moderately welded with phenocrysts comprising approximately 40-50% of the rock. Phenocrysts include plagioclase (25-30%) up to 2 mm in size, quartz (15-25%) up to 1.5 mm in size, sanidine (30-40%) up to 2 mm in size, and biotite (0-5%) up to 0.5 mm in size. The pumice fragments show well developed compaction foliation. The pumice fragments can range between 15 cm to approximately half a meter in length. The unit contains minor amounts of lithic fragments <1%. The age of the Upper Pyramid Spring tuff is 22.862 Ma  $\pm$  0.146 Ma.

#### Rhyolite of Dome B (Tdr)

The rhyolite of the Dome B is white to peach in color, coarsely porphyritic with phenocrysts making up 40-45% of the rock. The phenocrysts include quartz (15-25%) up to 1 mm in size, plagioclase (20-25%) up to 1 mm in size, sanidine (35-45%) up to 1.5 mm in size, and biotite (0-5%) up to 0.5 mm in size. The crystals are anhedral to subhedral with some resorbed crystals of quartz. The rhyolite that comprises Dome B lack lithic or pumice fragments. Flow foliation can be seen in the outcrop; however, the flow foliation is hard to observe microscopically.

## Rhyolite of Dome C

The rhyolite of Dome C is white to peach in color, coarsely porphyritic with phenocrysts making up to 40-45% of the rock. Phenocrysts include quartz (15-25%) up to 1 mm in size, plagioclase (20-25%) up to 1 mm in size, sanidine (35-45%) up to 1.5 mm in size, and biotite (0-5%) up to 0.5 mm in size. The crystals are anhedral to subhedral with some resorbed crystals of quartz. The rhyolite that comprises the Dome C contains no lithic fragments or pumice fragments. The rhyolite that composes Dome C is most likely the same that comprises Dome B.

## Volcaniclastic Sedimentary Units (Ts) (Reveille Range)

The volcaniclastic sedimentary units are fine grained sandstones composed of accretionary lapilli, coarse grained sandstones, and coarse grained conglomerates with clasts of dacite and rhyolite. The fine grained units commonly show soft sediment deformation. The conglomerates are clast supported with the matrix being primarily composed of silt and sand sized particles.

## Fang Ridge Dacite (Tfr) (Reveille Range)

The dacite of Fang Ridge is gray to white, coarsely crystalline with phenocrysts consisting about 50-60% of the rock. Phenocrysts include plagioclase (45-55%) up to 3-4 mm in size, quartz (15-25%) up to 1-2 mm in size, biotite (10-15%) up to 2 mm in size, sanidine (0-3%) up to 0.5 mm in size, and sphene (trace to 2%) up to 0.25 mm in size. Most of the crystals are anhedral to subhedral, except for biotite. Biotite is euhedral and

occurs in hexagonal books with a thickness of 1-3 mm. Iron staining occurs within the groundmass and along the outer edges of the crystals.

#### Episode-1 Basalts (Tb<sub>1</sub>) (Reveille Range)

Episode-1 basalts are grey in color consisting of 30-40% phenocrysts. Phenocrysts include plagioclase (75-95%; occurs as glomerocystic megacrysts) up to ~19 mm in length, iddingsitized olivine (3-21%) up to 1.5 mm in size, clinopyroxene (trace-2%) up to 2.4 mm in size, and Fe-Ti oxides (trace-2%) up to 0.5 mm in size (Naumann et al., 1991; Naumann and Martin, 1995). Episode-1 basalts lie conformably above upper Pyramid Springs tuff (Tps<sub>3</sub>). Episode-1 basalts commonly show reversed topography in areas in which the basalt was channeled or flowed into depressions. Episode-1 basalts range in age from  $5.13 \pm 0.15$  Ma to  $5.94 \pm 0.14$  Ma (Naumann et al., 1991). Thickness ranges from 0-25 m within the southern Reveille Range, but can be as thick as 100 m in the northern Reveille Range.

#### Episode-2 Basalts (Tb<sub>2</sub>) (Reveille Range)

Episode-2 basalts are porphyritic olivine basalts that are dark gray in color and contain 20-30% phenocrysts. Phenocrysts include plagioclase (10-20%) up to 12 mm in size, iddingsitized olivine (10%) up to 2 mm in size, orthopyroxene (0-5%) up to 2.8 mm in size, xenocrysts of hornblende (0-50%) up to 8 mm in size, and Fe-Ti oxides (trace-6%) (Naumann et al., 1991; Naumann and Martin, 1995; Rash, 1995). Episode-2 basalts are the youngest volcanic units within the Reveille Range ( $3.00 \pm 0.08$  Ma to  $4.64 \pm 0.14$

Ma). Thickness ranges from 10 m in the southern Reveille Range up to 100 m in other areas of the Reveille Range.

#### Tertiary/Quaternary colluvium

The Tertiary and Quaternary colluvium consist primarily of loose angular fragments of tuff, basalt, dacite, and volcanoclastic sedimentary units. Thickness is variable depending on the locality.

#### Tertiary/Quaternary Alluvium

The Tertiary and Quaternary alluvium consists of unconsolidated sands and gravels with quartz nodules in some areas. Most of the alluvium is restricted to the washes and alluvial fans.

## APPENDIX B

### $^{40}\text{Ar}/^{39}\text{Ar}$ LASER FUSION ANALYTICAL DATA

**McKelvey-UNLV, Tps<sub>i</sub>, single crystal sanidine, J = 0.00159999 ± 0.5369%**

4 amu discrimination = 1.02695 ± 0.50%, <sup>40</sup>/<sup>39</sup>K = 0.01868 ± 52.3%, <sup>36</sup>/<sup>37</sup>Ca = 0.00025867 ± 10.31%, <sup>39</sup>/<sup>37</sup>Ca = 0.00080803 ± 27.74%

Crystal	T (C)	t (min.)	<sup>36</sup> Ar	<sup>37</sup> Ar	<sup>38</sup> Ar	<sup>39</sup> Ar	<sup>40</sup> Ar	% <sup>40</sup> Ar*	Ca/K	<sup>40</sup> Ar*/ <sup>39</sup> ArK	Age (Ma)	Is.d.
1	1600	6	0.124	0.220	0.983	75.335	628.154	94.7	0.026055086	7.9206	22.718	0.194
2	1600	6	0.059	0.092	0.401	30.975	261.127	94.7	0.026499836	7.9747	22.872	0.196
3	1600	6	0.073	0.115	0.520	39.922	335.357	94.6	0.025701125	7.9529	22.810	0.202
4	1600	6	0.088	0.140	0.655	49.795	416.163	94.6	0.025084695	7.9182	22.711	0.198
5	1600	6	0.086	0.138	0.644	51.425	429.875	94.5	0.023942593	8.1178	23.280	0.197
6	1600	6	0.110	0.099	0.454	33.632	292.070	89.7	0.026263291	7.9848	22.901	0.196
7	1600	6	0.076	0.115	0.498	38.025	318.881	93.3	0.026983318	8.0297	23.029	0.194
8	1600	6	0.205	0.092	0.343	24.239	247.308	76.4	0.033864185	7.9827	22.895	0.210
9	1600	6	0.047	0.131	0.559	44.053	361.760	96.4	0.026531542	8.1277	23.308	0.192
10	1600	6	0.099	0.066	0.267	18.727	172.395	84.3	0.031444374	7.7322	22.181	0.164
11	1600	6	0.132	0.110	0.558	42.335	370.193	90.0	0.023182455	7.8859	22.619	0.162

note: isotope beams in mV rlsd = released, error in age includes J error, all errors 1 sigma  
(<sup>36</sup>Ar through <sup>40</sup>Ar are measured beam intensities, corrected for decay in age calculations)

Mean ± s.d. = 22.848 0.297  
Wtd mean = 22.892 0.154  
(omit xtal 10)  
Isochron age = 22.76 0.14  
(11 crystals)



McKelvey-UNLV, Tps<sub>3</sub>, single crystal sanidine, J = 0.00160352 ± 0.4995%

4 amu discrimination = 1.02695 ± 0.50%, <sup>40</sup>β<sup>39</sup>K = 0.01868 ± 52.3%, <sup>36/37</sup>Ca = 0.00025867 ± 10.31%, <sup>39/37</sup>Ca = 0.00080803 ± 27.74%

Crystal	T (C)	t (min.)	<sup>36</sup> Ar	<sup>37</sup> Ar	<sup>38</sup> Ar	<sup>39</sup> Ar	<sup>40</sup> Ar	% <sup>40</sup> Ar*	Ca/K	<sup>40</sup> Ar*/ <sup>39</sup> ArK	Age (Ma)	1s.d.	
1	1600	6	0.019	0.100	0.410	30.405	244.625	98.6	0.027477846	7.9104	22.740	0.190	
2	1600	6	0.016	0.078	0.262	21.431	174.962	98.6	0.030407463	7.9980	22.990	0.188	
3	1600	6	0.012	0.096	0.311	28.590	205.355	99.3	0.028053357	7.9371	22.816	0.197	
4	1600	6	0.020	0.153	0.007	49.440	396.981	99.2	0.025854758	7.9661	22.899	0.188	
5	1600	6	0.016	0.116	0.447	36.418	291.872	99.4	0.026611509	7.9479	22.847	0.188	
6	1600	6	0.031	0.121	0.553	43.679	350.842	98.2	0.023144079	7.8831	22.662	0.185	
7	1600	6	0.022	0.104	0.322	25.943	208.327	99.1	0.033492033	7.9300	22.796	0.189	
8	1600	6	0.017	0.065	0.274	20.733	167.161	99.8	0.026192609	7.9987	22.992	0.192	
9	1600	6	0.012	0.091	0.350	28.083	225.472	99.4	0.027072324	7.9616	22.886	0.186	
10	1600	6	0.013	0.091	0.339	27.100	218.925	99.2	0.028054327	7.9983	22.991	0.187	
11	1600	6	0.014	0.115	0.514	40.658	325.003	99.4	0.023630836	7.9514	22.857	0.190	
											Mean ± s.d. =	22.861	0.102
											Wtd mean =	22.862	0.146
											no isochron		

note: isotope beams in mV rlsd = released, error in age includes J error, all errors 1 sigma  
(<sup>36</sup>Ar through <sup>40</sup>Ar are measured beam intensities, corrected for decay in age calculations)

**McKelvey-UNLV, Dome B, single crystal sanidine, J = 0.00161775 ± 0.4933%**

4 amu discrimination = 1.02695 ± 0.50%,  $^{40}\text{S}^{39}\text{K}$  = 0.01868 ± 52.3%,  $^{36}\text{S}^{37}\text{Ca}$  = 0.00025867 ± 10.31%,  $^{39}\text{S}^{37}\text{Ca}$  = 0.00080803 ± 27.74%

Crystal	T (C)	t (min.)	$^{36}\text{Ar}$	$^{37}\text{Ar}$	$^{38}\text{Ar}$	$^{39}\text{Ar}$	$^{40}\text{Ar}$	% $^{40}\text{Ar}^*$	Ca/K	$^{40}\text{Ar}^*/^{39}\text{ArK}$	Age (Ma)	1s.d.	
1	1600	6	0.019	0.086	0.291	22.927	183.224	98.8	0.029130075	7.8811	22.856	0.190	
2	1600	6	0.020	0.051	0.196	15.017	122.562	98.1	0.026374065	7.9592	23.081	0.203	
3	1600	6	0.093	0.153	0.546	43.548	361.580	93.4	0.027284336	7.7708	22.538	0.187	
4	1600	6	0.029	0.140	0.508	39.756	318.185	98.3	0.027347368	7.8815	22.857	0.185	
5	1600	6	0.477	0.108	0.466	30.573	372.671	63.9	0.027433164	7.8048	22.636	0.228	
6	1600	6	0.077	0.167	0.673	51.479	422.972	95.0	0.025192793	7.8291	22.706	0.189	
7	1600	6	0.160	0.081	0.324	22.651	222.941	79.9	0.027770767	7.8679	22.818	0.212	
8	1600	6	0.029	0.121	0.478	36.607	296.893	97.6	0.025669135	7.9307	22.999	0.191	
9	1600	6	0.047	0.124	0.443	34.695	281.605	95.7	0.027755242	7.7749	22.550	0.192	
10	1600	6	0.026	0.132	0.447	35.264	276.808	97.8	0.029069177	7.6847	22.290	0.185	
11	1600	6	0.060	0.145	0.486	38.110	315.424	94.9	0.029547414	7.8711	22.827	0.191	
note: isotope beams in mV rlsd = released, error in age includes J error, all errors 1 sigma											Mean ± s.d. =	22.742	0.216
(36Ar through 40Ar are measured beam intensities, corrected for decay in age calculations)											Wtd mean =	22.788	0.151
											(omit xtal 10)		
											Isochron age =	22.79	0.14
											(omit xtal 10)		

McKelvey-UNLV, Fang Ridge, single crystal plagioclase&sanidine,  $J = 0.00161406 \pm 0.4851\%$

4 amu discrimination =  $1.02763 \pm 0.18\%$ ,  $^{40}/^{39}\text{K} = 0.01868 \pm 52.3\%$ ,  $^{36}/^{37}\text{Ca} = 0.00025867 \pm 10.31\%$ ,  $^{39}/^{37}\text{Ca} = 0.00080803 \pm 27.74\%$

Crystal	T (C)	t (min.)	$^{36}\text{Ar}$	$^{37}\text{Ar}$	$^{38}\text{Ar}$	$^{39}\text{Ar}$	$^{40}\text{Ar}$	% $^{40}\text{Ar}^*$	Ca/K	$^{40}\text{Ar}^*/^{39}\text{ArK}$	Age (Ma)	1s.d.	
1	1600	6	0.287	3.696	0.100	2.744	101.071	19.6	12.43493073	7.1605	20.731	0.575	
2	1600	6	0.758	4.030	0.205	2.732	236.475	8.3	13.62233558	7.2432	20.969	0.676	
3	1600	6	0.143	3.316	0.069	2.487	57.353	30.7	12.30892917	6.9299	20.067	0.593	
4	1600	6	0.164	2.337	0.059	1.645	57.594	20.3	13.11789303	7.0167	20.317	1.265	
5	1600	6	0.059	0.177	0.286	20.377	165.444	90.7	0.07993845	7.3363	21.237	0.154	
6	1600	6	0.088	2.714	0.053	1.917	37.619	37.0	13.07235866	7.0570	20.433	1.070	
7	1600	6	0.218	3.687	0.084	2.684	80.226	23.9	12.68275589	7.1014	20.561	0.833	
8	1600	6	0.213	3.680	0.081	2.474	79.713	25.2	13.73687829	8.0918	23.410	0.976	
9	1600	6	0.046	1.260	0.043	0.923	18.485	38.1	12.60326399	7.0851	20.514	2.198	
10	1600	6	0.105	2.425	0.043	1.658	42.498	33.7	13.50646163	8.4336	24.392	1.343	
11	1600	6	0.056	0.060	0.216	16.567	139.791	90.0	0.0333292	7.5507	21.854	0.206	
12	1600	6	0.109	3.923	0.071	2.782	48.649	40.7	13.0203193	6.9688	20.179	0.858	
13	1600	6	0.261	3.913	0.092	3.031	96.278	24.4	11.91686306	7.7075	22.305	0.707	
14	1600	6	0.079	4.090	0.070	2.596	41.156	51.5	14.55288286	7.9363	22.963	0.772	
15	1600	6	0.125	2.585	0.052	1.804	48.266	29.6	13.23146359	7.7785	22.509	1.141	
note: isotope beams in mV rlsd = released, error in age includes J error, all errors 1 sigma ( $^{36}\text{Ar}$ through $^{40}\text{Ar}$ are measured beam intensities, corrected for decay in age calculations)											Mean $\pm$ s.d. =	21.496	1.293
											Wtd mean =	21.385	0.206
											(omit #10)		
											no isochron		

APPENDIX C

MAJOR AND TRACE ELEMENT  
GEOCHEMISTRY DATA

Table 7. Major and trace element analyses of volcanic units in the southern Reveille Range

	Tps1	Tps2	Tps3	F. Ridge	F.Ridge-2	N. Dome	S. Dome	Tpsr
SiO <sub>2</sub>	67.33	70.1	64.8	65.16	65.26	75.26	73.02	75.25
TiO <sub>2</sub>	0.27	0.26	0.27	0.61	0.61	0.16	0.22	0.21
Al <sub>2</sub> O <sub>3</sub>	16.13	15.14	15.35	14.32	14.29	12.3	13.4	12.66
Fe <sub>2</sub> O <sub>3</sub>	1.66	1.37	1.85	3.91	3.87	1.01	1.45	1.32
MnO	0.15	0.04	0.03	0.068	0.07	0.05	0.01	0.02
MgO	1	0.4	0.57	1.32	1.3	0.27	0.4	0.47
CaO	1.34	1.45	2.15	4.2	4.16	0.99	0.92	1.02
Na <sub>2</sub> O	3.5	4.19	4.71	4.86	3.35	3.57	4.13	3.68
K <sub>2</sub> O	6.67	5.93	6.29	4.21	4.24	4.6	5.09	4.65
P <sub>2</sub> O <sub>5</sub>	0.14	0.084	0.11	0.221	0.22	0.1	0.78	0.06
LOI	1.2	1.3	2.2	1.42	2.3	1.2	0.67	0.35
Total	99.39	100.264	98.33	99.689	99.67	99.51	100.09	99.69
Sc	1.78	3.22	1.7	7.31	10.96	2	0	1.33
V	44.52	35.02	55.76	97.94	93.92	7.66	19.2	20.26
Cr	200.7	192.51	198.1	217.31	214.29	186.62	198.69	191.41
Co		10.53	24.63	13.42	21.29	23.68	23.3	14.47
Ni	4.02	2.98	2.43	9.69	8.83	1.7	1.9	2.92
Cu	3.23	3.5	3	9.75	8.95	2.01	2.64	2.8
Rb	170	143	123	146	141	117	104	163
Sr	213	265	510	645	651	129	165	161
Y	20.49	16	16	19.36	19.15	12.48	10.16	18.1
Zr	159	183	240	232	221	118	165	141
Nb	13.8	12.67	8.7	16.38	15.63	10.12	8.5	14.74
Cs	15.11	15.34	28.45	7.1	6.9	23.81	23.21	
Ba	968	982	1495	1232	1233	442	662	511
La	72.24	66.9	63.04	56.33	66.25	48.7	52.8	53.04
Ce	114.31	118.76	112.69	96.1	108.94	75.41	73.81	82.35
Nd	43	41	40	41	45	28	28	28
Sm	4	8		9	6		2	2
Yb	2.64	3.9	1	1.37	1.32	3.18	1.51	0.59
Hf	7.03	6.55	8.03	5.66	6.76	2.22	2	3.5
W	4.32	126.1	125.91	80.23	131.8	238.67	216.13	156
Pb	24.78	19.5	21.34	15.73	14.54	16.31	18.1	20.55
Th	16.15	16.8	12.1	18.95	20.67	14.2	11.6	18.75
U	7.3	6.91	7.5	9.74	8.31	5.91	5.8	6.73

APPENDIX D

PALEOMAGNETIC DATA FOR THE  
SOUTHERN REVELLE RANGE AND  
SURROUNDING REGIONS

Table 8. Paleomagnetic Data of the southern Great Basin Volcanics

Site Name	I, Deg	D, Deg	R	k	Alpha 95	Del
Squaw Flat, Little Fish Lake Valley *	-70.9	200.3	7.9398	116	5.2	7.5
Black Beauty Mesa, Pancake Range *	-66.6	199.7	5.9872	389	3.4	4.1
Forest Home, East Grant Range *	-56.7	192.1	7.9647	199	3.9	5.6
Shingle Spring, Egan Range *	-67.6	192.3	5.9363	79	7.6	9.2
White River Narrows, Seaman Range *	-63.6	175.5	5.9725	182	5	6.0
Pahroc Summit, North Pahroc Range *	-58.5	177.9	7.8356	43	8.6	12.4
Badger Valley, East Pahrangat Range *	-58.1	182.3	7.989	636	2.2	3.2
Southern Delmar Mountains *	-63.1	226	7.9268	96	5.7	8.3
Mud Spring, Saulsbury Wash, Monitor Range *	-60.6	153.8	7.9864	516	2.4	3.6
Red Bluff Spring, Quinn Canyon Range *	-54.5	182.7	7.9894	658	2.2	3.2
Queen City Summit, Quinn Canyon Range *	-39	195.4	7.9959	1688	1.3	2.0
White Blotch Spring, Chalk Mountain *	-54.1	197.5	5.9818	274	4.1	4.9
Coyote Summit, Timpahute Range *	-50.2	202.1	3.9958	718	3.4	3.0
Longstreets Ranch, N. Kawich *	-57.2	171.7	6.9622	159	4.8	6.4
Cedar Pass, S. Kawich Range *	-48.8	193.1	6.9707	205	4.2	5.7
Reveille Peak, Southern Reveille Range *	-51.3	200.1	2.9985	1341	3.4	2.2
Hiko Tuff, southeastern NV **	37.21	114.868	5.99	501	3	n/a
N. Dome, Reveille Range ***	N/A	N/A	N/A	N/A	N/A	N/A
L. Pyramid Spring tuff ***	-50.5	218.1	5 of 6	490.1	3.5	
M. Pyramid Spring tuff ***	-41.4	201.1	4 of 5	616.4	3.7	
U. Pyramid Spring tuff ***	-42.5	213.4	5 of 6	1008.6	2.4	
Tuff of Goblin Knobs ***	8.6	27.2	5 of 6	328.1	3.7	

\* Samples from Best and others (1995)

\*\* Samples from Hudson and others (1992)

\*\*\* Samples from this study

## REFERENCES CITED

- Axen, G.J., Taylor, W.J., and Bartley, J.M., 1993, Space-time patterns and tectonic controls of the Tertiary extension and magmatism in the Great Basin of the western United States: *Geological Society of America Bulletin*, v. 105, p. 56-76.
- Best, M.G., Christiansen, E.H., Dieno, A.L., Grommè, C.S., McKee, E.H., and Noble, D.C., 1989, Eocene through Miocene volcanism in the Great Basin of the western United States: *New Mexico Bureau of Mines and Mineral Resource Memoir* 47, p. 91-133.
- Best, M.G., and Christiansen, E.H., 1991, Limited extension during peak volcanism, Great Basin of Nevada and Utah: *Journal of Geophysical Research*, vol. 96, p. 13,509-13,528.
- Best, M.G., Scott, R.B., Rowley, P.D., Swadley, W.C., Anderson, R.E., Grommè, C.S., Harding, A.E., Deino, A. L., Christiansen, E.H., Tingey, D.G., Sullivan, K.R., 1993, Oligocene-Miocene caldera complexes, ash-flow sheets, and tectonism in the central and southeastern Great Basin, *in* Lahren, M.M., Trexler, J.H., and Spinosa, C. *eds.*, 1993, *Crustal Evolution of the Great Basin and Sierra Nevada: Cordilleran/Rocky Mountain Section*, Geological Society of America Guidebook, Department of Geological Sciences, University of Nevada, Reno, p. 285-311.
- Best, M.G., Christiansen, E.H., Deino, A.L., Grommè, C.S., and Tingey, D.G., 1995, Correlation and emplacement of a large, zoned, discontinuously exposed ash flow sheet: The  $^{40}\text{Ar}/^{39}\text{Ar}$  chronology, paleomagnetism, and petrology of the Pahranaagat Formation, Nevada: *Journal of Geophysical Research*, v.100, p. 24,593 - 24,609.
- Butler, Robert F., 1992, *Paleomagnetism: Magnetic Domains to Geologic Terranes*, Blackwell Scientific Publications, Boston, 319 pp.
- Cebula, G.T., M.J. Kunk, H.H. Mehnert, C.W. Naeser, J.D. Obradovich, and J.F. Sutter, The Fish Canyon Tuff, a potential standard for the  $^{40}\text{Ar}$ - $^{39}\text{Ar}$  and fission-track dating methods (abstract), *Terra Cognita (6th Int. Conf. on Geochronology, Cosmochronology and Isotope Geology)*, 6, 139, 1986.
- Coney, P.J., 1978, Mesozoic-Cenozoic Cordilleran plate tectonics, *in*: Smith, R.B., and Eaton, G.P., *Cenozoic tectonics and regional geophysics of the western Cordilleran*, *Geology Society of America Memorandum* 152, p.33-50.



- Ekren, E.B., Rogers, C.L., and Davis, G.L., 1973, Geologic and Bouger Gravity map of the Reveille quadrangle, Nye County, Nevada: U.S. Geological Survey Miscellaneous Geologic Investigations Map I-806.
- Fisher, R.A., 1953, Dispersion on a sphere: Proceedings of Royal Society of London, v. A217, p. 295-305.
- Gardner, J.N., Eddy, A.C., Goff, F.E. and Grafft, K.S., 1980, Reconnaissance geologic mapping of the northern Kawich and southern Reveille Ranges, Nye County, Nevada: Los Alamos Scientific Laboratory Map LA-8390 – UC-51.
- Honn, Denise, K., 2005, Nested calderas of the northern Kawich Range, central Nevada, M.S. Thesis, University of Nevada, Las Vegas, 97 p.
- Hudson, M., Rosenbaum, J.G., Scott, R.B., Rowley, P.D., 1992, Paleomagnetic data from the Miocene Hiko Tuff, southeastern Nevada, and their tectonic implications, U.S. Geologic Survey Bulletin 2056-A, p. 221-232.
- Hudson, M.R., John, D.A., Conrad, J.E., and McKee, E.H., 2000, Style and age of late Oligocene-early Miocene deformation in the southern Stillwater Range, west central Nevada: Paleomagnetism, geochronology, and field relations: Journal of Geophysical Research, v. 105, p. 929-954.
- Hurtubise, D. O., 1994, Silver King lineament, the missing link of a 50 km east-trending structure in the southern Great Basin, *in* Dobbs, S.W., and Taylor, W.J., eds., Structural and stratigraphic investigations and petroleum potential of Nevada, with special emphasis south of the Railroad Valley producing trend: Nevada Petroleum Society, Conference, Volume 2, p. 127–139.
- Irvine, T.N. and Baragar, W.R.A., 1971. A guide to the chemical classification of the common volcanic rocks. Canadian Journal of Earth Sciences, 8: 523-548.
- Johnson, C.M., 1991, Large-scale crust formation and lithosphere modification beneath middle to late Cenozoic calderas and volcanic fields, western North America: Journal of Geophysical Research, vol. 96, p. 13,485-13,507.
- Kirchvink, J.L., 1980, The least-squares line and plane and the analysis of paleomagnetic data: Geophysical Journal of the Royal Astronomical Society, v. 62, p. 699-718.
- Knight, M.D., Walker, G.P.L., Ellwood, B.B., and Diehl, J.F., 1986, Stratigraphy, paleomagnetism, and magnetic fabric of the Toba Tuffs: Constraints on the source and eruptive styles: Journal of Geophysical Research, v. 91, p. 10,355-10,382.

- Krogh, T.E., 1973, A low contamination method for hydrothermal decomposition of zircon and Pb for isotopic age determinations, *Geochimica et Cosmochimica Acta*, v.37, p.485-494.
- Lipman, P.W., 1997, Subsidence of ash-flow calderas: Relation to caldera size and magma chamber geometry, *Bulletin of Volcanology*, vol. 59, issue 3, pp. 198-218.
- Martin, M.W., and Naumann, T.R., 1995, Geologic map of the Reveille quadrangle, Nevada: Nevada Bureau of Mines and Geology, Map 104.
- McFadden, P.L., and Lowes, F.J., 1981, The discrimination of mean directions drawn from Fisher distributions: *Geophysical Journal of the Royal Astronomical Society*, v. 67, p. 19-33.
- Naumann, T.R., Smith, E.I., Shafiqullah, M., and Damon, P.E., 1991, New K-Ar ages for mafic to intermediate volcanic rocks in the Reveille Range, Nevada: *Isochron West*, p. 12-16.
- Norrish, K., and Hutton, J.T., 1969, An accurate X-ray spectrographic method for the analysis of a wide range of geological samples: *Geochimica et Cosmochimica Acta*, v. 33, p. 431-453.
- Patchet, P.J., and Ruiz, J., 1987, Nd isotopic ages of crust formation and metamorphism in the eastern and southern Mexico, *contributions to Mineralogy and Petrology*, v.96, p.523-528.
- Rash, K.B., 1995, Geology and geochemistry of the Tertiary volcanic rock in the northern Reveille and southern Pancake Ranges, Nye County, Nevada: M.S. Thesis, University of Nevada, Las Vegas, Las Vegas, Nevada, 171 p.
- Richard, P., Shimizu, N., and Allegre, C.J., 1976,  $^{143}\text{Nd}/^{146}\text{Nd}$ , a natural tracer: an application: *Earth and Planetary Science Letters*, v.31, p.269-278.
- Schmincke, H.U., 2004, *Volcanism*, Springer, Berlin Heidelberg NewYork, 324 p.
- Scott, R.B., Grommè, C.S., Best, M.G., Rosenbaum, J.R., and Hudson, M.R., 1995, Stratigraphic relationships of Tertiary volcanic rocks in central Lincoln County, southeastern Nevada, in *Geologic Studies in the Basin and Range to Colorado Plateau Transition of Nevada-Utah-Arizona Area*, U.S. Geologic Survey Bulletin 2056-A, p. 7-41.
- Steven, T.A., H.H. Mehnert, and J.D. Obradovich, Age of volcanic activity in the San Juan Mountains, Colorado, *U.S. Geol. Surv. Prof. Pap.*, 575-D, 47-55, 1967.
- Stewart, J.H., and Carlson, J.E., 1976, Cenozoic rocks of Nevada, Map 52, Nevada Bureau of Mines and Geology, Reno, NV.

- Sun, S. and McDonough, W.F., 1989. Chemical and isotopic systematics of ocean basalts: implications for mantle composition and processes. In: A.D.N. Saunders, M.J. (Editor), *Magmatism in the Ocean Basins*. Geological Society of London Special Publication. Geological Society of London, pp. 313-345.
- Vaniman, D.T., and Crowe, B.M., 1981, Geology and petrology of the basalt of Crater Flat: Applications to volcanic risk assessment for the Nevada nuclear waste and storage  
Investigations: Los Alamos National Laboratory Report LA-8845-MS.
- Wendt, I., and Carl, C., 1991, The statistical distribution of the mean squared weighted deviation, *Chemical Geology*, v. 86, p. 275-285.
- Wernicke, B., 1981, Low-angle normal faults in the Basin and Range province: nappe tectonics in an extending orogen, *Nature*, v. 291, p. 645-648.

## VITA

Graduate College  
University of Nevada, Las Vegas

Matthew A. McKelvey

### Home Address:

1943 Claymont Drive  
Clarksville, TN 37040

### Degrees:

Bachelor of Science, Geology, 1995  
Austin Peay State University

### Publications:

McKelvey, Matthew, and Smith, Eugene, 2004, Mid-Miocene calderas in the Reveille Range, Nevada, Denver Annual Geologic Society of America Meeting (November 7-10, 2004).

Drushke, Peter, Honn, Denise, McKelvey, Matt, Nastanski, Nicole, Rager, Audrey, Smith, Eugene I., and Belliveau, Robert, 2004, Volcanology of the Northern Eldorado Mountains, Nevada: New evidence for the source of the Tuff of Bridge Spring?, 2004 Denver Annual Geologic Society of America Meeting (November 7-10, 2004)..

McKelvey, M.A., and Deibert, J.E., 2000, Stratification features of eolian volcanoclastic sandstone units of the Miocene Humboldt Formation, northeast, Nevada: (abs.), Geological Society of America Abstracts with Programs, v. 32, p. A-272.

Thesis Title: Geology of the southern Reveille Range, Nye County, Nevada

### Thesis Examination Committee:

Chairperson, Dr. Eugene I. Smith, Ph. D.  
Committee Member: Dr. Terry Spell, Ph. D.  
Committee Member: Dr. Andrew Hanson, Ph. D.  
Graduate Faculty Representative: Dr. Stephen Lepp, Ph. D.